



1 Space Weather Forecasting: What We Know Now and What 2 Are the Current and Future Challenges?

3

4 Bruce T. Tsurutani¹, Gurbax S. Lakhina², Rajkumar Hajra³

5

6 ¹Jet Propulsion Laboratory, California Institute of Technology, Pasadena, Calif, USA

7 ²Indian Institute for Geomagnetism, Navi Mumbai, India

8 ³National Atmospheric Research Laboratory, Gadanki, India

9

10 ABSTRACT

11 Geomagnetic storms are caused by solar wind southward magnetic fields that impinge upon
12 the Earth's magnetosphere (Dungey, 1961). How can we forecast the occurrence of these
13 interplanetary events? We view this as the most important challenge in Space Weather. We
14 discuss the case for magnetic clouds (MCs), interplanetary sheaths upstream of ICMEs,
15 corotating interaction regions (CIRs) and high speed streams (HSSs). The sheath- and
16 CIR-related magnetic storms will be difficult to predict and will require better knowledge
17 of the slow solar wind and modeling to solve. There are challenges for forecasting the
18 fluences and spectra of solar energetic particles. This will require better knowledge of
19 interplanetary shock properties from the Sun to 1 AU (and beyond), the upstream slow
20 solar wind and energetic "seed" particles. Dayside aurora, triggering of nightside
21 substorms, and formation of new radiation belts can all be caused by shock and
22 interplanetary ram pressure impingements onto the Earth's magnetosphere. The
23 acceleration and loss of relativistic magnetospheric "killer" electrons and penetrating
24 electric fields in terms of causing positive and negative ionospheric storms are currently
25 reasonable well understood, but refinements can still be made. The forecasting of extreme
26 events (extreme shocks, extreme solar energetic particle events, and extreme geomagnetic
27 storms ("Carrington" events or greater)) are also discussed. Energetic particle precipitation
28 and ozone destruction is briefly discussed. For many of the studies, the Parker Solar Probe,
29 Solar Orbiter, Magnetospheric Multiscale Mission (MMS), Arase, and SWARM data will
30 be useful.



31

32 1. INTRODUCTION

33 1.1. Some Comments on the History of Space Weather

34

35 Space Weather is a new term for an old topic. Prior to the space age where we have satellites
36 orbiting the Earth, probing interplanetary space and viewing the Sun in UV, EUV and X-ray
37 wavelengths, it was clearly realized that solar phenomena caused geomagnetic activity at the Earth.
38 For example Carrington (1859) noted that there was a magnetic storm that followed ~17 hr 40 min
39 after the well-documented optical solar flare which he reported. This storm (Chapman and Bartels,
40 1940) was only more recently studied in detail by Tsurutani et al. (2003) and Lakhina et al. (2012),
41 but the hints of a causal relationship was there in 1859. Later, Hale (1931), Newton (1943) and
42 others showed that magnetic storms were delayed by several days from intense solar flares. These
43 types of magnetic storms are now known to be caused by interplanetary coronal mass ejections or
44 ICMEs. Details will be discussed later in this review.

45

46 Maunder (1904) showed that geomagnetic activity often had a ~27 day recurrence, associated with
47 some mysteriously unseen (by visible light) feature on the Sun. Chree (1913) showed that these
48 data were statistically significant, thus inventing the Chree “superposed epoch analysis”, a
49 technique which is often used today. The mysteriously unseen solar features responsible for the
50 geomagnetic activity were called “M-regions” by Bartels (1934) where the “M” stood for
51 “magnetically active”. It is now known that M-regions are coronal holes (Krieger et al., 1973),
52 solar regions from which high speed solar wind streams (HSSs) emanate, causing geomagnetic
53 activity at the Earth (Sheeley et al., 1976, 1977; Tsurutani et al. 1995). The current status of
54 geomagnetic activity associated with HSSs and future work needed to predict the various facets of
55 space weather events will be discussed.

56

57 With the advent of rockets and satellites, the interplanetary medium has been probed by magnetic
58 field, plasma, and energetic particle detectors. The Sun has been viewed in many different
59 wavelengths. The Earth’s auroral regions have recently been viewed by UV imagers giving a
60 global view of auroras including the dayside. The ionosphere has been probed by global
61 positioning system (GPS) dual frequency radio signals, allowing a global map of the ionospheric



62 total electron content (TEC) in relatively high spatial and temporal resolution. The purpose of this
63 review article will be to give a reasonably comprehensive review of some of the major Space
64 Weather effects in the magnetosphere, ionosphere and atmosphere and in interplanetary space, in
65 order to explain what the solar and interplanetary causes are or are expected to be. The most useful
66 part of this review will be to focus on what future advances in Space Weather might be in the next
67 10 to 25 years. In particular we will mention what outstanding problems the Parker Solar Probe,
68 Solar Orbiter, MMS, Arase, ICON, GOLD, and SWARM data might be useful in solving.

69

70 Our discussion will first start with phenomena that occur during solar maxima (flares, CMEs and
71 interplanetary CME (ICME)-induced magnetic storms). We will explain to the solar scientists what
72 is meant by an ICME and why we distinguish this from a CME. Next, phenomena associated with
73 the declining phase of the solar cycle will be addressed. These include corotating interaction
74 regions (CIRs), high speed streams (HSSs) which cause high-intensity long-duration continuous
75 AE activity (HILDCAA) events, and the acceleration and loss of magnetospheric relativistic
76 electrons. We will then return to the topic of interplanetary shocks and their acceleration of
77 energetic particles in interplanetary space and also their creating new radiation belts inside the
78 magnetosphere. Interplanetary shock impingement onto the magnetosphere create dayside auroras
79 and also trigger nightside substorms. Prompt penetration electric fields during magnetic storm
80 main phases will be discussed with the consequences of positive and negative ionospheric storms,
81 depending on the local time of the observation and the phase of the magnetic storm. Two relatively
82 new topics, that of supersubstorms and the possibility of precipitating magnetospheric relativistic
83 electrons affecting atmospheric weather will be discussed. A glossary will be provided to give
84 definition of the terms used in this review article.

85

86 1.2. Organization of Paper

87

88 The concept of magnetic reconnection is introduced first for the nonspace plasma readers. This is
89 the physical process responsible for transferring solar wind energy into the magnetosphere during
90 magnetic storms. We have organized the rest of the paper by discussing space weather phenomena
91 by solar cycle intervals. However it should be mentioned that this is not totally successful since
92 some phenomena span all parts of the solar cycle.



93

94 Solar maximum phenomena such as Coronal Mass Ejections (CMEs), Interplanetary CMEs
95 (ICMEs), fast shocks, sheaths, and the forecasting of geomagnetic storms associated with the
96 above are covered in subsections 2.1 to 2.4. The space weather phenomena associated with the
97 declining phase of the solar cycle are discussed in section 3.0. Topics such as CIRs, CIR storms,
98 high speed solar wind streams, embedded Alfvén wave trains, High-Intensity Long-Duration
99 Continuous AE Activity (HILDCAA) events, relativistic magnetospheric electron acceleration and
100 loss, and electron precipitation and ozone depletion are discussed in subsections 3.1 to 3.6.
101 Although interplanetary shocks are primarily features associated with fast ICMEs and thus a solar
102 maximum phenomenon, shocks can also bound CIRs (~20% of the time) at 1 AU during the solar
103 cycle declining phase as well. Shocks and the high density plasmas that they create can input ram
104 energy into the magnetosphere. Topics such as solar cosmic ray particle acceleration, dayside
105 auroras, triggering of nightside substorms and the creation of new magnetospheric radiation belts
106 are covered in subsections 4.1 to 4.4. Solar flares and ionospheric total electron content (TEC)
107 increases is another space weather effect causing direct solar-ionospheric coupling not involving
108 interplanetary space nor the magnetosphere. This is briefly discussed in Section 5.0. Prompt
109 Penetration Electric Fields (PPEFs) and ionospheric TEC increases (and decreases) occurs during
110 magnetic storms. Although the biggest effects are observed during ICME magnetic storms (solar
111 maximum), effects have been noted in CIR magnetic storms as well. This is discussed in section
112 6.0. The “Carrington” magnetic storm is the most intense magnetic storm in recorded history. The
113 aurora associated with the storm reached 23° from the geomagnetic equator (Kimball, 1960), the
114 lowest in recorded history. Since this event has been used as an example for extreme space weather
115 and events of this type are a problem for the U.S. Homeland Security, we felt that there should be
116 a separate section on this topic, section 7.0. We discuss the possibility of events even larger than
117 the Carrington storm occurring. In section 8.0 supersubstorms are discussed. Why is this topic
118 covered in this paper? It is possible that supersubstorms which occur within superstorms are the
119 actual causes for the extreme ionospheric currents that are responsible for potential power grid
120 failures and not the geomagnetic storms themselves. Section 9.0 gives our summary/conclusions
121 for forecasting space weather events. Section 10.0 is a glossary of space weather terms used by
122 researchers in the field. Most of the definitions were carefully constructed and were reviewed in



123 a previous publication. These should be useful for an ionospheric person looking up solar terms or
124 vice versa. It could be particularly useful for the nonspace plasma readership.

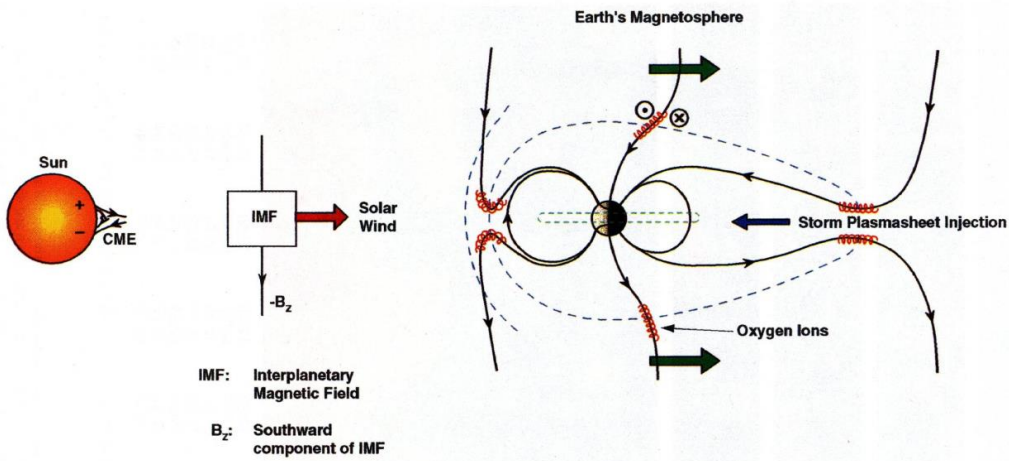
125

126 W

127 2. RESULTS: Solar Maximum

128 2.1. Southward Interplanetary Magnetic Fields, Magnetic Reconnection and Magnetic 129 Storms

130



131

132 Figure 1. Magnetic reconnection powering geomagnetic storms and substorms. Adapted from
133 Dungey (1961).

134

135 Figure 1 shows the Dungey (1961) scenario of magnetic reconnection. A one-to-one relationship
136 between southward magnetic fields and magnetic storms has been shown by Echer et al. (2008a)
137 for 90 magnetic storms that occurred during Solar Cycle 23. If the interplanetary magnetic field
138 is directed southward, it will interconnect with the Earth's magnetopause northward magnetic
139 fields (the Earth's north magnetic pole is located in the southern hemisphere near the south
140 rotational pole). The solar wind drags the interconnected magnetic fields and plasma downstream
141 (in the antisunward direction). The open magnetic fields then reconnect in the tail. Reconnection
142 leads to strong convection of the plasmashell into the nightside magnetosphere.

143



144 What is known by theory and verified by observations is that the stronger the southward
145 component of the interplanetary magnetic field, the stronger the solar wind-magnetospheric system
146 is driven (e.g., Gonzalez et al., 1994). Intense IMF B_{south} in MCs (and sheaths) drive intense
147 magnetic reconnection at the dayside magnetopause and intense reconnection on the nightside.
148 Strong nightside magnetic reconnection leads to strong inward convection of the plasmasheet. The
149 stronger the magnetotail reconnection, the stronger the inward convection. Via conservation of the
150 first two adiabatic invariants (Alfvén, 1950), the greater the convection, the greater the
151 energization of the radiation belt particles.

152

153 As the midnight sector plasmasheet is convected inward to lower L, the initially ~100 eV to 1 keV
154 plasmasheet electrons and protons are adiabatically compressed (kinetically energized) so that the
155 perpendicular (to the ambient magnetic field) energy becomes greater than the parallel energy.
156 This leads to plasma instabilities, wave growth and wave-particle interactions (Kennel and
157 Petschek, 1966). The resultant effect is the “diffuse aurora” caused by the precipitation of the ~10
158 to 100 keV electrons and protons into the upper atmosphere/lower ionosphere. At the same time
159 double layers are formed just above the ionosphere, giving rise to ~1 to 10 keV electron
160 acceleration and precipitation in the formation of “discrete auroras” (Carlson et al., 1998).

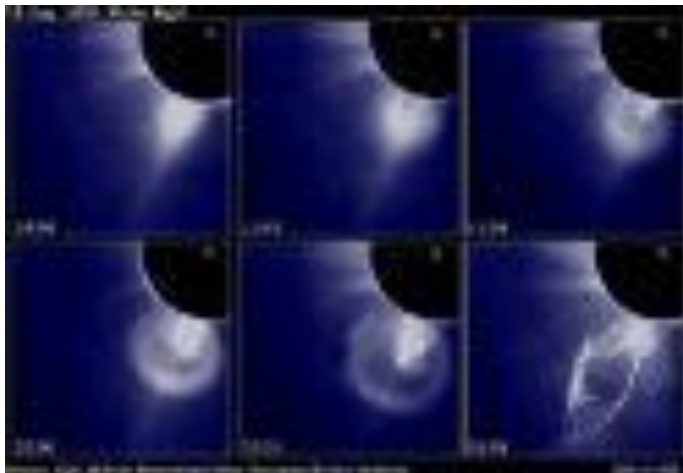
161

162 After the southward field decreases or changes orientation to northward fields, the magnetic storm
163 recovers. The recovery is associated with a multitude of physical processes associated with the
164 loss of the energetic ring current particles: charge exchange, Coulomb collisions, wave-particle
165 interactions and convection out the dayside magnetopause (Kozyra et al. 1997, 2006a; Jordanova
166 et al., 1998; Daglis et al. 1999). A typical time for storm recovery is 10 to 24 hrs (Burton et al.,
167 1975; Hamilton et al., 1988; Ebihara and Ejiri, 1998; O'Brien and McPherron, 2000; Dasso et al.,
168 2002; Kozyra et al., 2002; Wang et al., 2003; Weygand and McPherron, 2006; Montreal MacMahon
169 and Llop, 2008).

170

171 **2.2. Coronal Mass Ejections (CMEs), Interplanetary Coronal Mass Ejections (ICMEs) and** 172 **Magnetic Storms**

173



174

175 Figure 2. A sequence of images showing the emergence of parts of a coronal mass ejection (CME)
176 coming from the Sun. The time sequence starts at the upper left and ends at the lower right. Taken
177 from Illing and Hundhausen (1986).

178

179 What are the solar and interplanetary sources of intense interplanetary magnetic fields that lead to
180 magnetic reconnection at Earth and intense magnetic storms? What we know from space age
181 observations is that these magnetic fields come from parts of a coronal mass ejection, a giant blob
182 of plasma and magnetic fields which are released from the Sun associated with solar flares and
183 disappearing filaments (Tang et al., 1989). Figure 2 shows the emergence of a CME from behind
184 a solar occulting disc. The time sequence starts at the upper left, goes to the right and then to the
185 bottom left, and ends at the bottom right. The three parts of a CME are best noted in the image on
186 the bottom left. There is a bright outer loop most distant from the Sun, followed by a “dark region”,
187 and then closest to the Sun is the solar filament.

188

189 **2.3. Forecasting Magnetic Storms and Extreme Storms Associated with ICMEs**

190

191 We will precede ourselves and state here that for the limited number of cases studied to date, the
192 most geoeffective part of the CME is the “dark region”. Interplanetary scientists (Burlaga et al.,
193 1981; Choe et al., 1982; Tsurutani and Gonzalez, 1994) have identified this as the low plasma beta
194 region called a magnetic cloud (MC), first identified by Burlaga et al.(1981) and Klein and Burlaga
195 (1982) in interplanetary space by magnetic field and plasma measurements. When there are



196 southward component magnetic fields within the magnetic cloud (thought to typically be a giant
197 fluxrope), a magnetic storm results (Gonzalez and Tsurutani, 1987; Gonzalez et al. 1994; Zhang
198 et al., 2007; Echer et al. 2008a).

199

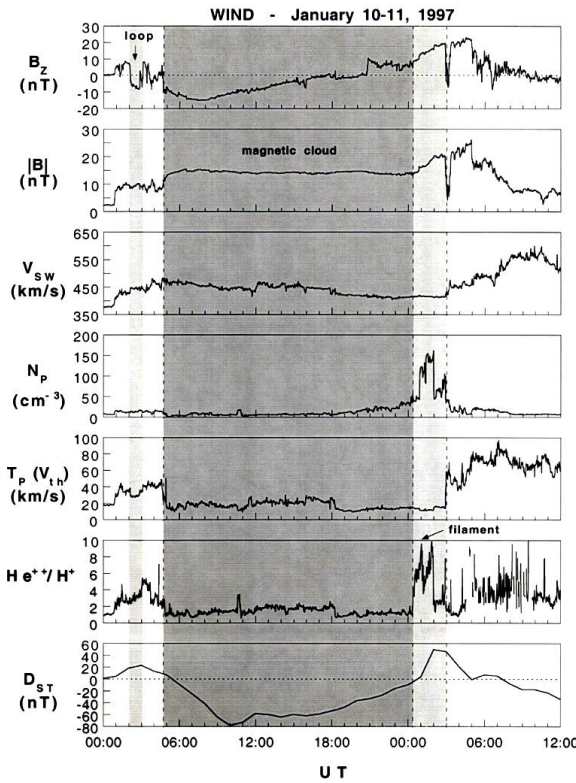
200 Interplanetary and magnetospheric scientists have developed the term ICME or interplanetary
201 CME because it is not known how the CME evolves as it propagates from the Sun to the Earth and
202 beyond. For example the bright outer loops are seldomly identified at 1 AU (one rare case was
203 identified by Tsurutani et al., 1998) and the filaments are typically not found within the ICME at
204 1 AU. A rare case was reported by Burlaga et al. (1998). For statistical results we direct the reader
205 to Lepri and Zurbuchen (2010). Where have the bright outer loops and filaments gone to? Have
206 they simply detached only to impinge onto the magnetosphere at a later time, or do they go back
207 into the Sun? Observations from the Parker Solar Probe, Solar Orbiter and ACE plus ground-
208 based solar observations could perhaps help address this question.

209

210 It should be remarked that the high density solar filaments could be extremely geoeffective if they
211 collided with the Earth's magnetosphere (this is covered later in Section 3.2.5). Modeling and
212 examining the Parker Solar Probe and Solar Orbiter data could help us understand whether the MC
213 evolves as it propagates through interplanetary space. Is it possible for the MC to rotate so that
214 initially southward magnetic fields become northward components? Can the MC fields be
215 compressed or expanded by interplanetary interactions? Can magnetic reconnection be taking
216 place within the ICME between the solar corona and 1 AU as suggested by Manchester et al.
217 (2006) and Kozyna et al., (2013)? If so, how often does this occur and can it be predicted?

218

219 Of course the most important goal for space weather is predicting the southward magnetic fields
220 within the ICME. This extremely difficult task is the holy grail of space weather. It is more
221 important than predicting the time of the release of a CME, its speed and its direction.



222

223 Figure 3. An ICME detected at 1 AU just upstream of the Earth.

224

225 Figure 3 shows a rare case of an ICME where all three parts of a CME are detected at 1 AU. The
226 MC is indicated by the shaded region in the figure. The outer loop was identified by Tsurutani et
227 al. (1998) and the filament by Burlaga et al. (1998).

228

229 From top to bottom are the interplanetary magnetic field (IMF) B_z component (in geocentric solar
230 magnetospheric/GSM coordinates), the field magnitude, the solar wind velocity, density,
231 temperature and the He^{++}/H^+ ratio. The bottom panel gives the ground based Dst index whose
232 amplitude is used as an indicator of the occurrence of a magnetic storm. Dst becomes negative
233 when the Earth's magnetosphere is filled with storm-time energetic $\sim 10\text{-}300$ keV electrons and
234 ions (Williams et al., 1990). Dessler and Parker (1959) and Sckopke (1966) have shown that the
235 amount of magnetic decrease is linearly related to the total kinetic energy of the enhanced radiation
236 belt particles. This is because the energetic particles which comprise the storm-time ring current,



237 through gradient drift of the charged particles, form a diamagnetic current which decreases the
238 Earth's magnetic field inside the current. We refer the reader to Sugiura (1964) and Davis and
239 Sugiura (1966) for futher discussions of the Dst index. The Dst index is a one hr index. More
240 recently a 1 min SYM-H index (Iyemori, 1990; Wanliss and Showalter, 2006) has been developed.
241 This is more useful for high time resolution studies. Both indices are produced by the Kyoto Data
242 Center.

243

244 In this example (top panel of Figure 3) the MC fields start with a strong southward ($B_z < 0$ nT)
245 component and then later turns northward. In the bottom panel, the magnetic storm Dst index
246 becomes negative with very little delay from the southward magnetic fields. The energy transfer
247 mechanism is magnetic reconnection (Dungey, 1961) as discussed in Section 2.1. The high density
248 filament (fourth panel from the top) is present after the MC passage. Values as high as ~ 160 cm $^{-3}$
249 have been detected. These values are extreme values with the nominal solar wind density being \sim
250 3 to 5 cm $^{-3}$ (Tsurutani et al., 2018a). The high densities impinging on the magnetosphere in this
251 case caused the Dst index to reach a maximum of $\sim +55$ nT.

252

253 The stronger the southward component of the MC fields, the more intense the magnetic storm at
254 the Earth. In extreme cases storms with intensities of $Dst < -250$ nT can occur (Tsurutani et al.
255 1992a; Echer et al. 2008b). An empirical relationship between the speed of the MC at 1 AU and
256 its magnetic intensity has been shown by Gonzalez et al. (1998). A hypothetical explanation is the
257 “melon seed model”: squeezing a melon seed will cause it to squirt out, squeezing it harder will
258 make it come out fast. A larger magnetic field will require greater pressure to release it. However
259 a real MHD or plasma kinetic model is need to explain this empirical relationship.

260

261 Because extremely strong MC magnetic fields are needed to produce extreme magnetic storms
262 like the “Carrington” event (Tsurutani et al., 2003; Lakhina and Tsurutani, 2017), one should focus
263 on extremely fast events for forecasting purposes. The geoeffective interplanetary dawn-to-dusk
264 electric field is $V_{sw} \times B_{south}$. Because Gonzalez et al (1998) have shown that $|B|$ is empirically
265 proportional to V_{sw} , the dawn-to-dusk interplanetary electric field has a V_{sw}^2 dependence. The
266 Carrington ICME took ~ 17 hr 40 min to go from the Sun to Earth (Carrington, 1859) causing the
267 largest magnetic storm in history, Dst estimated to be -1760 nT. However the August 1972 event



268 was even faster, taking only ~14 hr 40 min to go from the Sun to Earth (Vaisberg and Zastenker
269 1976; Zastenker et al. 1978). Although the 1972 MC was indeed extreme in speed and magnetic
270 field intensity, the direction of the magnetic field was northward and thus geomagnetic quiet during
271 the MC impingement onto the magnetosphere (Tsurutani et al. 1992b). So again, predicting the
272 ICME magnetic field direction is paramount in importance.

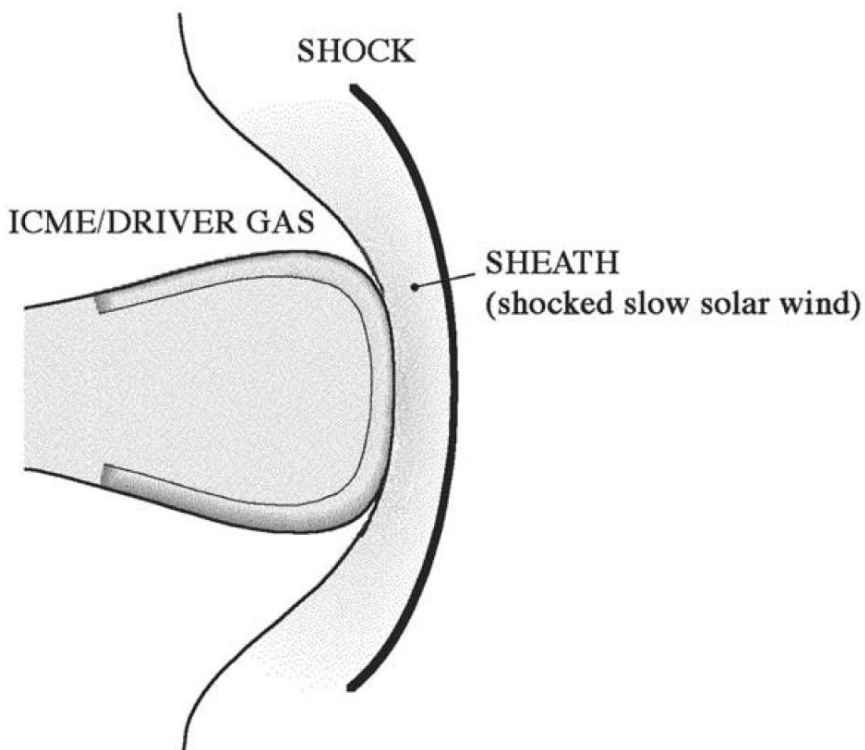
273

274 Modeling of ICME propagation in interplanetary space during disturbed AR periods has met only
275 limited success (Echer et al., 2009; Mostl et al., 2015). Sometimes it is difficult to even identify
276 which flare or disappearing filament a detected ICME is related to (see Tang et al., 1989). The
277 propagation times from the Sun to 1 AU has often been in error by days (Zhao and Dryer, 2014).
278 The additional information provided by the Parker Solar Probe and Solar Orbiter and examination
279 of present ICME propagation codes will help improve the ability to make more accurate forecasts.

280

281 **2.4. Fast Shocks, Sheaths and Magnetic Storms**

282



283

284 Figure 4. A schematic of an interplanetary sheath antisunward of an ICME. In this diagram the
285 Sun is on the left (not shown).

286

287 Figure 4 shows a schematic of a shock and sheath upstream of an ICME. “Fast” CMEs/ICMEs can
288 create upstream fast forward shocks (Tsurutani et al., 1988). By “fast” it is meant that the
289 CME/ICME is moving at a speed higher than the upstream magnetosonic (fast wave mode) speed
290 relative to the upstream plasma and by “forward” we mean that the shock is propagating in the
291 same direction as the “driver gas” or the CME/ICME, antisunward. When a shock is formed, it
292 compresses the upstream plasma and magnetic fields. In this terminology, the upstream direction
293 is the direction in which the shock is propagating (antisunward in this case) and the downstream
294 direction is towards the Sun (see Kennel et al., 1985 and Tsurutani et al., 2011 for details on
295 shocks). The compressed plasma and magnetic fields downstream of the shock is the “sheath”.
296 The shock and sheath are not part of the CME/ICME. The origin of this plasma and magnetic
297 fields is the slow solar wind, altered by shock compression. This is important to realize if one

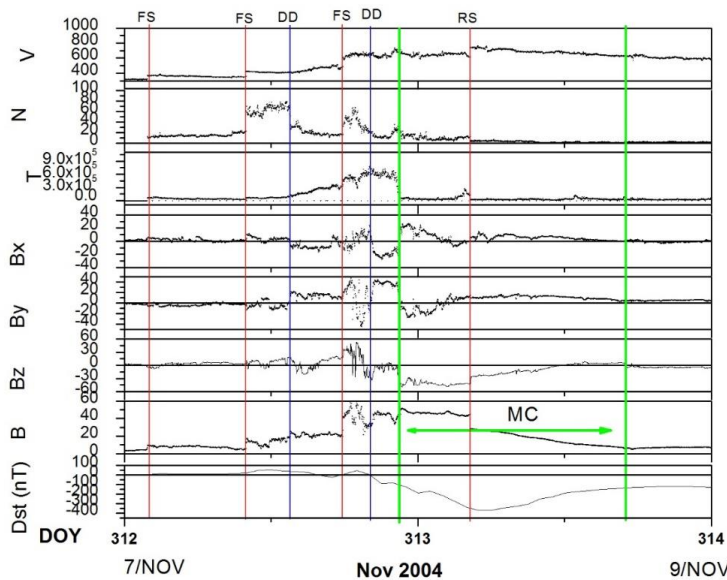


298 wishes to predict magnetic storms caused by interplanetary sheath southward magnetic fields. It
299 should be noted that “slow” ICMEs have been detected at 1 AU (Tsurutani et al., 2004a). These
300 phenomena do not necessarily have upstream shocks and sheaths, as expected. However the
301 southward MC magnetic fields still cause magnetic storms.

302

303 Kennel et al. (1985) used MHD simulations to show that the plasma densities and magnetic field
304 magnitudes downstream of shocks are roughly related to the shock magnetosonic Mach numbers.
305 This relationship holds up to a Mach number of ~4. For higher Mach numbers MHD predicts that
306 the compression will remain at a factor of ~4. Since interplanetary shocks detected at 1 AU
307 typically have Mach numbers only of 1 to 3 (Tsurutani and Lin, 1985; Echer et al., 2011; Meng et
308 al. 2019), 1 to 3 are the typical shock magnetic field and density compressions detected at 1 AU.
309 One question for future studies is “does the MHD relationships of magnetic field magnitude and
310 density jumps hold for extreme shocks?” If not, there will be important consequences for extreme
311 space weather.

312



313

314 Figure 5. An example of three fast forward shocks pumping up the interplanetary magnetic field
315 intensity. Taken from Tsurutani et al. (2008a).



316

317 Figure 5 shows a complex interplanetary event that was selected by the CAWSES II team to study
318 in detail. The full information on this event from the Sun to the atmosphere can be found in the
319 special issue: Large Geomagnetic Storms of Solar Cycle 23
320 ([https://agupubs.onlinelibrary.wiley.com/doi/toc/10.1002/\(ISSN\)1944-8007.CYCLE231](https://agupubs.onlinelibrary.wiley.com/doi/toc/10.1002/(ISSN)1944-8007.CYCLE231)). What
321 is important is that this event was associated with a solar active region (AR) and the results are
322 quite important in terms not only for interplanetary disturbance phenomena but also for
323 geomagnetic activity at the Earth.

324

325 From top to bottom in Figure 5 are the solar wind speed, density, and temperature, the IMF Bx,
326 By and Bz components and the magnetic field magnitude in GSM coordinates. In this coordinate
327 system, **x** points in the direction of the Sun, **y** is $(\Omega \times \mathbf{x})/|\Omega \times \mathbf{x}|$ where Ω is the Earth's south
328 magnetic pole and **z** completes the right hand system. The magnetic storm Dst index is given at
329 the bottom. Fast forward shocks are denoted by the three vertical red lines on 7 November 2004.
330 There are sudden increases in the velocity, density, temperature and magnetic field magnitude at
331 all three events. The Rankine-Hugoniot relationships have been applied to the plasma and
332 magnetic field data to determine that they are indeed fast shocks.

333

334 The point of showing this case is to indicate that each shock pumps up the interplanetary sheath
335 magnetic field by factors of ~2 to 3. The initial magnetic field magnitude started with a value of
336 ~4 nT and at the peak value after three shocks, it reached a value of ~60 nT. This final value was
337 higher than the MC magnetic field which was ~45 nT. Details concerning the shocks and
338 compressions can be found in the original paper for readers who are interested. What is important
339 here is how intense interplanetary magnetic fields are created. They can come from the MCs
340 themselves or the sheaths, as shown here. However in this case the southward magnetic fields that
341 caused the magnetic storm came from the MC and not the sheath.

342

343 In the above example it is believed that three fast forward shocks were associated with three ICMEs
344 released from the AR. The longitudinal extent of shocks are, however, wider than the MCs, so
345 only one MC was detected in the event. A similar situation was found for the August 1972 event
346 discussed earlier.



347

348 It should be noted that a fast reverse wave (here by “reverse” we mean that the wave is propagating
349 in the solar direction) was detected during the Figure 5 event. It is identified as the red vertical line
350 on 8 November. In detailed examination of the Rankine-Hugoniot conservation equations, this
351 wave was found to propagate at a speed below the upstream magnetosonic speed and thus was a
352 magnetosonic wave and not a shock. This reverse wave caused a decrease in the MC magnetic
353 field (and the southward component) and thus the start of the recovery phase of the magnetic storm.
354 The reader should note that fast reverse waves and shocks are also important for geomagnetic
355 activity. A detailed discussion of shock and discontinuity effects on geomagnetic activity can be
356 found in Tsurutani et al. (2011).

357

358 **2.4.1. Forecasting ICME sheath magnetic storms**

359

360 Determination of the IMF Bz component in the sheaths will be a difficult task. To do this, more
361 effort on predicting the slow solar wind plasma and magnetic field will be required. To date, there
362 has been little effort expended in this area. This is, however easy for us to hope for, but in practice
363 is far more difficult to do. Use of data from Solar Probe, Solar Orbiter and a 1 AU spacecraft such
364 as ACE will help in these analyses.

365

366 This problem has recently been emphasized by results from Meng et al. (2019). Meng et al. have
367 shown that superstorms ($Dst < -250$ nT) that occurred during the space age (1957 to present) are
368 mostly driven by sheath fields or a combination of sheath plus a following magnetic cloud (MC).

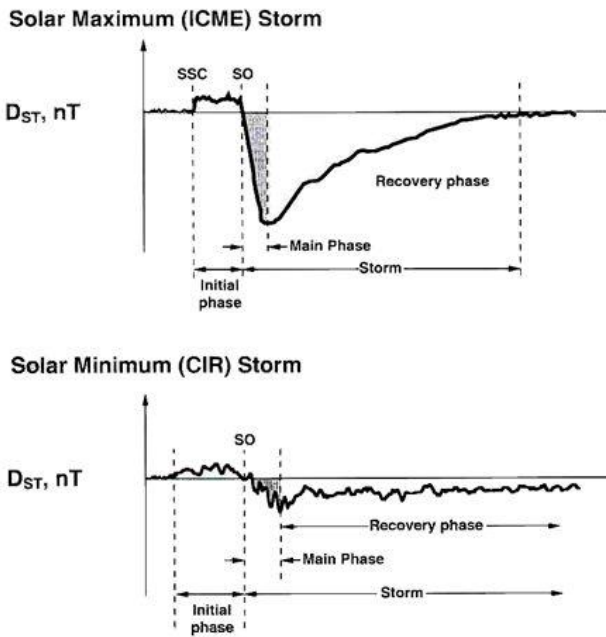
369

370 Substorms are generated by lower intensity southward magnetic fields with the process of
371 magnetic reconnection being the same as above. However substorm plasmashell injections only
372 go in to $L \sim 4$, the outer part of the magnetosphere (Soraas et al., 2004). The auroras associated
373 with substorms appear in the “auroral zone”, 60° to 70° magnetic latitudes (MLATs). Magnetic
374 storms associated with much larger IMF Bsouth are detected at subauroral zone latitudes.

375

376 **3.0. RESULTS: Declining Phase of the Solar Cycle**

377 **3.1. Corotating Interaction Region (CIR) Magnetic Storms**



378

379 Figure 6. The magnetic Dst profiles of a CIR magnetic storm (bottom) and an ICME magnetic
380 storm (top). Taken from Tsurutani (2000).

381

382 During the declining phase of the solar cycle a different type of solar and interplanetary activity
383 dominates the cause of magnetic storms, that of solar coronal holes and Corotating Interaction
384 Regions (CIRs). The magnetic storms caused by CIRs are quite different from storms caused by
385 ICMEs and/or their sheaths. Figure 6 shows the difference in profiles of two different types of
386 magnetic storms. The profile of a CIR magnetic storm is shown on the bottom and that of a shock
387 sheath ahead of an ICME MC magnetic storm on top.

388

389 The ICME MC magnetic storm Dst profile, discussed briefly earlier (see Figure 3), is reasonably
390 easy to identify (top panel). There is a sudden, ~tens of second duration positive increase in Dst
391 which is caused by the sudden increase in solar wind ram pressure caused by the passage of the
392 sheath high density jump downstream of the shock. This compresses the magnetosphere, creating
393 the sudden impulse (SI⁺: see Joselyn and Tsurutani, 1990) detected everywhere on the ground
394 (Araki et al., 2009). Later, in either the sheath or the MC there may be a southward IMF which
395 causes the magnetic storm. If there is a southward component in the MC, it is usually smoothly



396 varying in intensity and direction. This leads to a smooth monochromatic storm main phase as
397 seen in the Dst index (and illustrated in the Figure 6 (and Figure 3). The loss of the ring current
398 particles is the storm recovery phase. The details of storm recovery phase durations and causative
399 mechanisms will be an interesting topic for magnetospheric scientists to study in the near future.
400 The Arase mission data will be quite useful for these studies.

401

402 The bottom panel of Figure 6 shows the typical profile of a CIR magnetic storm. It is quite different
403 from a MC magnetic storm profile. There is no SI⁺ associated with the beginning of the
404 geomagnetic disturbance. This is because CIRs detected at 1 AU typically are not led by fast
405 forward shocks (Smith and Wolf, 1976; Tsurutani et al. 1995). The positive increase in Dst is
406 associated with the impact of a high density region near the heliospheric current sheet (HCS)
407 (Smith et al., 1978; Tsurutani et al. 2006a) called the heliospheric plasmashell (Winterhalter et al.,
408 1994) and/or associated with the compressed plasma at the leading edge of the CIR. These are
409 slow solar wind plasma densities. The most distinguishing feature of the CIR storm main phase is
410 the lack of smoothness, in sharp contrast to the MC magnetic storm. This irregular Dst storm main
411 phase is caused by large Bz fluctuations within the CIR.

412

413 CIR magnetic fields have magnitudes of ~20 to 30 nT and typically do not reach the much higher
414 magnetic field intensities that MC fields do. For this reason and also because of the Bz
415 fluctuations, CIR magnetic storms are typically have intensities Dst \geq -100 nT (smaller magnetic
416 storms). Extreme magnetic storms with Dst $<$ -250 nT caused by CIRs are rare, if they occur at
417 all (none found in the Meng et al. 2019 study). However it is clear that compound events involving
418 both CIRs and ICMEs could certainly cause extreme magnetic storm events.

419

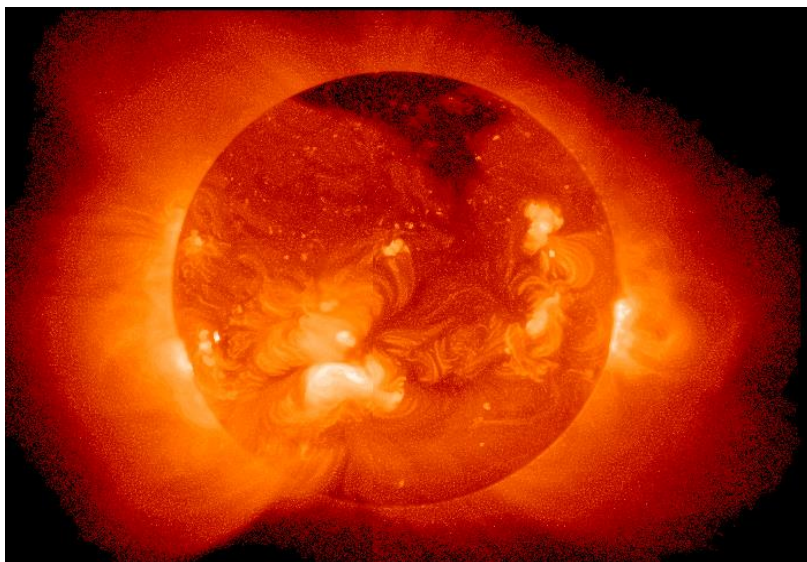
420 CIR related magnetic storms occur most frequently during the declining phase of the solar cycle
421 and ICME magnetic storms typically occur near the maximum phase of the solar cycle. However
422 have said that, it should be noted that both CIR storms and ICME MC magnetic storms can occur
423 during any phase of the solar cycle. We have simply ordered things by solar cycle so that it will
424 be easier to give the reader the general picture of space weather.

425

426 **3.2 Coronal Holes, High Speed Solar Wind Streams and Geomagnetic Activity**



427 3.2.1. Coronal holes and high speed solar wind streams



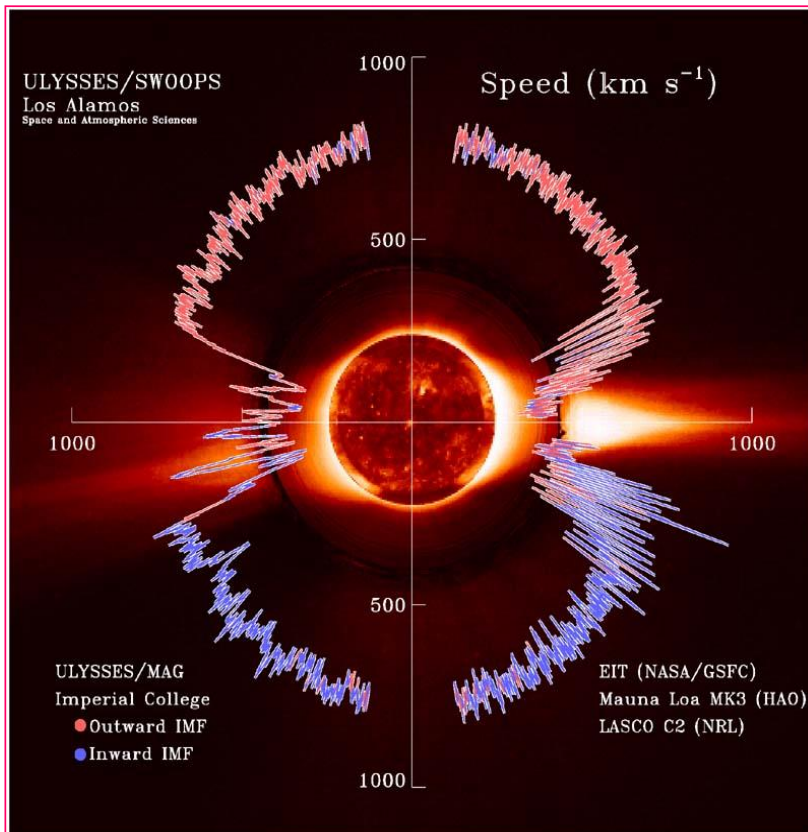
428

429 Figure 7. A giant polar coronal hole near the north pole of the Sun.

430

431 Figure 7 shows a polar coronal hole at the north pole of the Sun. This image was taken by Solar
432 Dynamic Observatory, NASA (<https://sdo.gsfc.nasa.gov/>) in soft x-rays showing the dark (low
433 temperature) region at the pole. Large polar coronal holes occur typically in the declining phase
434 of the solar cycle (Bravo and Otaola, 1989; Bravo and Stewart, 1997; Zhang et al., 2005).

435



436

437 Figure 8. High speed solar wind streams emanating from coronal holes in the north and south
438 solar poles. The figure was taken from Phillips et al. (1995) and McComas et al. (2002).

439

440 Figure 8 gives a “dial plot” of the solar wind speed for the first traversal of the Ulysses spacecraft
441 over the Sun’s poles. The radius from the center of the Sun to the trace indicates the solar wind
442 speed. The magnetic field polarity is indicated by the color of the trace, red for outward IMFs and
443 blue for inward IMFs. A SOHO EIT soft x-ray image of the Sun is placed at the center of the figure
444 and a High Altitude Observatory Mauna Loa coronagraph image is superposed onto the Figure.

445

446 Two large polar coronal holes are detected at the Sun, one at the north pole and the other at the
447 south pole. It is noted that HSSs of ~750 to 800 km/s are detected at Ulysses when over the polar
448 coronal hole regions. When Ulysses was near the solar equatorial region where helmet streamers
449 are present, the solar wind speeds are of the slow solar wind variety, $V_{sw} \sim 400$ km/s. The reader

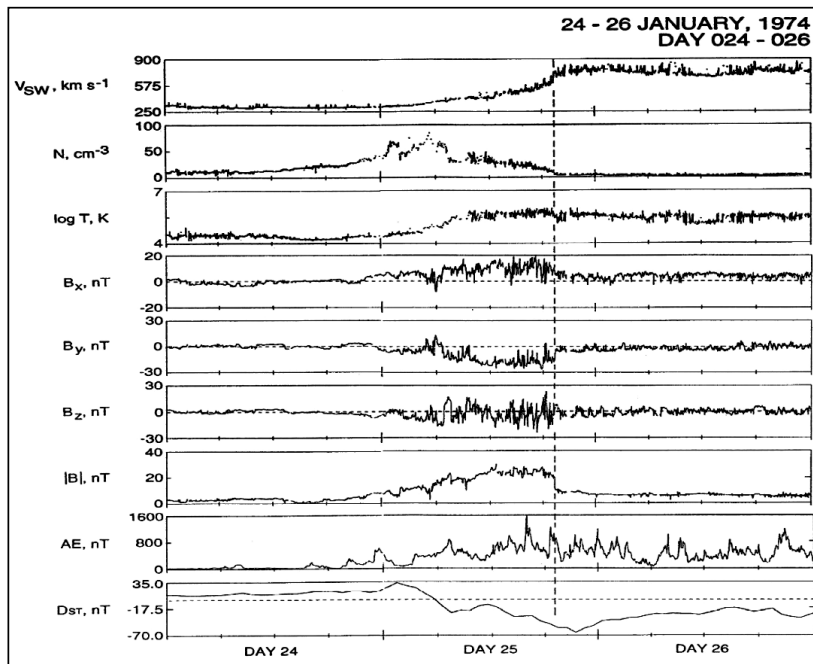


450 should note that it took years for Ulysses to make this polar orbit while the solar and coronal
451 images were taken at one point in time. However this composite figure is useful to illustrate the
452 main points about the origins of HSSs.

453

454 **3.2.2 High speed solar wind streams and the formation of CIRs**

455



456

457 Figure 9. A high speed solar wind stream-slow solar wind interaction and the formation of a CIR.
458 The format is the same as in Figure 4 except that the AE index is given in the next to bottom panel.
459 The figure is taken from Tsurutani et al. (2006a).

460

461 Figure 9 shows a HSS-slow speed stream interaction. The right portion of the top panel on day 26
462 shows a HSS with speeds of 750-800 km/s at 1 AU. On day 24, the top panel left indicates a solar
463 wind speed of ~300 km/s, or the slow solar wind. The effects of the stream-stream interaction
464 occurs on day 25. This is best seen in the IMF magnitude panel, 7th from the top. The stream-
465 stream interaction creates intense magnetic fields of ~25 nT. The 6th from the top panel is the IMF
466 Bz component (in GSM coordinates). The Bz is highly fluctuating. Magnetic reconnection



467 between the IMF southward components and the magnetopause magnetic fields leads to the
468 irregularly shaped storm main phase shown in the bottom (Dst) panel.

469

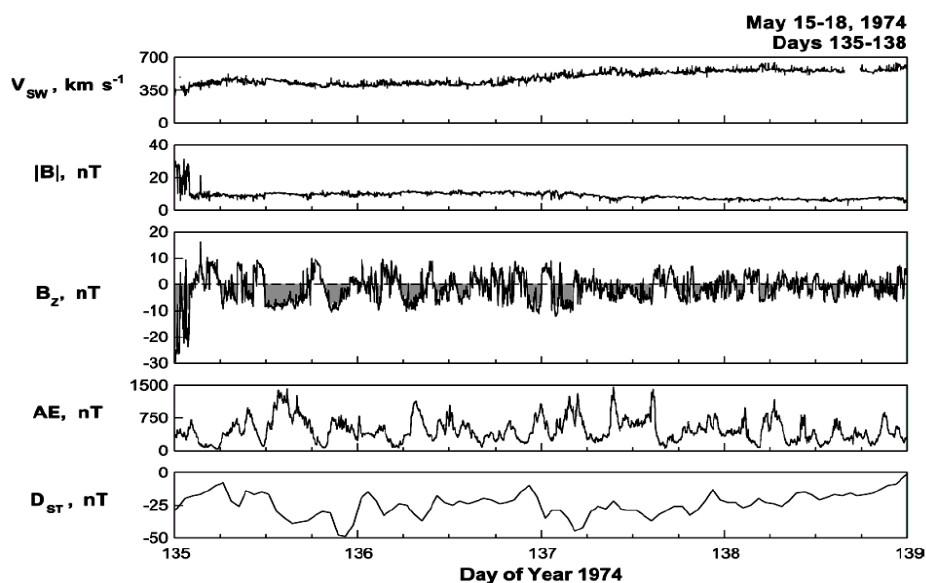
470 To be able to forecast a CIR magnetic storm, one would have to first understand the sources of the
471 IMF Bz fields. For example are they compressed upstream Alfvén waves (Tsurutani et al. 1995,
472 2006b)? Or could they be waves generated by the shock interaction with upstream waves in the
473 slow solar wind? That would be only the first step for forecasting, of course. Then with knowledge
474 of the properties of the slow speed stream, the details of the wave compression/interaction would
475 then have to be calculated/modeled.

476

477 Another approach would be to determine if there is an underlying southward component of the
478 IMF within the CIR. This would most likely be caused by the geometry of the HSS-slow speed
479 stream interaction and may be predictable from MHD modeling. If this is correct, then the wave
480 fluctuations can be modeled as being superposed on top of these dc magnetic fields. The Parker
481 Solar Probe, Solar Orbiter and ACE data could be useful in these endeavors.

482

483 3.2.3. High speed solar wind streams, Alfvén waves and HILDCAAs



484



485 Figure 10. A high-intensity, long-duration continuous AE activity (HILDCAA) event. Taken from
486 Tsurutani et al. (2006b).

487

488 The schematic in Figure 6 showed a long “recovery phase” that trails the CIR magnetic storm main
489 phase (see Tsurutani and Gonzalez, 1987 and Yermolaev et al. 2014 for a contrast in
490 interpretation). However we now know that the storm wasn’t “recovering” as in the case of an MC
491 magnetic storm but that something else was occurring. This “recovery” can last from days to
492 weeks. Thus processes of charge exchange, Coulomb collisions, etc. for particle losses are not
493 tenable to explain such long “recoveries”.

494

495 Figure 10 shows the interplanetary cause of this extended geomagnetic activity. It occurs primarily
496 during HSSs independent of whether a CIR magnetic storm occurred prior to it or not (Tsurutani
497 and Gonzalez, 1987; Tsurutani et al., 1995, 2006a; Kozyra et al. 2006b; Turner et al. 2006; Hajra
498 et al. 2013, 2014a, 2014b, 2014c, 2017). From top to bottom are the solar wind speed, the IMF
499 magnitude, the IMF B_z component (in GSM coordinates) and the auroral electrojet (AE) index.
500 The bottom panel is the Dst index.

501

502 The interplanetary data were taken from the IMP-8 spacecraft, an Earth orbiting satellite that was
503 located upstream of the magnetosphere in the solar wind at this time. The location was inside 40
504 Re, where an Re is an Earth radius. The magnetic B_z fluctuations have been shown to be Alfvén
505 waves which are of large nonlinear amplitudes in HSSs (Belcher and Davis, 1971; Tsurutani and
506 Gonzalez, 1987; Tsurutani et al., 2018b). What is apparent from this figure is that every time the
507 IMF B_z is negative (southward), there is an AE increase and a Dst decrease. This has been
508 interpreted as being due to magnetic reconnection between the southward components of the
509 Alfvén waves and the Earth magnetopause. The AE is enhanced by the same magnetic
510 reconnection process that occurs during substorms, and a small parcel of plasmasheet plasma is
511 injected into the nightside magnetosphere suppressing the Dst index slightly. It is noted that there
512 are many southward IMF B_z dips in this four day interval of data shown in Figure 10. There are
513 also many corresponding AE increases and Dst decreases. Thus the interpretation of the
514 constant/average Dst value of ~ -25 nT for four days is that continuous plasma injection and decay
515 is occurring. This is clearly not a “recovery phase” where the ring current particles are simply



516 lost, it only appears as a recovery from the Dst trace. Soraas et al. (2004) have shown that particles
517 are injected during these events but only to L values of 4 and greater. These are shallow injections
518 as suggested above.

519

520 These geomagnetic activity events have been named High-Intensity, Long-Duration Continuous
521 AE events or HILDCAAs (Tsurutani and Gonzalez, 1987). This is simply a description of the
522 events without an interpretation. In 2004 when a detailed examination using Polar EUV auroral
523 imaging was applied, it was found that many phenomena besides simple isolated substorms
524 occurred (Guarnieri, 2006; Guarnieri et al., 2006). Although substorms occur during HILDCAA
525 events, there are AE increases (injection events?) that are not well-correlated with substorm onsets
526 (Tsurutani et al., 2004b). The full extent of HILCAAs is not well understood (see also Souza et
527 al., 2016, 2018; Mendes et al., 2017). Data from SWARM, MMS and Arase could help answer
528 this question.

529

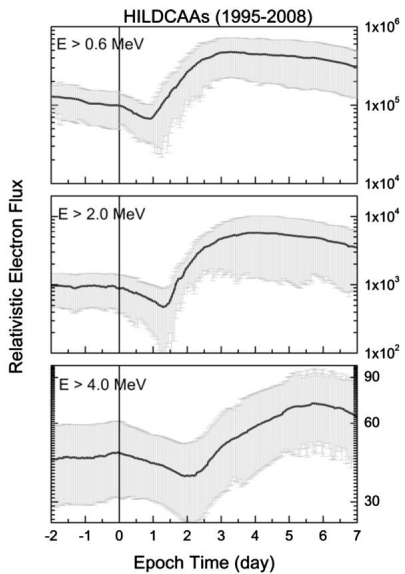
530 There is also the question of the origin of the interplanetary Alfvén waves? Do they originate at
531 the Sun caused by supergranular circulation, or is that mechanism untenable as argued by Hollweg
532 (2006)? Could the waves be generated locally between the Sun and Earth as speculated by Matteini
533 et al. (2006, 2007) and Hellinger and Travnicek (2008)? The Parker Solar Probe and Solar Orbiter
534 mission data could be useful in helping answer these questions.

535

536 The original requirement for identifying a HILCAA event was quite strict. The event had to occur
537 outside of a magnetic storm main phase (Dst was required to be > -50 nT: Gonzalez et al. 1994),
538 the peak AE intensity had to be greater than 1,000 nT (high-intensity), the event had to last longer
539 than 2 days (long-duration), and there could not be any dips in AE less than 200 nT for longer than
540 two hrs (continuous). Clearly there are HILDCAAs with the same interplanetary causes and
541 geomagnetic effects as for the strict definition. However the strict definition is useful for further
542 studies using different data sets.

543

544 **3.2.4. HILDCAAs and the Acceleration of Relativistic Magnetospheric Electrons**



545

546 Figure 11. The relationship between HILDCAAs and relativistic electron acceleration. The figure
547 is from Hajra et al. (2015a).

548

549 One of the consequences of HSSs and HILDCAAs is the acceleration of relativistic electrons.
550 These energetic particles can damage orbiting satellite electronic components (Wrenn, 1995).
551 Figure 11 shows the relationship between the onset of HILCAA events (vertical line) and
552 relativistic electron fluxes. From top to bottom are the $E > 0.6$ MeV, the $E > 2.0$ MeV and the E
553 > 4.0 MeV electrons detected by the GOES-8 and GOES-12 satellites located at $L = 6.6$. This
554 figure is a superposed epoch analysis (Chree, 1913) result of all of the HILDCAA events in solar
555 cycle 23 which are not preceded by magnetic storms. This was done to avoid contamination by
556 storm-time particle acceleration. The zero epoch time (vertical line) corresponds to the HILDCAA
557 onset time. Here the “strict” definition of HILDCAAs was used to define the onset times.

558

559 The figure shows that the appearance of $E > 0.6$ MeV electrons is statistically delayed by ~ 1.0 day
560 from the onset of the HILDCAAs. The $E > 4.0$ MeV electrons are statistically delayed by ~ 2.0
561 days from the HILDCAA onset. It is thus possible that HILCAAs may be used to forecast
562 relativistic electron enhancements in the magnetosphere (see Hajra et al., 2015b; Tsurutani et al.,
563 2016a; Hajra and Tsurutani, 2018a; Guarneri et al., 2018). This however has not been done yet
564 and could be implemented by scientists today.



565

566 The physics for the electron acceleration has been well-developed by magnetospheric scientists.
567 Two competing acceleration mechanisms have been developed. In one mechanism, with each
568 injection of plasmashell particles on the nightside magnetosphere, the anisotropic ~10 to 100 keV
569 electrons generate electromagnetic whistler mode chorus waves (Tsurutani and Smith, 1974;
570 Meredith et al. 2002) by the loss cone/temperature anisotropy instability (Brice, 1964; Kennel and
571 Petschek, 1966; Tsurutani et al., 1979; Tsurutani and Lakhina, 1997). The chorus then interacts
572 with the ~100 keV injected electrons to energize them to ~0.6 MeV energies (Inan et al., 1978;
573 Horne and Thorne, 1998; Thorne et al., 2005, 2013; Summers et al., 2007; Tsurutani et al., 2010;
574 Reeves et al., 2013; Boyd et al., 2014). The lower-frequency part of the chorus in turn interact
575 with the ~0.6 MeV electrons to accelerate them to ~2.0 MeV energies, etc. This bootstrapping
576 mechanism has been suggested by several authors (Baker et al., 1979, 1998; Li et al., 2005; Turner
577 and Li, 2008; Boyd et al., 2014, 2016; Reeves et al., 2016).

578

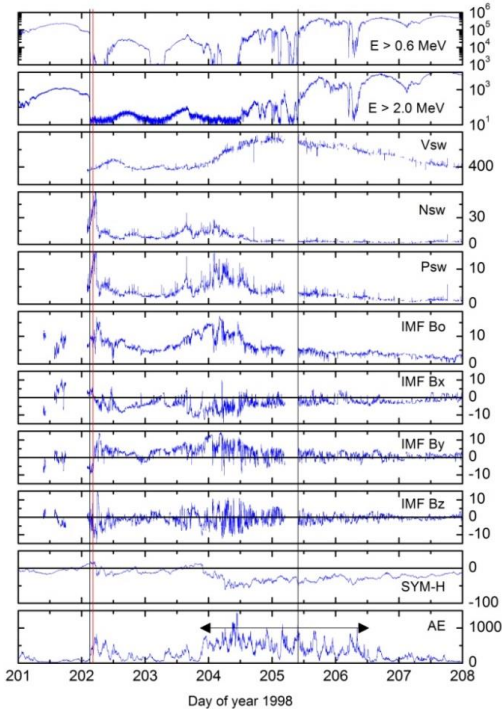
579 An alternative scenario is that relativistic electrons are created through particle radial diffusion
580 driven by micropulsations (Elkington et al., 1999, 2003; Hudson et al., 1999; Li et al., 2001, O'Brien et
581 al., 2001; Mann et al., 2004; Miyoshi et al., 2004). However the same general scenario would hold as for
582 chorus acceleration. The substorms and convection events within HILDCAAs would be the sources for the
583 micropulsations and the micropulsations would last from days to weeks in duration. Bootstrapping of
584 energy would still take place.

585

586 A few important questions for researchers are: "How high can the relativistic magnetospheric
587 electron energy get?". If there are two HSSs, one from the south pole and another from the north
588 pole so that Earth's magnetosphere is bathed in HSSs for years, as happened during 1973-1975
589 (Sheeley et al., 1976, 1977; Gosling et al. 1976; Tsurutani et al. 1995), will the energies go above
590 ~10 MeV? What will physically limit the energy range? This is important for keeping Earth-
591 orbiting satellites safe during such events.

592

593 **3.2.5. Solar wind ram pressure pulses and the loss of relativistic electrons**



594

595 Figure 12. A relativistic electron decrease (RED) event and later acceleration. Taken from
596 Tsurutani et al. (2016b).

597

598 Figure 12 shows a relativistic electron decrease (RED) event. From top to bottom are the $E > 0.6$
599 MeV electron fluxes, the $E > 2.0$ MeV electron fluxes, the solar wind speed, density and ram
600 pressure, and the IMF magnitude, B_x , B_y and B_z component in the GSM coordinate system. The
601 bottom two panels are the 1 min SYM-H index (think of this as a high resolution Dst index:
602 Wanliss and Showalter, 2006) and the AE index. The relativistic electron measurements were
603 taken at $L = 6.6$.

604

605 At the beginning of day 202, a vertical black line indicates the onset of a high density heliospheric
606 plasmashell (HPS: Winterhalter et al., 1994) that is identified in the fourth panel from the top. The
607 HPS is by definition located adjacent to the HCS (Smith et al. 1978). The HCS is noted by the
608 reversal in the signs of the IMF B_x and B_y components (seventh and eighth panels from the top).
609 The onset of the HPS is followed within one hr by the vertical red line, the sudden disappearance



610 of the $E > 0.6$ MeV (first panel) and $E > 2.0$ MeV (second panel) relativistic electrons. Tsurutani
611 et al. (2016b) has shown that for 8 relativistic electron disappearance events during solar cycle 23
612 all of the disappearances were associated with HPS impingements onto the magnetosphere.

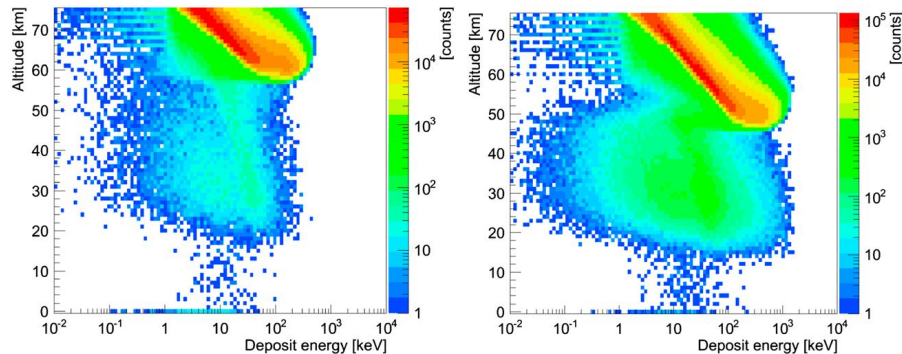
613

614 Where have the relativistic electrons gone? There are two primary possibilities. One is that the
615 energetic electrons have gradient drifted out of the magnetosphere through the dayside
616 magnetopause, a feature that has been called “magnetopause shadowing” by West et al. (1972).
617 However a second possible mechanism is electron pitch angle scattering by electromagnetic ion
618 cyclotron (EMIC) waves. We think that this second possibility is more intriguing and has far more
619 interesting consequences, if correct. One might ask where the EMIC waves come from and why is
620 pitch angle scattering particularly important? It has been shown by Remya et al. (2015) that when
621 the magnetosphere is compressed, both electromagnetic chorus (electron) waves (Thorne et al.,
622 1974; Tsurutani and Smith, 1974; Meredith et al. 2002) and EMIC (ion) waves (Cornwall, 1965;
623 Kennel and Petschek, 1966; Olsen and Lee, 1983; Anderson and Hamilton, 1993; Engebretson et
624 al., 2002; Halford et al. 2010; Usanova, 2012; Saikin, 2016) are generated. The compression of
625 the magnetosphere causes betatron acceleration of remnant \sim 10 to 100 keV electrons and protons,
626 and thus plasma instabilities associated with both particle populations occur. What is particularly
627 important is that the EMIC waves are coherent (Remya et al., 2015), leading to extremely rapid
628 pitch angle scattering of \sim 1 MeV electrons by the waves. The scattering rate has been shown to
629 be three orders of magnitude faster than that with incoherent waves (Tsurutani et al., 2016b).

630

631 Another possible loss mechanism is associated with possible generation of PC waves by the HPS
632 impingement followed by radial diffusion of the relativistic electrons. Wygant et al. (1998) and
633 Halford et al. (2015) have mentioned that larger loss cone sizes at lower L could be a source of
634 loss to the ionosphere. Rae et al. (2018) has shown that superposition of compressional PC waves
635 and the conservation of the first two adiabatic invariants could enhance particle losses. However
636 one should mention that there are not observations of PC wave generation during HPS
637 impingements and this needs to be tested. It is also uncertain how rapidly the relativistic electrons
638 would be lost by the above processes. It has been shown that the total loss of $L > 6.6$ relativistic
639 electrons occurs in \sim 1 hr (Tsurutani et al., 2016b).

640



641

642 Figure 13. The GEANT4 code runs for the precipitation of $E > 0.6$ MeV electrons (left panel) and
643 $E > 2.0$ MeV electrons. The vertical scale is altitude above the ground and the horizontal scale is
644 energy deposition. The color scheme gives the amount of counts. Taken from Tsurutani et al.
645 (2016b).

646

647 Why can the loss of relativistic electrons to the atmosphere be important? Figure 13 shows the
648 results of the GEometry ANd Tracking 4 (GEANT4) code developed by the European
649 Organization for Nuclear Research (Agostinelli et al., 2003) applied to the relativistic electron
650 disappearance problem. The GEANT4 code takes into account Rayleigh scattering, Compton
651 scattering, photon absorption, gamma ray pair production, multiple scattering, ionization,
652 bremsstrahlung for electrons and positrons and annihilation of positrons (positron formation is not
653 germane for these “low energy” relativistic particles, but the code includes it anyway). A standard
654 atmosphere was used.

655

656 Figure 13 shows the GEANT4 Monte Carlo results for the electron shower for $E > 0.6$ MeV
657 electrons on the left and for $E > 2.0$ MeV electrons on the right. Two important features should be
658 noticed. First the bulk of energy deposition (the red areas) go down to ~ 60 km for the $E > 0.6$
659 MeV electron simulation and down to ~ 50 km for the $E > 2.0$ MeV electron simulation. This
660 portion of the energy from the incident electrons is due to direct ionization and particle energy
661 cascading. However there is a second region which might be extremely important. That is the
662 blue-green area that goes down to ~ 20 km for the $E > 0.6$ MeV simulation and ~ 16 km for the $E >$
663 2.0 MeV simulation. There are also “hits” seen on the ground. This lower altitude energy
664 deposition is due to the relativistic electrons interacting with atmospheric atomic and molecular



665 nuclei creating bremsstrahlung X-rays and γ -rays. X-rays and γ -rays have very large mean free
666 paths and thus can freely propagate through the dense atmosphere without interactions. They
667 propagate to much lower altitudes where they interact and have energy cascading again.

668

669 The reason why this process may be quite an important space weather topic is that it might relate
670 to atmospheric weather as well. Wilcox et al. (1973) discovered a correlation between
671 interplanetary HCS crossings and high atmospheric vorticity winds at 300 mb altitude. Over the
672 years a number of different explanations for the physics of the trigger has been offered (Tinsley
673 and Deen, 1991; Lam et al., 2013). Tsurutani et al. (2016) presented the above relativistic electron
674 dumping scenario (instead of HCS crossings) for the possible triggers of high atmospheric vorticity
675 winds. Quantitative estimates of potential energy deposition at different atmospheric altitudes
676 were provided in the original paper.

677

678 It is noted that the energy deposition should occur in a limited spatial region of the globe (just
679 inside the auroral zone and a small region of the dayside atmosphere) which is more geoeffective
680 than either cosmic ray energy or solar flare particle deposition. The fact that it is electron
681 precipitation gives an additional advantage that substantial energy is deposited at quite low
682 altitudes.

683

684 Advances to this problem can be made in a number of different ways. Simultaneous ground-
685 detected EMIC waves, γ -rays and atmospheric heating could be sought. Correlation with such
686 events with solar wind pressure pulses like the HPSs or interplanetary shocks (see Hajra and
687 Tsurutani, 2018b) would advance our knowledge of the details of such events.

688

689 Atmospheric heating events known as Sudden Stratospheric Warnings (SSWs) (Scherhag, 1960;
690 Harada et al., 2010) occur at subauroral latitudes by unknown causes. They are known to be related
691 to atmospheric wind system changes, perhaps the same phenomenon as the Wilcox et al. (1973)
692 effect. Atmospheric scientists generally assume that SSWs are created by gravity waves
693 propagating from lower atmosphere upward, but so far no one-to-one correlated case has been
694 found. Thus it would be quite interesting to see if space weather can have a major impact on

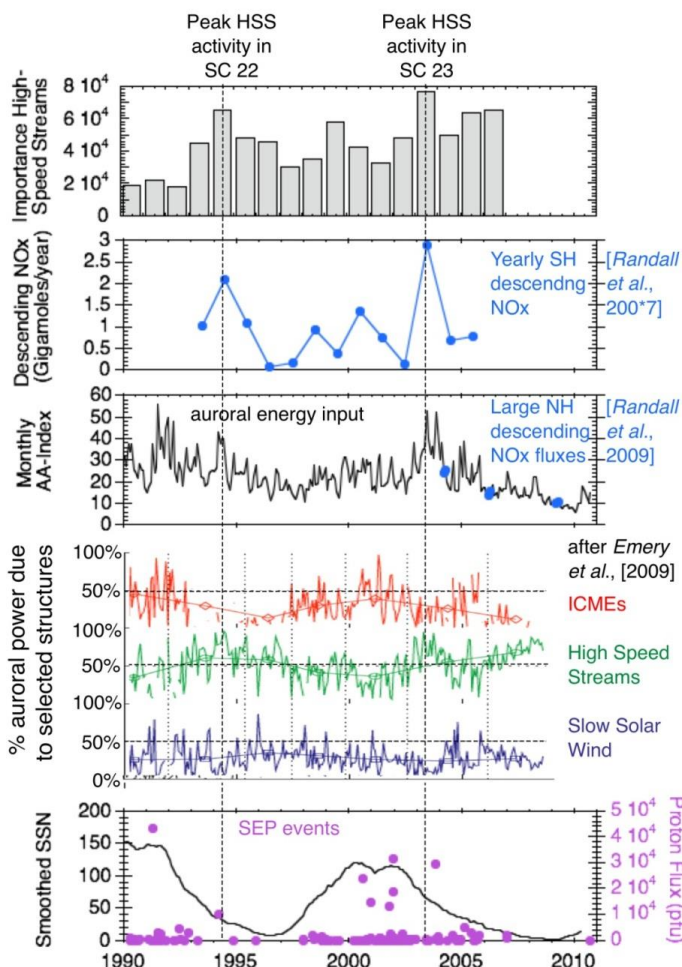


695 atmospheric weather. The connection between these two disciplines will be quite interesting for
696 the next generation of space weather scientists.

697

698 3.2.6. Energetic particle precipitation and ozone depletion

699



700
701 Figure 14. The dashed vertical lines show the peaks in solar wind high speed streams during SC
702 22 and SC23. These are coincident with the peaks in auroral energy input and the peaks in yearly
703 NOx descent. We thank J.U. Kozyra for this unpublished figure.

704

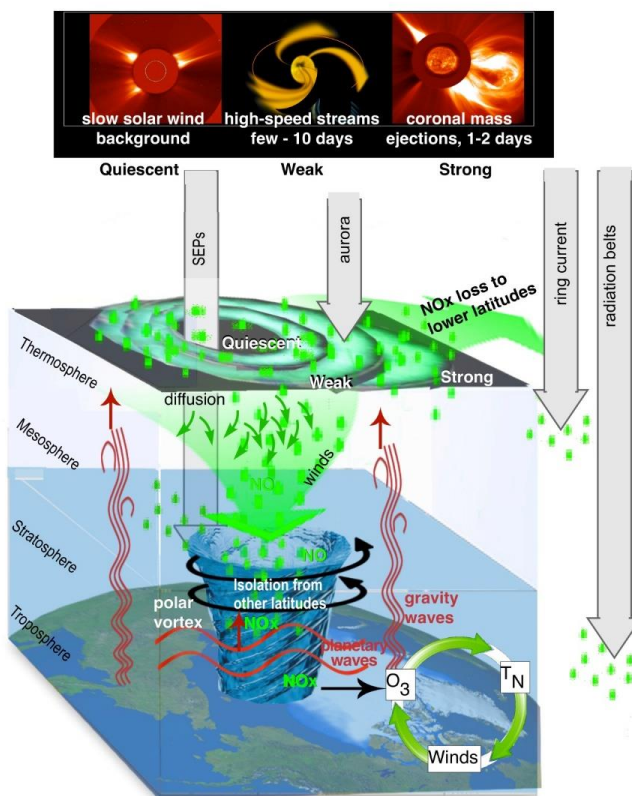


705 Figure 14 shows two solar cycles of data, SC22 and SC23. From top to bottom are the
706 “importance” of high speed streams, the descending NO_x, the monthly AA index, the percent
707 auroral power due to three types of solar wind phenomena (ICMEs, HSSs and slow solar wind),
708 and the bottom panel solid line trace is the sunspot number (SSN). Also shown in the bottom panel
709 is the solar energetic particle (SEP) flux.

710

711 There are two vertical dashed lines. They correspond to the peaks in HSS activity for SC22 and
712 SC23 (top panel), peaks in auroral energy input (third panel from the top), and peaks in the yearly
713 descending NO_x (second panel from the top). It is noted that all three peaks are aligned in time.
714 The bottom panel shows that both dashed vertical lines correspond to times in the descending
715 phase of the solar cycle.

716



717



718 Figure 15. The scenario for polar cap ozone destruction using the observations shown in Figure
719 27. We thank J.U. Kozyra and her colleagues for this unpublished figure.

720

721 Figure 15 shows the Kozyra et al. (2015) scenario for ozone destruction over the polar cap. The
722 top of the Figure shows the various types of solar wind that can affect atmospheric ozone. The
723 quiet solar wind will lead to quiescence. HSSs lasting a few to ten days have weak effects and
724 ICMEs (and of course shock acceleration of energy particles) can have much strong effects.

725

726 The energetic particles associated with HILDCAAs and interplanetary shock acceleration will be
727 deposited in the near-polar regions of the both the north and south ionospheres. Particles from
728 HILDCAA events will deposit their energy on closed auroral zone ($\sim 60^\circ$ to 70°) magnetic field
729 lines. Solar energetic particles from interplanetary ICME shocks can propagate down the open
730 magnetic field lines of the polar caps. If the particles are energetic enough with sufficient gyroradii,
731 they can reach to as low latitudes as $\sim 50^\circ$ magnetic latitude.

732

733 The energetic particle entering the atmosphere lose a portion of their energy in the dissociation of
734 N^2 into $N + N$. The nitrogen atoms will attach to oxygen atoms to form NOx. Auroral HILDCAA
735 ~ 10 -100 kev energy particles will only penetrate to depths of ~ 75 km above the surface of the
736 Earth. Solar energetic particles with greater kinetic energies can penetrate lower into the
737 atmosphere to ~ 50 to 60 km. If there is a polar vortex, this vortex can “entrain” the NOx molecules
738 and atmospheric diffusion can bring them down to lower altitudes over months time duration. The
739 NOx can act as a catalyst in the destruction of ozone.

740

741 One interesting consequence of extreme ICME shocks is that one would expect extreme Mach
742 numbers to lead to both extreme SEP fluences and also extremely high energies. The former will
743 lead to greater production of NOx at the polar regions and the latter to deeper penetration and thus
744 less loss of NOx as they diffuse downward. Alternatively there is a scenario where radiation belt
745 “killer” relativistic electrons can play an important role. If there are large solar polar coronal holes
746 like in 1973-1975, HSSs could produce extremely intense and energetic relativistic electrons.
747 Shocks and HPS impingements on the magnetosphere could cause loss of the electrons to the lower
748 atmosphere. This magnetospheric energy pumping and dumping may have important



749 consequences for NO_x production. The topic of shock acceleration of energetic particles will be
750 discussed in more details in Section 4.1.

751

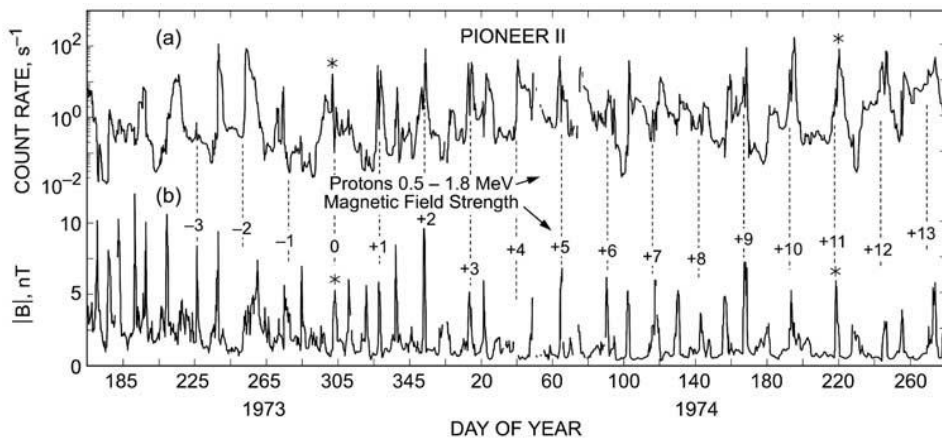
752 4.0. RESULTS: Interplanetary Shocks

753 4.1. Interplanetary Shocks and Energetic Charged Particle Acceleration

754

755 Interplanetary shocks have a variety of effects both in interplanetary space and the Earth's
756 magnetosphere. It is important for the reader to note that these space weather phenomena can occur
757 with or without the occurrence of magnetic storms. Shock and magnetic storm intensities are
758 related but only in a loose sense. The physical mechanism for energy transfer for different
759 phenomena is different. As one example, interplanetary shock acceleration of energetic charged
760 particles (called "solar cosmic rays") are due to an ICME ram energy driving the fast shocks which
761 then transfers energy to the charged particles. Solar cosmic ray events can occur with or without
762 magnetic storms (Halford et al. 2015, 2016; Mays et al., 2015; Foster et al. 2015). Some of the
763 major extreme space weather topics will be addressed below.

764



765

766 Figure 16. Energetic ~0.5 to 1.8 MeV protons accelerated by interplanetary fast forward and fast
767 reverse shocks. Taken from Tsurutani et al. (1982).

768

769 Acceleration of energetic particles in deep space was discovered by Pioneer 11 energetic particle
770 scientists (McDonald et al., 1976; Barnes and Simpson, 1976; Pesses et al., 1978, 1979; Van



771 Hollebeke et al., 1978; Christon and Simpson, 1979). As the Pioneer 11 spacecraft traveled away
772 from the Sun, it was found that the particle fluences kept increasing, contrary to the concept of
773 adiabatic deceleration. The interplanetary magnetic field magnitude decreases with increasing
774 distance from the Sun, so one would expect energetic particle deceleration with distance. Thus it
775 was clear to scientists that something must be accelerating these particles in the interplanetary
776 medium. Figure 16 shows one channel of the Pioneer 11 energetic proton count rate, ~0.5 to 1.8
777 MeV (see Simpson et al., 1974) The bottom panel is the Pioneer 11 magnetic field (Smith et al.,
778 1975). Some of the peak magnetic fields are numbered, corresponding to a ~25 day recurrence of
779 these magnetic structures. The magnetic magnitude structures are identified as well-developed
780 CIRs (see Smith and Wolfe, 1976), bounded by fast forward and fast reverse shocks.

781

782 Tsurutani et al. (1982) identified the shocks and showed statistically that both forward and reverse
783 shocks were related to proton peak count rates. One of the results, which still remains to be solved,
784 is that the proton peaks were generally higher at the reverse shocks. What is the mechanism for
785 greater particle acceleration at fast reverse shocks? This has received little attention and should be
786 addressed in the future.

787

788 Reames (1999) has argued that fast forward shocks upstream (anti-solarward) of ICMEs are the
789 most important component of “solar flare” particle events. Particle acceleration occurs throughout
790 interplanetary space from near the Sun (where the shocks first form) to 1 AU and beyond as the
791 shocks propagate through the heliosphere. Studies of this acceleration as a function of longitudinal
792 distance away from magnetic connection to the flare site (this gives the variations in the shock
793 normal angle and thus dominant mechanism for acceleration—see Lee (2017) and references
794 therein) have been done by Lario (2012). The features of the energetic particles in space have
795 different characteristics depending on these distances and the portion of the shock that the particles
796 are being accelerated from.

797

798 Forecasting the solar flare/interplanetary shock features such as the fluence, energy, spectra and
799 composition will require knowledge of the upstream seed population, upstream (and downstream)
800 waves, and shock properties such as the magnetosonic Mach number and shock normal angle.
801 This is a very difficult task since knowledge of the entire slow solar wind plasma from the Sun to



802 1 AU will be required for accurate forecasting. But again, the Parker Solar Probe and Solar Orbiter
803 may help in developing two points of measurements for modeling of specific events.

804

805 A more fundamental problem that can be answered by the Parker Solar Probe, Solar Orbiter and
806 ACE is why are interplanetary fast forward shock Mach numbers so low? As previously
807 mentioned, Tsurutani and Lin (1985) from ISEE-3 measurements have found that at 1 AU, the
808 measured magnetosonic Mach numbers were typically only 1 to 3. Tsurutani et al (2014) have
809 identified a shock with Mach number ~9 and Riley et al. (2016) has identified an event with
810 magnetosonic Mach number ~28. The latter event was associated with the SOHO 2012 extreme
811 ICME which did not impact the Earth's magnetosphere. The above are extreme events and little
812 or no events have been detected with intermediate values.

813

814 **4.2. Extreme Interplanetary Shocks and Extreme Interplanetary Energetic Particle
815 Acceleration**

816 Tsurutani and Lakhina (2014) have shown from simple calculations that with CME observed
817 speeds of 3,000 km/s (Yashiro et al., 2004; Gopalswamy, 2011), shock Mach numbers of ~45 are
818 possible. These Mach numbers are getting close to supernova shock numbers. Why haven't such
819 strong shocks been observed at 1 AU? If such events are possible, what would the energetic particle
820 fluences be? Experts on shock particle acceleration will hopefully answer this complex question.
821 It is well known that such solar flare particles enter the polar regions of the Earth's atmosphere
822 and cause radio blackouts. Will extreme solar flare particle fluence precipitation cause different
823 ionospheric effects other than those known today? This latter question might be addressed by
824 ionospheric modelers.

825

826 It should be noted that although space weather is a chain of events/phenomena going from the Sun
827 to interplanetary space to the magnetosphere, ionosphere and atmosphere, there is often not a direct
828 link between different facets of space weather. Each feature of space weather should be examined
829 separately and it should not be assumed that an extreme flare will cause extreme cascading space
830 weather phenomena. We use solar flare particles as an example for the readership. The largest
831 solar flare particle event in the space age occurred in August 1972 (Dryer et al., 1976 and
832 references therein). However there was no magnetic storm caused by the MC impact onto the



833 Earth's magnetosphere (the MC field direction was entirely northward, leading to geomagnetic
834 quiet: Tsurutani et al. 1992b). On the other hand, the largest magnetic storm on record is the
835 "Carrington" storm. The storm intensity will be discussed further in Section 7.0. There is little or
836 no evidence of large solar flare particle fluences in Greenland ice core data from that event (Wolff
837 et al., 2012; Schrijver et al., 2012). Usoskin and Kovfaltsov (2012) examining historical proxy
838 data (^{14}C and ^{10}Be) also find a lack of any signature associated with the Carrington flare. Although
839 this is an extreme example, it is useful to mention it to illustrate the point.

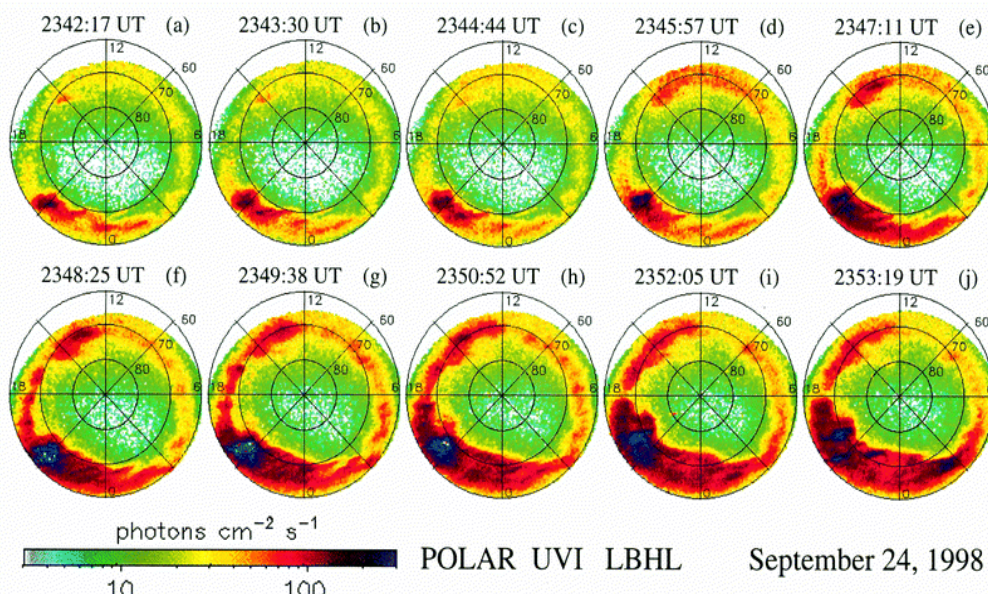
840

841 An area that has received a lot of attention lately is ancient solar flares. Miyake et al. (2012)
842 discovered an anomalous 12% rapid increase in ^{14}C content from 774 to 775 AD in Japanese cedar
843 tree rings. Usoskin et al. (2013) have argued that such an extreme radiation event could be
844 associated with an extreme solar energetic particle event (or a sequence of events). The latter
845 authors estimate the fluence of > 30 MeV particles was about $4.5 \times 10^{10} \text{ cm}^{-2}$. Could such an
846 extreme particle event be associated with an extremely strong interplanetary shock or series of
847 shocks? Space weather scientists are currently working on this problem.

848

849 4.3. Interplanetary shocks, dayside aurora and nightside substorms

850



851



852 Figure 17. Interplanetary shocks cause dayside auroras and trigger nightside substorms. Northern
853 polar views of polar cap and auroral zones taken in UV wavelengths. Figure is taken from Zhou
854 and Tsurutani (2001).

855

856 Interplanetary shocks can trigger the precipitation of energetic ~10 to 100 keV electrons into the
857 auroral ionosphere (Halford et al. 2015). In fact, low energy ($E < 10$ keV) electron precipitation
858 can occur as well. Figure 17 show interplanetary shock impingement auroral UV effects for an
859 event on September 23, 1998. Each image has the north pole at the center and 60° magnetic
860 latitude (MLAT) shown at the outer edge. Noon is at the top and dawn is at the right. The cadence
861 between images is ~1min 13 s. From ACE measurements and propagation calculations it is known
862 that the fast forward shock arrived the magnetosphere between the images c), 2344:44 UT and d),
863 2345:47 UT. What is apparent in panel d) is the sudden appearance of aurora on the dayside (Zhou
864 and Tsurutani et al., 1999). From further analyses of these shock auroral events, Zhou et al. (2003)
865 has shown that magnetospheric compression of preexisting ~10 to 100 keV electrons and protons
866 will generate both electromagnetic electron and proton plasma waves and diffuse auroras (as
867 discussed previously). Also noted were the generation of field-aligned dayside currents.
868 Compression of the magnetosphere will generate Alfvén waves (Haerendel, 1994) which will
869 propagate along the magnetic fields lines down to the ionosphere. Wave damping could provide
870 substantial ionospheric heating.

871

872 The mechanism for energy transfer from the solar wind to the magnetosphere is the absorption of
873 the solar wind ram energy. Dayside auroras occur with shock impingement irrespective of the
874 interplanetary magnetic field B_z direction. Another possible mechanism for the dayside aurora
875 not mentioned above are double layers above the ionosphere (Carlson et al., 1998) with the
876 acceleration of ~1 to 10 keV electrons and the formation of discrete dayside auroras. What is the
877 relative importance of these three different auroral energy mechanisms? This would be an
878 excellent topic for the SWARM and Arase satellite missions. Coordinated ground measurements
879 would be useful.

880

881 Returning back to Figure 17 panel e) 2347:11UT, there is a substorm intensification centered at
882 ~2100 magnetic local time (MLT). The substorm further intensification and expansion can be



883 noted in the sequence of images. Interplanetary shock triggering of substorms has been known to
884 occur before the advent of imaging polar orbiting spacecraft (Heppner, 1955; Akasofu and Chao,
885 1980). The AE index had been used to identify these events.

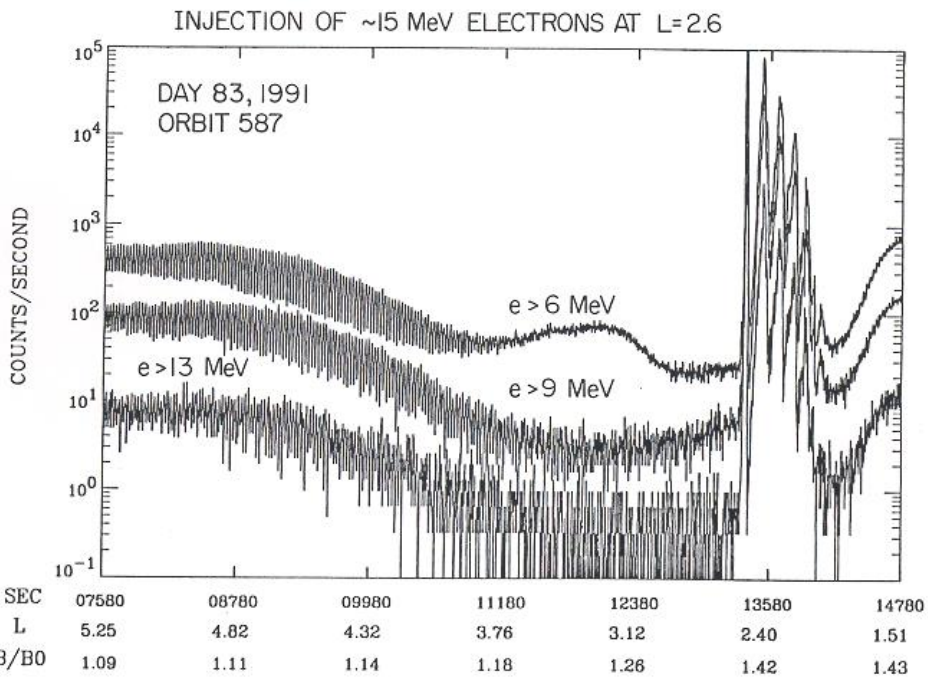
886

887 Important topics are be where in the tail/magnetosphere does the substorm get initiated and by
888 what physical mechanism? Is it reconnection or plasma instabilities (Akasofu, 1972; Hones, 1979;
889 Lui et al., 1991; Lui, 1996; Baker et al., 1996; Lakhina, 2000)? Where does the energy come
890 from, recent solar wind inputs as suggested by Zhou and Tsurutani (1999) or stored tail energy or
891 even possibly solar wind ram energy (see Hajra and Tsurutani, 2018b)? The rapid response of the
892 magnetosphere to the shock should limit the downstream location of the substorm initiation point.
893 It should be noted that there are probably several different mechanisms for causing substorms.
894 Although this is only the shock triggering case, knowledge of this may help understand other cases.
895 The MMS mission will be ideally suited for addressing this question in the tail phase of the
896 mission.

897

898 **4.4. Interplanetary shocks and the formation of new radiation belts**

899



901 Figure 18. Shock creation of a new radiation belt in the magnetosphere. Figure taken from Blake
902 et al. (1992).

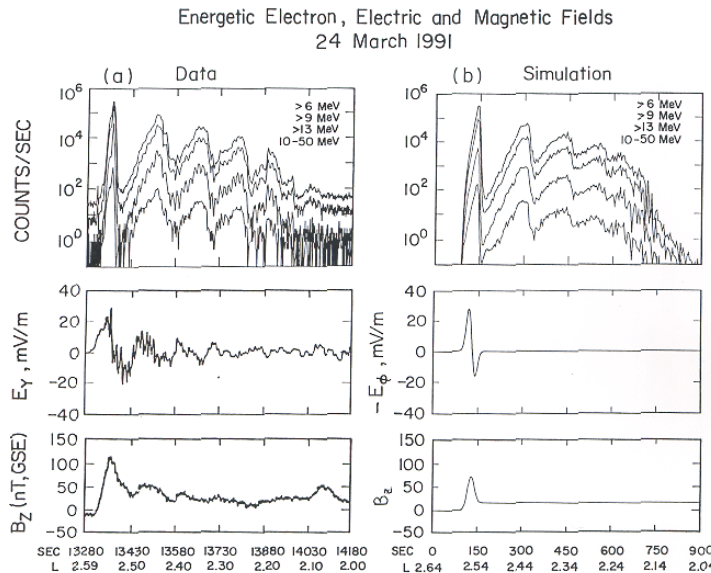
903

904 Figure 18 shows evidence of a new “radiation belt” triggered by a strong interplanetary shock. The
905 Figure shows three traces, $E > 6$ MeV, > 9 MeV and > 13 MeV fluences. At the time of the strong
906 increase in all energy fluxes, the spacecraft was at $L = 2.6$. With increasing time, a second, then
907 third, etc., pulse appear. These are “drift echos” where the energetic electrons gradient drift around
908 the magnetosphere to return to the initial location.

909

910 4.4.1. What is the mechanism to create this new radiation belt?

911



912

913 Figure 19. An expanded version of the relativistic electron pulse and measured magnetospheric
914 electric field and magnetic field Bz on the left and simulation results on the right. Taken from Li
915 et al. (2003).

916

917 The left hand column of Figure 19 show an expanded version of Figure 16 on the top with the
918 addition of the ~10 to 50 MeV count rate channel included. Next is the d.c. electric field in the Y
919 direction, and magnetospheric Bz on the bottom. The right hand column bottom shows a magnetic
920 pulse input into the system. This generates a time varying azimuthal electric field (right middle)
921 and the relativistic electron flux at the top right.

922

923 Using the input of a single magnetospheric magnetic pulse into the magnetosphere, Li et al. (2003)
924 simulated the acceleration and injection of $E > 40$ MeV electrons. What is interesting is that the
925 origin of the electrons was $L > 6$ with energies of only a few MeV. The reader should read Li et
926 al. (2003) for more details of the simulation and the results. Related works on acceleration of
927 magnetospheric electrons by shock impact on the magnetosphere can be found in Wygant et al.
928 (1994), Kellerman and Shprits, 2012; Kellerman et al., 2014; Foster et al. (2015).

929

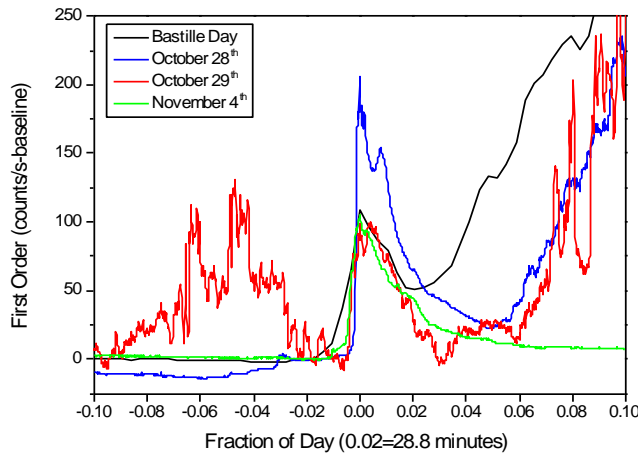


930 How strong was the interplanetary shock? At this time it is because there were not any spacecraft
931 upstream of the Earth at the time of the event. However Araki (2014) has noted that this shock
932 caused a SI^+ of magnitude 202 nT. This is the second largest SI^+ in recorded history. In Tsurutani
933 and Lakhina (2014) with the assumption of a 3,000 km/s CME and only a 10% deceleration from
934 the Sun to 1 AU, they estimated a maximum SI^+ of 234 nT under normal conditions. Could this
935 1991 shock may have been close to the $M = 45$ estimate mentioned earlier? However one cannot
936 really tell because the shock number strongly depends on the upstream plasma conditions which
937 can only be estimated. Also Tsurutani and Lakhina (2014) estimated a dB/dt six times larger than
938 the one used in the Li et al. (2003) modeling. What would a maximum dB/dt cause in a new
939 radiation belt formation?

940

941 5.0. RESULTS: Solar Flares and Ionospheric Total Electron Content

942



943

944 Figure 20. The largest solar EUV flare in recorded history, October 28, 2003. Taken from
945 Tsurutani et al. (2005b).

946

947 Figure 18 shows four well-recognized solar X-ray flare events but taken in a narrow band 26-34
948 nm EUV spectrum. This was done because some of the flare X-ray and EUV fluxes were so
949 intense that most spacecraft detectors became saturated (all except the SOHO SEM narrowband



950 EUV detector). The flare intensities could only be estimated from fitting techniques for the
951 saturated data. Here we use the narrow band channel of the SOHO SEM detector where the four
952 above flares were not saturated. The four flare intensity profiles are the Bastille day (July 14,
953 2000) flare and three “Halloween” flares occurring on October 28, 29 and November 4, 2003. The
954 four flare count rate profiles were aligned so that they start at time zero. What is particularly
955 remarkable is that the October 28, 2003 flare has the highest EUV peak intensity of all four events
956 and was greater by a factor of ~2. This is the most intense EUV solar flare in recorded history.

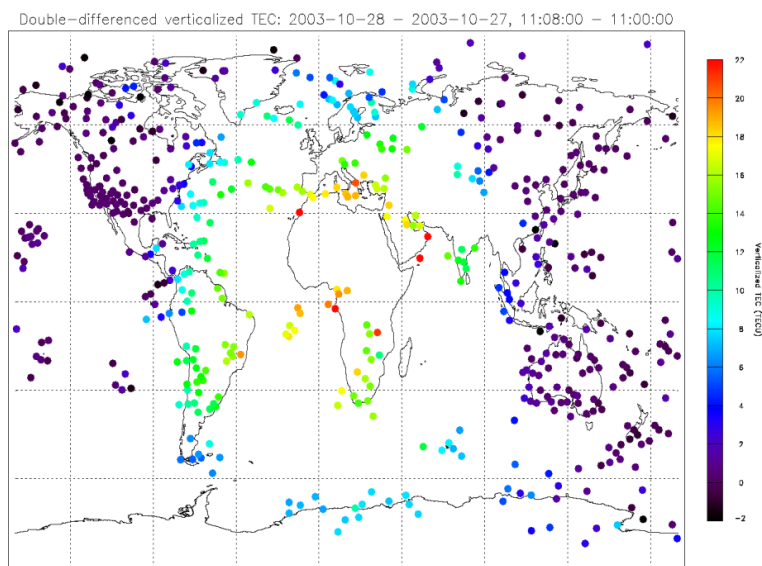
957

958 After each flare reached a peak intensity and then decreased in count rate, there was often a
959 following increase in count rate. This is particularly notable in the Bastille day (black trace) flare.
960 This is contamination due to delayed energetic electrons reaching the spacecraft. The November
961 4 flare (green) did not have such contamination because it was a limb flare and presumably
962 (magnetic) connection from the flare site to the spacecraft was poor.

963

964 NOAA has estimated the November 4 flare as having an intensity of ~X28. This event saturated
965 the detector so this is a conservative estimate. Thomson et al. (2004) using a different technique
966 estimated a value of X45 for this event.

967

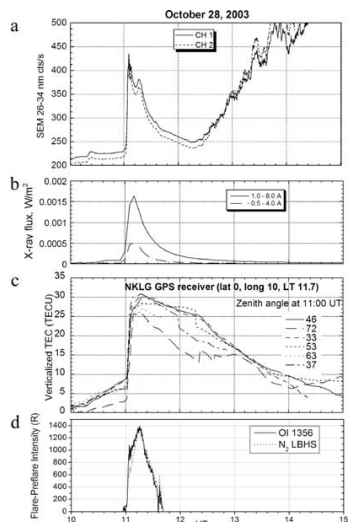




969 Figure 21. The global TEC during the October 28, 2003 solar flare. The scale is given on the right.
970 The figure is taken from Tsurutani et al. (2005b).

971
972 Figure 21 shows the global total electron content (TEC) in the ionosphere after the October 28,
973 2003 solar flare. The map has been adjusted so Africa, the subsolar point, is in the center of the
974 Figure. The top and bottom of the plot correspond to the poles and the left side and right side
975 edges local midnight. The enhanced TEC area corresponds to the sunlit hemisphere. The nightside
976 hemisphere shows no TEC enhancement, as expected. The TEC enhancement is due to ionization
977 by both X-rays, EUV photons and UV photons, all part of the solar flare spectrum.

978



979
980 Figure 22. The ionospheric and atmospheric effects of the October 28, 2003 solar flare.

981

982 Figure 22 shows the effects of the October 28 solar flare. From top to bottom are the SOHO SEM
983 EUV count rate, the GOES X-ray flux, the Libreville, Gabon TEC data and the GUVI O and N²
984 dayglow data. It is noted that the flare profiles in EUV and X-rays last ~tens of mins and are similar
985 in profile to each other. However the TEC over Libreville last hours. This is due to the EUV
986 portion of the solar flare. These photons deposit their energy at ~170 to 220 km altitude where the
987 recombination time scales are ~ 3 to 4 hours. Thus EUV photon ionization has longer lasting
988 ionospheric TEC effects. The X-ray portion of the solar flare spectrum deposit their energy in the



989 ~80 to 100 km altitude range where the recombination time scale is tens of min (Thomson et al.,
990 2005, and references therein).

991

992 Some future space weather problems are to understand if the solar flare spectrum varies and why
993 this happens. We have indicated that the 28 October 2003 and the 4 November 2003 flares were
994 significantly different. The question is why and how often does this happen? Ionospheric satellites
995 like the Constellation Observing System for Meteorology, Ionosphere and Climate-2 (COSMIC
996 II) and SWARM can probe for detailed altitude dependence of ionization to work backwards to
997 attempt to identify what spectrum would cause the layered ionization detected. Other questions are
998 how large can X-ray and EUV flares become? What will their ionospheric effects be?

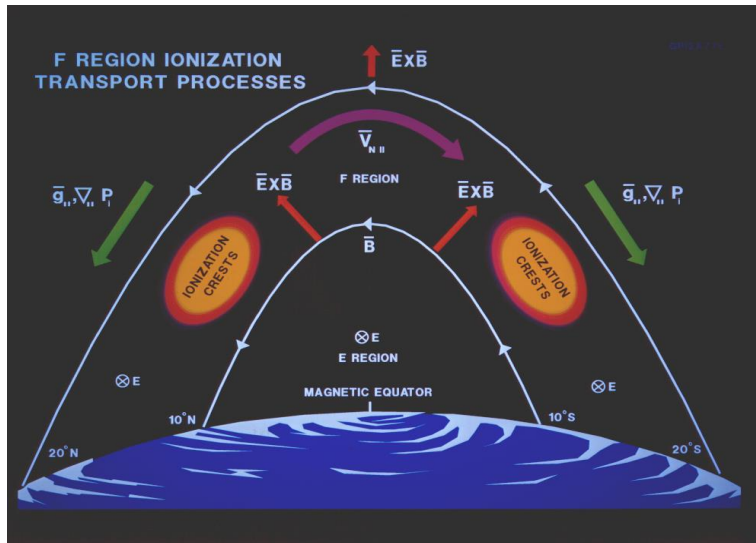
999

1000 **6.0. RESULTS: Magnetic Storms and Prompt Penetrating Electric Fields
(PPEFs)**

1002

1003 For substorms, PPEFs occurring in the ionosphere have been known for a long time (Nishida and
1004 Jacobs, 1962; Obayashi, 1967; Nishida, 1968; Kelley et al. 1979, 2003). In the last 10 years lots
1005 of work was done on PPEFs during magnetic storms. Why didn't people look at storms earlier?
1006 Because it was theoretically predicted that the PPEFs would be shielded out. Why doesn't
1007 shielding happen? This is a very good question for future works.

1008



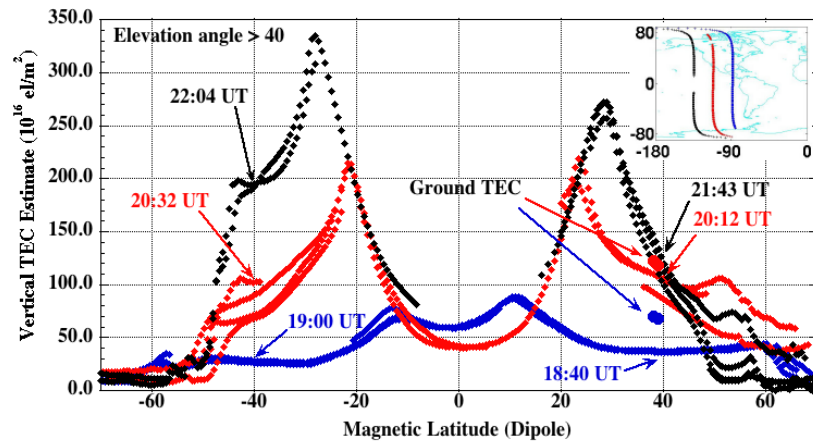
1009

1010 Figure 23. Dayside near equatorial ionization anomalies (EIAs) located $\sim \pm 10^\circ$ on both sides of
1011 the magnetic equator. The local Earth magnetic field is shown in this schematic. The figure is
1012 taken from Anderson et al. (1996).

1013

1014 Figure 23 show the geometry of the Earth's magnetic field near the magnetic equator. It is parallel
1015 to the Earth's surface at the equator but where the equatorial ionization anomalies (EIAs) are
1016 located, the magnetic field is slanted. The EIAs are standardly located at $\sim \pm 10^\circ$ MLAT in the
1017 dayside magnetosphere. With red arrows, the figure also shows the direction of $E \times B$ convection.
1018 At exactly the magnetic equator, $E \times B$ is in a purely upward direction. At the positions of the
1019 EIAs, the $E \times B$ direction is both upward and to higher magnetic latitudes.

1020



1021

1022 Figure 24. Three passes of the CHAMP satellite measuring the near equatorial and midlatitude
1023 TEC during October 30, 2003. CHAMP was at an altitude of ~430 km, so the TEC measured was
1024 the thermal electron content above that altitude. The figure is taken from Mannucci et al. (2005).

1025

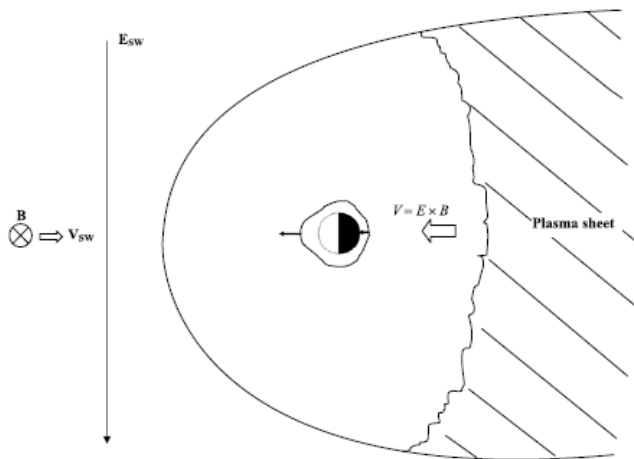
1026 Figure 24 shows three passes of the CHAMP satellite in polar orbit with an altitude of ~430 km at
1027 the near equatorial crossings. The three orbits are given in the upper right hand portion of the
1028 Figure. The first TEC trace shown in blue is before the onset of the October 30-31 magnetic storm.
1029 The two EIAs are identified by the TEC enhancements at $\sim \pm 10^\circ$ with peak intensities of ~ 80 TEC
1030 units. In the next pass (red trace), the EIAs are located at $\sim \pm 21^\circ$ MLAT and the peak intensities
1031 are ~ 210 TEC units. During the next satellite pass, the EIAs are located near $\pm 30^\circ$ and the TEC
1032 values become as high as ~ 330 TEC units. This “movement” of the EIAs to higher magnetic
1033 latitudes can be explained by a convective electric field (PPEF) in the east-west direction causing
1034 an uplift to both EIAs by $E \times B$ convection as explained earlier associated with Figure 23. However
1035 why does the TEC increase to such high values?

1036

1037 The answer is as the PPEF removes the plasma from the ionospheric lower F region and brings it
1038 to higher altitudes where recombination is long (hrs), the Sun’s EUV photons replace the plasma
1039 by photoionization of the upper atmosphere, replacing the lost plasma and thus increasing the “total
1040 electron content” of the ionosphere. This is one cause of a “positive ionospheric storm”.



1041



1042

1043 Figure 25. The interplanetary, magnetospheric and equatorial ionospheric electric fields during a
1044 PPEF event. The Figure is taken from Tsurutani et al. (2004c; 2008b).

1045

1046 Figure 25 shows the interplanetary motional electric field for southward interplanetary B_z . The
1047 electric field will be in the dawn-to-dusk direction. When magnetic reconnection takes place in
1048 the nightside plasmashell, the convective electric field will be in the same direction but with a
1049 reduced amplitude. This electric field brings the plasmashell plasma into the nightside low L
1050 magnetosphere during magnetic storms. The PPEFs penetrate into the dayside equatorial
1051 ionosphere (shown in Figure 24) and also the nightside equatorial ionosphere. However
1052 significantly different from the dayside case, the $E \times B$ convection on the nightside will bring the
1053 ionosphere to lower altitudes, leading to recombination and reduction in TEC. This is one form of
1054 a “negative ionospheric storm”. See Mannucci et al. (2005, 2008) for discussions of positive and
1055 negative ionospheric storms.

1056

1057 There are many important questions about PPEFs which are almost always present during major
1058 magnetic storms. As previously mentioned, “why aren’t the electric fields shielded out?” What is
1059 the mechanism for generating PPEFs, wave propagation from the polar ionosphere as suggested
1060 by Kikuchi and Hashimoto (2016) or a more global picture as Figure 25 and Nishida and Jacobs
1061 (1962) suggest? Figure 25 is a simple schematic. What are the real local time dependences of the
1062 PPEF? Does this vary from storm to storm, and if so, why? Why does the PPEF magnitude vary

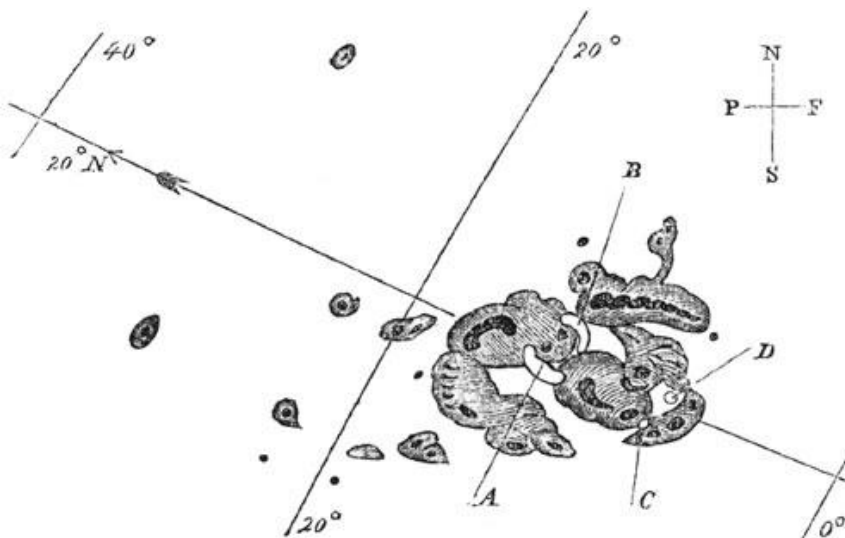


1063 from one storm to the next? Again future spacecraft and ground based studies will be able to help
1064 answer these questions.

1065

1066 **7.0 RESULTS: The Carrington Storm**

1067



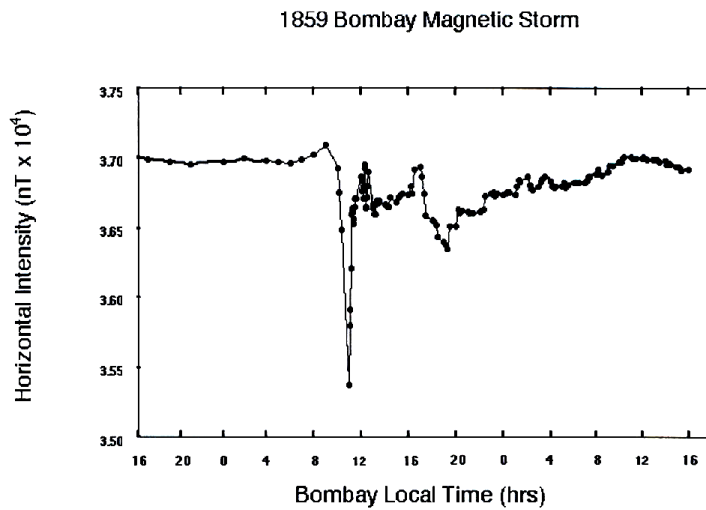
1068

1069 Figure 26. The solar active region during the Carrington 1 September 1859 optical solar flare. The
1070 figure is taken from Carrington (1859).

1071

1072 Figure 26 is the active region (AR) that was hand-drawn by Richard Carrington. This was the
1073 source of the optical solar flare that he and Hodgson (1859) saw and reported on 1 September
1074 1859. See Cliver (2006) for a nice accounting of the observational activity taken during 1859 flare
1075 interval and Kimball (1960) for an accounting of the aurora during the storm. The optical part of
1076 the flare lasted only ~ 5 min. Some ~17 hr 40 min later a magnetic storm occurred at Earth
1077 (Carrington, 1859).

1078



1079

1080 Figure 27. The Carrington storm detected in the Colaba, India magnetometer. The Figure is taken
1081 from Tsurutani et al. 2003 and Lakhina et al. 2012.

1082

1083 Figure 27 shows the H-component magnetic field taken by the Colaba magnetic observatory during
1084 the “Carrington” magnetic storm. The SI^+ is estimated to be ~ 110 nT and the magnetic decrease
1085 ~ 1600 nT at Colaba (Mumbai, India). The SI^+ and storm main phase has been recently shown to
1086 be most likely caused by an upstream solar wind density of 5 particles cm^{-3} and a MC with intensity
1087 ~ 90 nT (pointed totally southward) by Tsurutani et al. (2018a). No particularly unusual solar wind
1088 conditions are believed to have been necessary, in contrast to the conclusions of Ngwira et al.
1089 (2014).

1090

1091 The intensity of the “Carrington” storm was estimated as $Dst = -1760$ nT (Tsurutani et al., 2003)
1092 based on observations of the lowest latitude of red auroras being at $\pm 23^\circ$ (Kimball, 1960). The
1093 storm intensity was calculated using recent theoretical expressions of magnetospheric potentials
1094 needed to convect plasma into such low latitudes. Siscoe (1979) basing his estimate on a model
1095 that treats the pressure as a constant along the magnetic flux tube came up with a value of $Dst = -$
1096 2000 nT.

1097



1098 It should be mentioned that some researchers have taken exception with the Colaba magnetogram
1099 as an indication of ring current effects (see Comment by Akasofu and Kamide (2005) and Reply
1100 by Tsurutani et al. (2005a)). The Colaba magnetic profile is unlike those of ICME magnetic storms
1101 discussed in Sections 2.3, 2.4 and 3.1 of this paper. Several researchers have estimated the storm
1102 intensity based on the Colaba magnetogram (see articles in a special journal edited by Clauer and
1103 Siscoe, 2006; Acero et al. 2018). The Colaba data clearly show that the storm had exceptionally
1104 large geomagnetic effects, irregardless of the interpretation of the Colaba data.

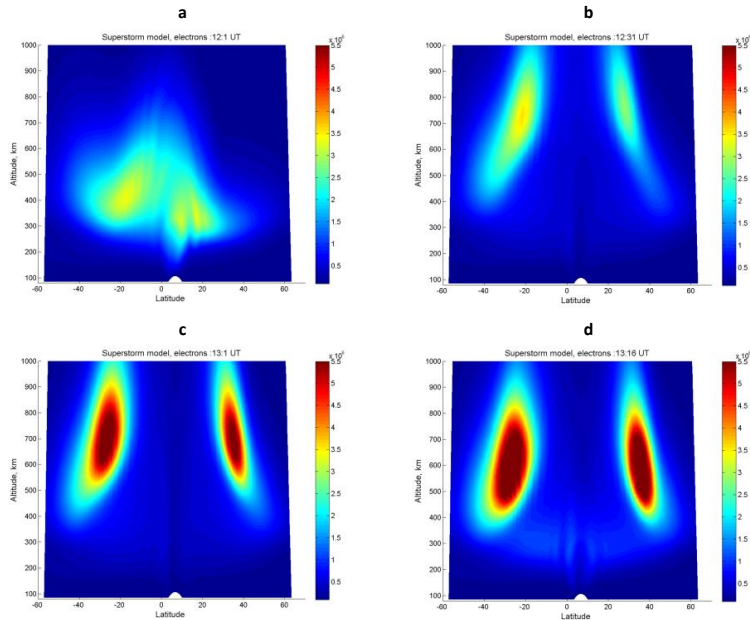
1105

1106 The most accurate method of estimating a magnetic storm intensity is by using the latitude of the
1107 aurora. Red auroras (Stable Auroral Red or SAR arcs) are presumably an indication of the location
1108 of the plasmapause (R.M. Thorne, private communication, 2002). Kimball (1960) noted that “red
1109 glows” were detected at $\pm 23^\circ$ from the geomagnetic equator during the Carrington event. In 1960
1110 the term “SAR arc” was not in use, but we can assume that this was what he was reporting. At the
1111 present time, this is the most equatorward SAR arcs that have been observed (thus the most intense
1112 magnetic storm). That is until researchers find records of lower latitude auroras!

1113

1114 Comments on the short duration of the recovery phase has been made by Li et al. (2006). A high
1115 density filament was used to explain this unusual feature of the magnetic storm profile. Tsurutani
1116 et al. (2018a) have recently proposed another possibility. During extreme events when the storm
1117 time convection brings the plasmasheet into very low L, all of the standard ring current loss
1118 processes will be enhanced. There will be greater Coulomb scattering, greater charge exchange
1119 losses and greater plasma wave growth with consequential greater wave-particle pitch angle
1120 scattering and losses to the atmosphere. Tsurutani et al. (2018a) focused particularly on wave-
1121 particle interactions because the size of the loss cone will increase dramatically with decreasing L.
1122 This, plus greater energetic particle compression due to inward convection, will lead to stronger
1123 loss cone/temperature anisotropy instabilities, greater wave growth and thus greater losses. This
1124 hypothesis can be easily tested by magnetospheric spacecraft observations during large magnetic
1125 storms and by magnetospheric modeling perhaps bringing some light to the unusual Colaba
1126 magnetic signature.

1127



1128

1129 Figure 28. A model of the PPEF effects of the Carrington storm on the dayside ionosphere. The
1130 input electric field was taken from Tsurutani et al. (2003) and the simulation was performed on
1131 the Huba et al. (2000, 2002) SAMI2 code. The figure is taken from Tsurutani et al. (2012).

1132

1133 7.1. The Carrington PPEF

1134

1135 One of the big worries for extreme space weather is the possible effects of PPEFs and the daytime
1136 superfountain effect on the uplift of O^+ ions (positive ionospheric storms). Higher ion densities in
1137 the exosphere will lead to the possibility of enhanced low altitude satellite drag. In Tsurutani et
1138 al. (2003), the authors used modern theories of the electric magnetospheric potential given by
1139 Volland (1973), Stern (1975) and Nishida (1978) to determine the electric field during the
1140 Carrington storm main phase. The former authors obtained an estimate of ~ 20 mV/m. They then
1141 applied this electric field in the SAMI2 model with the results shown in Figure 26.

1142

1143 Figure 28 shows the SAMI2 results of the modeled dayside ionosphere with a ~ 20 mV/m added
1144 to the diurnal variation electric field. The quiet ionosphere is shown at the upper left. The uplift
1145 of the O^+ ions both in altitude and MLAT after ~ 30 min is given on the upper right panel. The



1146 maximum time that the electric field was applied was 1 hr. The ionosphere at that time is shown
1147 on the lower left. The storm time equatorial ionospheric anomalies (EIAs) are located at $|MLAT|$
1148 $\sim 30^\circ$ to 40° and an altitude of ~ 550 to 900 km for the most dense portion of the EIAs. The bottom
1149 right panel shows that the EIAs have come down in altitude but at higher latitudes ~ 15 min after
1150 the termination of the PPEF application. Parts of the still intense EIAs are now beyond $|MLAT| >$
1151 40° and now the bulk of the maximum density portion is at ~ 400 to 800 km altitude.

1152

1153 It was found that at altitudes of ~ 700 to $1,000$ km, the O^+ densities are predicted to be 300 times
1154 that of the quiet time neutral densities. It has been also been shown by Tsurutani and Lakhina
1155 (2014) that in extreme cases, the magnetospheric/ionospheric electric field can be twice as large
1156 as the Carrington storm and six times as large as the 1991 event. Even if the magnetospheric
1157 radiation belt is saturated (and there are other scientific papers that state that magnetospheric beta
1158 can be greater than one: Chan et al. 1994; Saitoh et al. 2014; Nishiura et al., 2015), this is a different
1159 facet of space weather and the electric field may not be saturated. What will be the ionospheric
1160 effects of these even larger electric fields?

1161

1162 A fundamental question for the future is “can the upward O^+ ion flow drag sufficient numbers of
1163 oxygen neutrals upward so that the oxygen ions plus neutral densities are substantially higher?”
1164 A short time interval analytic calculation done by Lakhina and Tsurutani (2017) and a mini-
1165 Carrington event modeled by Deng et al. (2018) have indicated that the answer is “yes”. However
1166 a full code needs to be developed and run to answer this question quantitatively. This is an
1167 interesting future problem for computer modelers.

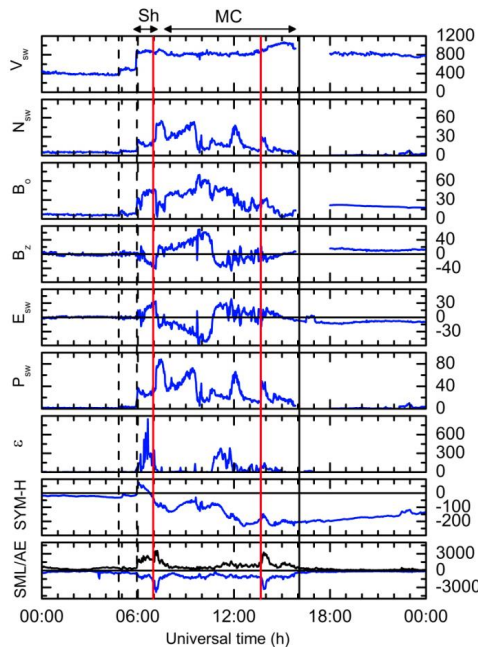
1168

8.0 RESULTS: Supersubstorms

1170

1171 Superintense substorms (supersubstorms: SSSs) appear to be externally (solar wind) triggered.
1172 Why are they important? They might be the feature within extreme magnetic storms that cause
1173 geomagneticall induced currents (GICs)/power outages. This hypothesis needs to be tested.

1174



1175

1176 Figure 29. Two supersubstorms (SSSs) that occur during a two-phase magnetic storm. The onsets
1177 of the supersubstorms are indicated by the vertical red lines. The figure is taken from Tsurutani et
1178 al. (2015).

1179

1180 Figure 29 shows the solar wind data during an intense magnetic storm and two SSSs. From top to
1181 bottom are the solar wind speed and density, the magnetic field magnitude and Bz component, and
1182 the interplanetary motional electric field, ram pressure and Akasofu epsilon parameter (Perreault
1183 and Akasofu, 1978). The bottom two parameters are the SYM-H index and the SML index (blue)
1184 and AE index (black). An initial forward shock is indicated by a vertical dashed line at ~0500 UT,
1185 a second shock at ~0600 UT, and the two SSS onsets by red vertical lines. The criterion for a SSS
1186 event was a SML peak value < -2500 nT (an arbitrary number, but chosen to be an extremely high
1187 value). At the top of the diagram, the sheath region is indicated by a “Sh” and the magnetic cloud
1188 region by “MC”. The first storm main phase is caused by southward Bz in the sheath and the
1189 second, more intense main phase by southward Bz in the MC.

1190

1191 It is noted that the SSS events in this case are not triggered at either of the two shocks nor do they
1192 occur during the peak negative SYM-H values of the storm main phases. However the first SSS

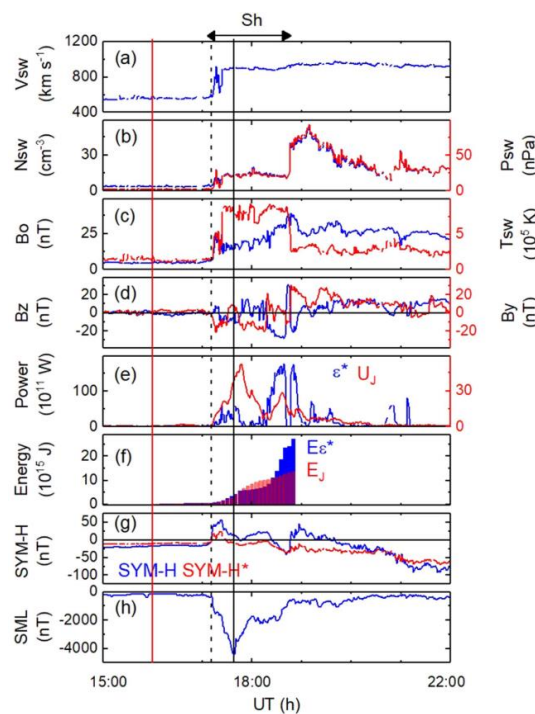


1193 event is collocated with a peak Esw and a peak southward Bz of the sheath plasma. The SSS event
1194 is also collocated with a large solar wind pressure pulse which is caused by an intense solar wind
1195 density feature. The second SSS event occurred in the recovery phase of the second magnetic
1196 storm. The IMF Bz was \sim 0 nT. The second SSS event was associated with a solar wind pressure
1197 pulse associated with a small density enhancement.

1198

1199 A study of SSSs from 1981 to 2012 was conducted by Hajra et al. (2016). In that study a variety
1200 of solar wind features were found to be associated with SSS onsets. In that survey it was noted
1201 that two SSS events were triggered by fast forward shocks. One of these events will be discussed
1202 below.

1203



1204

1205 Figure 30. A SSS triggered by an interplanetary shock on 21 January 2005. The dashed vertical
1206 line indicates a fast forward shock and the solid black line the peak intensity of the SSS event. The
1207 figure is taken from Hajra and Tsurutani (2018b).

1208

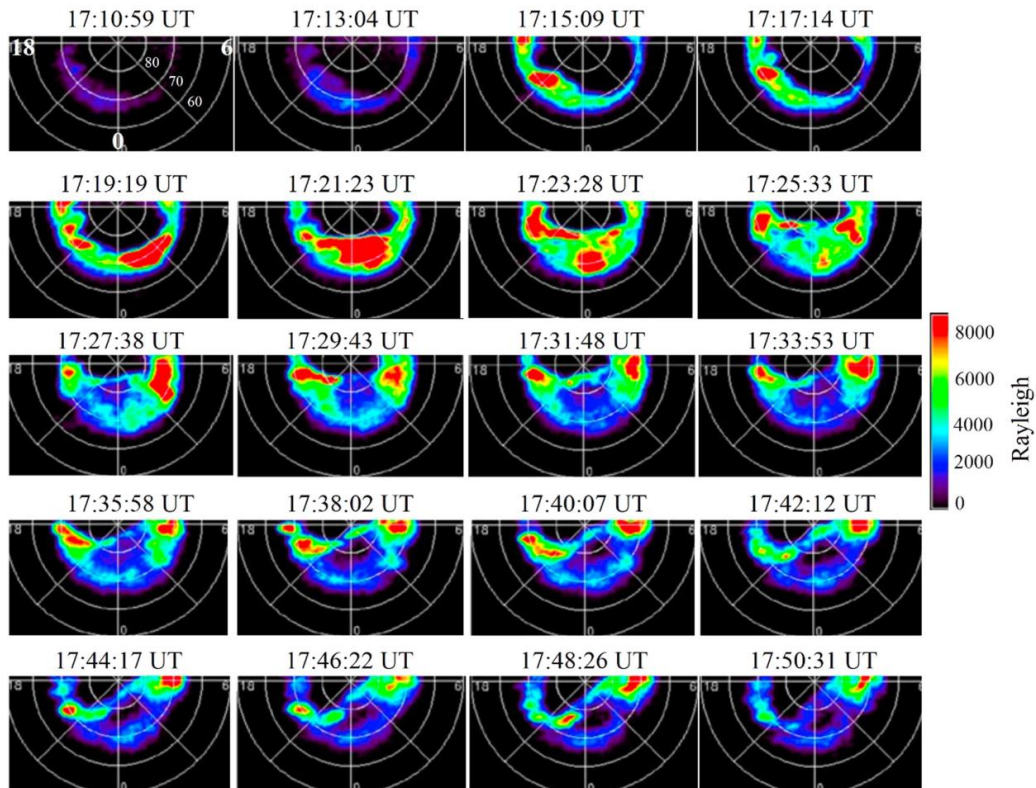


1209 Figure 30 shows solar wind/interplanetary parameters and geomagnetic parameters during a SSS
1210 event on 21 January 2005. From top to bottom are the solar wind speed, density and ram pressure,
1211 the magnetic field magnitude and solar wind temperature (in the same panel), the IMF B_z and B_y
1212 components (GSM coordinates), Joule energy and the Akasofu epsilon pressure corrected
1213 parameter ε^* , the time-integrated energy input into the magnetosphere and time-integrated joule
1214 energy. The next to the bottom panel contains the SYM-H* index and the pressure corrected SYM-
1215 H index. The bottom panel is the SML index. A dashed vertical line denotes the occurrence of a
1216 fast forward shock. A vertical solid line indicates the peak of the SSS event.

1217

1218 The SSS event onset at 1711 UT coincided with a shock with magnetosonic Mach number of ~ 5.5
1219 with a shock normal angle of 81° . The high density sheath sunward of the shock causes a SI⁺ of
1220 ~ 57 nT. The solar feature associated with this event was an X7 class flare that occurred at ~ 0700
1221 UT January 20 (Bombardier et al., 2008; Saldanha et al., 2008; Pérez-Peraza et al., 2009; Wang
1222 et al., 2009; Firoz et al., 2012; Bieber et al., 2013; Tan, 2013). The IMF B_z turned abruptly
1223 southward at the time of the shock so this is part of the energy driving the event. When the IMF
1224 B_z turned abruptly northward at ~ 1738 UT, the SSS began a recovery phase. This was followed
1225 by a solar filament (Kozyra et al., 2013) but the latter was not geoeffective in this case.

1226



1227

1228 Figure 31. IMAGE-FUV images taken from ~1711 UT to ~1751 UT on January 21. These selected
1229 auroral images correspond to the SSS event in Figure 30.

1230

1231 Figure 31 contains the Imager for Magnetopause-to-Aurora global Exploration (IMAGE) far
1232 ultraviolet images for the SSS event in Figure 30. At ~1713 UT there was a small brightening at
1233 ~68° MLAT, which was a very small substorm or pseudobreakup (Elvey, 1957; Tsurutani et al.,
1234 1998; Aikio et al., 1999). At ~1715 UT, 2 min later there was a ~2100 MLT premidnight
1235 brightening of the aurora at ~68° to 75°. At ~1719 UT the most intense aurora was located at ~68°
1236 to 72° in the postmidnight/morning sector, ~0000 to 0400 MLT. The aurora moved from a
1237 dominant premidnight location to a postmidnight location in ~4 min.

1238

1239 By ~1726 UT there was almost no aurora of significant intensity at local midnight. At the peak of
1240 the SML value at ~1738 UT until ~1751, there were both intense premidnight and postmidnight
1241 auroras.



1242

1243 The SSS event did not exhibit the Akasofu (1964) standard model of a substorm with an
1244 intensification at midnight and then expansion to the west, east and north. The changes in the
1245 location of intense auroras were too rapid to track with the IMAGE cadence of ~2 min.

1246

1247 The SSS events display rapid auroral movements which may entail the appearance of sudden local
1248 field-aligned currents. Even smooth motion of auroral forms will cause strong dB/dt effects over
1249 local ground stations. SSS events may be features that can cause GIC effects that have been
1250 attributed to “magnetic storms”. Thus it might be the SSS events within magnetic storms which
1251 are the real cause. SWARM satellites are excellently instrumented spacecraft that can study the
1252 SSS events in detail and possible resultant GIC effects. However as noted in the auroral images,
1253 there is a need for even higher time resolution global images than is present today.

1254

1255 8.0. CONCLUSIONS: Forecasting Space Weather

1256

1257 We have discussed the current knowledge about various facets of space weather. There are others
1258 which we have not touched upon because of limited time and knowledge. The reader should know
1259 that other areas of space weather exist which may be equally important. Perhaps other reviews
1260 will cover those topics.

1261

1262 The most critical area for forecasting magnetic storms, either during solar maximum or the
1263 declining phase of the solar cycle is the prediction of the magnetic field Bz in front of the Earth’s
1264 magnetosphere. For CME storms (primarily during solar maximum), this is identifying MC Bz
1265 near the Sun and understanding and predicting the evolution of the MC from the Sun to Earth.
1266 This major challenge will be applicable for the prediction of extreme magnetic storms and
1267 hopefully great progress will be made in the next 5 to 10 years.

1268

1269 For sheaths upstream of ICMEs during solar maximum and CIRs during the declining phase, the
1270 problem is different. Detailed knowledge of the slow solar wind in the space between the Sun and
1271 Earth are needed to accurately describe and predict the IMF Bz that impacts the Earth. So far little



1272 work has been applied towards predicting the slow solar wind (plus verification). Effort needs to
1273 be placed in this area to be able to forecast intense to moderate magnetic storms.

1274

1275 A great deal of knowledge presently exists for establishing SEP events, those energetic particles
1276 associated with acceleration at ICME shock fronts. What is needed for better forecasting is to
1277 understand the Mach number of the shocks, the shock normal angles and possibly upstream “seed”
1278 particles. The upstream seed particle population is similar to the sheath Bz problem in that this
1279 component of the slow solar wind needs to be modeled more carefully. Three spacecraft in the
1280 solar wind at different distances from the Sun should help a lot.

1281

1282 The appearance of HSSs at 1 AU is a very tractable problem. That is if the coronal hole boundaries
1283 in the photosphere can be established firmly and the HSS propagation to 1 AU can be done
1284 accurately. However the most difficult task again is the IMF Bz. If Alfvén waves are generated
1285 in the interplanetary medium, this will make the task even more difficult. One solution is to
1286 measure the interplanetary magnetic field at 1 AU and use filtering techniques (Guarnieri et al.
1287 2018) or again have large apogee Earth orbiters like the IMP-8 spacecraft again. Another
1288 possibility is developing some type of statistical IMF Bz generator.

1289

1290 Predicting the interplanetary shock Mach numbers and ram pressure jumps will allow
1291 foreknowledge of new radiation belt formation, SI⁺ effects and magnetospheric and ionospheric
1292 dB/dt effects. Dayside auroral intensities and nightside substorm triggering will also be enhanced
1293 by predicting oncoming shocks.

1294

1295 Several spacecraft missions have been mentioned in relationship to some forecasting problems.
1296 However the reader should note that the missions and/or their data alone will not solve these
1297 problems. It will be the scientists either on these missions or perhaps totally independent scientists
1298 who will make the most progress on these problems. An example is magnetic storms caused by
1299 interplanetary shocks/sheaths and CIRs. How long will it take scientists to be able to accurately
1300 forecast the time of occurrence of the storm (the easiest part) and the intensity (the hardest part)?
1301 Here we will not make an estimate of how long this will take. Shock acceleration of solar flare
1302 particles is clearly a fundamental part of space weather. How long will it take for scientists to be able to



1303 predict the fluence and spectral shape at a variety of distances away from the Sun? This is a
1304 fundamental problem which space agencies are not currently directly addressing.

1305

1306

1307

1308 10.0 GLOSSARY

1309 **Partially taken from:** “*From the Sun: Auroras, Magnetic Storms, Solar Flares, Cosmic*
1310 *Rays*” (Suess and Tsurutani, 1998, AGU Press)

1311

1312 **Adiabatic Invariant:** In a nearly collisionless, ionized gas, electrically charged particles orbit
1313 around magnetic lines of force. Certain physical quantities are approximately constant for
1314 slow (adiabatic) changes of the magnetic field in time or in space and these quantities are
1315 called *adiabatic invariants*. For example, the magnetic moment of a charged particle,
1316 $\mu = mV_{\perp}^2/(2B)$, is such a constant where V_{\perp} is the velocity of the particle perpendicular to
1317 the magnetic field, B is the magnetic field strength, and m is the particle mass. In a
1318 converging field such as in approaching the pole of a dipole magnetic, the field strength
1319 increases and therefore V_{\perp} increases as well because μ has to remain constant.

1320 **Aeronomy:** The science of the (upper) regions of atmospheres, those regions where dissociation
1321 of molecules and ionization are present.

1322 **Alfvén Wave** (magnetohydrodynamic shear wave): A transverse wave in magnetized plasma
1323 characterized by a change of direction of the magnetic field with no change in either the
1324 intensity of the field or the plasma density.

1325 **Anisotropic Plasma:** A Plasma whose properties vary with direction relative to the ambient
1326 magnetic field direction. This can be due, for example, to the presence of a magnetic or
1327 electric field. See also Isotropic Plasma; Plasma.

1328 **Arase satellite, formerly called Exploration of energization and Radiation in Geospace or**
1329 **ERG:** a scientific satellite developed by the Institute of Space and Astronautical Science



1330 (ISAS) of the Japanese Aerospace Exploration Agency (JAXA) to study the Van Allen
1331 radiation belts.

1332 **Astronomical Unit (AU):** The mean radius of the Earth's orbit, 1.496×10^{13} cm.

1333 **Aurora:** A visual phenomenon that occurs mainly in the high-latitude night sky. Auroras occur
1334 within a band of latitudes known as the auroral oval, the location of which is dependent
1335 on the intensity of geomagnetic activity. Auroras are a result of collisions between
1336 atmospheric gases and charged particles (mostly electrons) precipitating from the outer
1337 parts of the magnetosphere and guided by the geomagnetic field. Each gas (oxygen and
1338 nitrogen molecules and atoms) emits its own when bombarded by the precipitating
1339 particles. Since the atmospheric composition varies with altitude, and the faster
1340 precipitating particles penetrate deeper into the atmosphere, certain auroral colors
1341 originate preferentially from certain heights in the sky. The auroral altitude range is 80 to
1342 500 km, but typical auroras occur 90 to 250 km above the ground. The color of the
1343 typical aurora is yellow-green, from a specific transition line of atomic oxygen. Auroral
1344 light from lower levels in the atmosphere is dominated by blue and red bands from
1345 molecular nitrogen and molecular oxygen. Above 250 km, auroral light is characterized
1346 by a red spectral line of atomic oxygen. To an observer on the ground, the combined light
1347 of these three fluctuating, primary colors produces an extraordinary visual display.
1348 Auroras in the Northern Hemisphere are called the aurora borealis or “northern lights”.
1349 Auroras in the Southern Hemisphere are called aurora australis. The patterns and forms of
1350 the aurora include quiescent “arcs”, rapidly moving “rays” and “curtains,” “patches,” and
1351 “veils.”

1352 **Auroral Electrojet (AE):** See Electrojet.

1353 **Auroral Oval:** An elliptical band around each geomagnetic pole ranging from about 75 degrees
1354 magnetic latitude at local noon to about 67 degrees magnetic latitude at midnight under
1355 average conditions. It is the locus of those locations of the maximum occurrence of
1356 auroras, and widens to both higher and lower latitudes during the expansion phase of a
1357 magnetic substorm.



1358 **Beta** (e.g., low-beta plasma): The ratio of the thermal pressure to the magnetic 'pressure' in a
1359 plasma - $p/(B^2/(8\pi))$ in centimeter-gram-second (c.g.s.)

1360 **Bow Shock** (Earth, heliosphere): A collisionless shock wave in front of the magnetosphere
1361 arising from the interaction of the supersonic solar wind with the Earth's magnetic field.
1362 An analogous shock is the heliospheric bow shock which exists in front of the
1363 heliosphere and is due to the interaction of the interstellar wind with the solar wind and
1364 the interplanetary magnetic field.

1365 **Charge Exchange**: An interaction between a charged particle and a neutral atom wherein the
1366 charged particle becomes neutral and the neutral particle becomes charged through the
1367 exchange of an electron.

1368 **Cloud** (magnetic): see Magnetic Cloud.

1369 **Collisional (de-) Excitation**: Excitation of an atom or molecule to a higher energy state due to a
1370 collision with another atom, molecule, or ion. The higher energy state generally refers to
1371 electrons in higher energy around atoms. Deexcitation is the reduction of a higher
1372 electron energy state to a lower one, usually accomplished by a collision with another
1373 atom, molecule or ion.

1374 **Convection** (magnetospheric, plasma, thermal): The bulk transport of plasma (or gas) from one
1375 place to another, in response to mechanical forces (for example, viscous interaction with
1376 the solar wind) or electromagnetic forces. Thermal convection, due to heating from below
1377 and the gravitational field, is what drives convection inside the Sun. Magnetospheric
1378 convection is driven by the dragging of the Earth's magnetic field and plasma together by
1379 the solar wind when the magnetic field becomes attached to the magnetic field in the
1380 solar wind.

1381 **Coriolis Force**: In the frame of a rotating body (such as the Earth), a force due to the bodily
1382 rotation. All bodies that are not acted upon by some force have the tendency to remain in
1383 a state of rest or of uniform rectilinear motion (Newton's First Law) so that this force is
1384 called a "fictitious" force. It is a consequence of the continuous acceleration which must
1385 be applied to keep a body at rest in a rotating frame of reference.



1386 **Corona:** The outermost layer of the solar atmosphere, characterized by low densities ($<10^9 \text{ cm}^{-3}$
1387 or 10^{15} m^{-3}) and high temperatures ($>10^6 \text{ K}$).

1388 **Coronal Hole:** An extended region of the solar corona characterized by exceptionally low
1389 density and in a unipolar photospheric magnetic field having "open" magnetic field
1390 topology. Coronal holes are largest and most stable at or near the solar poles, and are a
1391 source of high speed (700-800 km/s) solar wind. Coronal holes are visible in several
1392 wavelengths, most notably solar x-rays visible only from space, but also in the He 1083
1393 nm line which is detectable from the surface of the Earth. In soft x-ray images (photon
1394 energy of $\sim 0.1\text{-}1.0 \text{ keV}$ or a wavelength of 10-100 Å), these regions are dark, thus the
1395 name "holes".

1396 **Coronal Mass Ejection (CME):** A transient outflow of plasma from or through the solar
1397 corona. CMEs are often but not always associated with erupting prominences,
1398 disappearing solar filaments, and flares.

1399 **Corotation** (with the Earth): A plasma in the magnetosphere of the Earth is said to be corotating
1400 with the Earth if the magnetic field drags the plasma with it and together they have a 24
1401 hour rotation period.

1402 **Cosmic Ray** (galactic, solar): Extremely energetic (relativistic) charged particles or
1403 electromagnetic radiation, primarily originating outside of the Earth's magnetosphere.
1404 Cosmic rays usually interact with the atoms and molecules of the atmosphere before
1405 reaching the surface of the Earth. The nuclear interactions lead to formation of daughter
1406 products, and they in turn to granddaughter products, etc.; thus there is a chain of
1407 reactions and a "cosmic ray shower" Some cosmic rays come from outside the solar
1408 system while others are emitted from the Sun in solar flares. See also Anomalous Cosmic
1409 Ray; Energetic Particle; Solar Energetic Particle (SEP) Event.

1410 **Constellation Observing System for Meteorology, Ionosphere and Climate-2 (COSMIC II):**
1411 A joint Taiwan National Space Organization (NSPO)-U.S. National Oceanic and Atmospheric
1412 Administration (NOAA) mission of six satellites in low-inclination orbit to study the Earth's
1413 ionosphere.

1414



1415 **Corotating Interaction Region (CIR):** An interplanetary region of high magnetic fields and
1416 plasma densities created by the interaction of a high speed solar wind stream with the upstream
1417 slow solar wind. The antisunward portion of the CIR is compressed slow solar wind plasma and
1418 magnetic fields, and the sunward portion is compressed fast solar wind plasma and magnetic
1419 fields. The two regions of the CIR are separated by a tangential discontinuity.

1420

1421 **Cyclotron Frequency:** When a particle of charge q moves in a magnetic field B , the particle
1422 orbits, or gyrates around the magnetic field lines. The cyclotron frequency is the
1423 frequency of this gyration, and is given by $\omega_c = q|B|/mc$, where m is the mass of the
1424 particle, and c is the velocity of light (in centimeter-gram-second (c.g.s.) units).

1425 **Cyclotron Resonance:** The frequency at which a charged particle experiences a Doppler-shifted
1426 wave at the particle's cyclotron frequency. Because the particle and wave may be
1427 traveling at different speeds and in different directions, there is usually a Doppler shift
1428 involved.

1429 **D Region:** A daytime region of the Earth's ionosphere beginning at approximately 40 km,
1430 extending to 90 km altitude. Radio wave absorption in this region can be significantly
1431 increased due to increasing ionization associated with the precipitation of solar energetic
1432 particles through the magnetosphere and into the ionosphere.

1433 **Diffusion:** The slow, stochastic motion of particles.

1434 **Diffusive Shock Acceleration:** Charged particle acceleration at a collisionless shock due to
1435 stochastic scattering processes caused by waves and plasma turbulence. See also Shock
1436 Wave (collisionless).

1437 **Dipole Magnetic Field:** A magnetic field whose intensity decreases as the cube of the distance
1438 from the source. A bar magnet's field and the magnetic field originating in the Earth's
1439 core are both approximately dipole magnetic fields.

1440 **Drift** (of ions/electrons): As particles gyrate around magnetic field lines, their orbits may "drift"
1441 perpendicular to the local direction of the magnetic field. This occurs if there is a force



1442 also perpendicular to the field - e.g. an electric field, curvature in the magnetic field
1443 direction, or gravity.

1444 **Driver Gas:** A mass of plasma and entrained magnetic field that is ejected from the Sun, that has
1445 a velocity higher than the upstream plasma, and which "drives" a (usually collisionless)
1446 shock wave ahead of itself. The magnetic cloud within an ICME is the same thing as a
1447 driver gas.

1448 **Dst Index:** A measure of variation in the geomagnetic field due to the equatorial ring current. It
1449 is computed from the H-components at approximately four near-equatorial stations at
1450 hourly intervals. At a given time, the Dst index is the average of variation over all
1451 longitudes; the reference level is set so that Dst is statistically zero on internationally
1452 designated quiet days. An index of -50 nT (nanoTesla) or less indicates a storm-level
1453 disturbance, and an index of -200 nT or less is associated with middle- latitude auroras.
1454 Dst is determined by the World Data Center C2 for Geomagnetism, Kyoto University,
1455 Kyoto, Japan.

1456 **Dynamo** (solar magnetospheric): The conversion of mechanical energy (rotation in the case of
1457 the Sun) into electrical current. This is the process by which magnetic fields are amplified
1458 by the induction of plasmas being forced to move perpendicular to the magnetic field
1459 lines. See also Mean Field Electro-Dynamics.

1460 **E-Region:** A daytime region of the Earth's ionosphere roughly between the altitudes of 90 and
1461 160 km. The E-region characteristics (electron density, height, etc.) depend on the solar
1462 zenith angle and the solar activity. The ionization in the E layer is caused mainly by x-
1463 rays in the range 0.8 to 10.4 nm coming from the Sun.

1464 **Ecliptic Plane:** The plane of the Earth's orbit about the Sun. It is also the Sun's apparent annual
1465 path, or orbit, across the celestial sphere.

1466 **Electrically Charged Particle:** Electrons and protons, for example, or any atom from which
1467 electrons have been removed to make it into a positively charged ion. The elemental
1468 charge of particles is 4.8×10^{-10} esu. An electron and proton have this charge. Combined (a
1469 hydrogen atom), the charge is zero. Ions have multiples of this charge, depending on the
1470 number of electrons which have been removed (or added).

1471 **Electrojet:** (1) Auroral Electrojet (AE): A current that flows in the ionosphere at a height of
1472 ~100 km in the auroral zone. (2) Equatorial Electrojet: A thin electric current layer in the
1473 ionosphere over the dip equator at about 100 to 115 km altitude.

1474 **Electron Plasma Frequency/Wave:** The natural frequency of oscillation of electrons in a
1475 neutral plasma (e.g., equal numbers of electrons and protons).

1476 **Electron Volt (eV):** The kinetic energy gained by an electron or proton being accelerated in a
1477 potential drop of one Volt.

1478 **ESA:** European Space Agency

1479 **Extreme Ultraviolet (EUV):** A portion of the electromagnetic spectrum from approximately 10
1480 to 100 nm.

1481 **Extremely Low Frequency (ELF):** That portion of the radio frequency spectrum from 30 to
1482 3000 Hz.

1483 **Fast Mode (wave/speed):** In magnetohydrodynamics, the fastest wave speed possible.
1484 Numerically, this is equal to the square root of the sum of the squares of the Alfvén speed
1485 and plasma sound speed.

1486 **Field Aligned Current:** A current flowing along (or opposite to) the magnetic field direction.

1487 **Filament:** A mass of gas suspended over the chromosphere by magnetic fields and seen as dark
1488 ribbons threaded over the solar disk. A filament on the limb of the Sun seen in emission
1489 against the dark sky is called a prominence. Filaments occur directly over magnetic-
1490 polarity inversion lines, unless they are active.

1491 **Flare:** A sudden eruption of energy in the solar atmosphere lasting minutes to hours, from which
1492 radiation and energetic charged particles are emitted. Flares are classified on the basis of
1493 area at the time of maximum brightness in H alpha.

1494 Importance 0 (Subflare): < 2.0 hemispheric square degrees

1495 Importance 1: 2.1-5.1 square degrees

1496 Importance 2: 5.2-12.4 square degrees



1497 Importance 3: 12.5-24.7 square degrees

1498 Importance 4: ≥ 24.8 square degrees

1499 [One square degree is equal to $(1.214 \times 10^4 \text{ km})$ squared = 48.5 millionths of the visible solar hemisphere.] A brightness qualifier F, N, or B is generally appended to the importance character to indicate faint, normal, or brilliant (for example, 2B).

1503 **Flux Rope:** A magnetic phenomenon which has a force-free field configuration.

1504 **Force Free Field:** A magnetic field which exerts no force on the surrounding plasma. This can
1505 either be a field with no flowing electrical currents or a field in which the electrical
1506 currents all flow parallel to the field.

1507 **Free Energy** (of a plasma): When an electron or ion distribution is either non-Maxwellian or
1508 anisotropic, they are said to have free energy" from which plasma waves can be
1509 generated via instabilities. The waves scatter the particles so they become more isotropic,
1510 reducing the free energy.

1511 **Frozen-in Field:** In a tenuous, collisionless plasma, the weak magnetic fields embedded in the
1512 plasma are convected with the plasma. i.e., they are "frozen in."

1513 **Galactic Cosmic Ray (GCR):** See Cosmic Ray.

1514 **Gamma Ray:** Electromagnetic radiation at frequencies higher than x-rays.

1515 **Geomagnetic Storm:** A worldwide disturbance of the Earth's magnetic field, distinct from
1516 regular diurnal variations. A storm is precisely defined as occurring when D_{ST} becomes
1517 less than -50 nT (See geomagnetic activity).

1518 Main Phase: Of a geomagnetic storm, that period when the horizontal magnetic field at
1519 middle latitudes decreases, owing to the effects of an increasing magnetospheric ring
1520 current. The main phase can last for hours, but typically lasts less than 1 day.

1521 Recovery Phase: Of a geomagnetic storm, that period when the depressed northward field
1522 component returns to normal levels. Recovery is typically complete in one to two days.



1523 **Geosynchronous Orbit:** Term applied to any equatorial satellite with an orbital velocity equal to
1524 the rotational velocity of the Earth. The geosynchronous altitude is near 6.6 Earth radii
1525 (approximately 36,000 km above the Earth's surface). To be geostationary as well, the
1526 satellite must satisfy the additional restriction that its orbital inclination be exactly zero
1527 degrees. The net effect is that a geostationary satellite is virtually motionless with respect
1528 to an observer on the ground.

1529 **GeV:** 10^9 electron Volts (Giga-electron Volt).

1530 **Global Positioning System (GPS):** is a global navigation satellite system that provides
1531 geolocation and time information to a GPS receiver anywhere on or near the Earth where
1532 there is an unobstructed line of sight to four or more GPS satellites.

1533 **Global-scale Observations of the Limb and Disk (GOLD):** a NASA mission to “ investigate
1534 the dynamic intermingling of space and Earth’s uppermost atmosphere”

1535 **Heliosphere:** The magnetic cavity surrounding the Sun, carved out of the galaxy by the solar
1536 wind.

1537 **Heliospheric Current Sheet (HCS):** This is the surface dividing the northern and southern
1538 magnetic field hemispheres in the solar wind. The magnetic field is generally one polarity
1539 in the north and the opposite in the south so just one surface divides the two polarities.
1540 However, the Sun's magnetic field changes over the 11-year solar sunspot cycle and
1541 reverses polarity at solar maximum. The same thing happens in the magnetic field carried
1542 away from the Sun by the solar wind so the HCS only lies in the equator near solar
1543 minimum. It is called a "current sheet" because it carries an electrical current to balance
1544 the oppositely directed field on either side of the surface. It is very thin on the scale of the
1545 solar system - usually only a few proton gyroradii, or less than 100,000 km.

1546 **Helmet Streamer:** See Streamer.

1547 **High Frequency (HF):** That portion of the radio frequency spectrum between 3 and 30 MHz.

1548 **Heliospheric Plasma Sheet (HPS):** A high density slow solar wind region that is located
1549 adjacent to the heliospheric current sheet (HCS).



1550 **High Speed Solar Wind (HSS):** A solar wind with speeds of 750 to 800 km/s emanating from
1551 solar coronal holes. The HSS is characterized by embedded, particularly large amplitude
1552 Alfvén waves. At the edges of HSSs, the velocities can be less due to superradial
1553 expansion effects.

1554 **Instability:** When an electron or ion distribution is sufficiently anisotropic, it becomes unstable
1555 (instability), generating plasma waves. The anisotropic distribution provides a source of
1556 free energy for the instability. A simple analog is a stick, which if stood on end is
1557 "unstable," but which if laid on its side is "stable." In this analog, gravity pulls on the
1558 stick and provides a source of free energy when the stick is stood on end.

1559 **Interplanetary Magnetic Field (IMF, Parker spiral):** The magnetic field carried with the solar
1560 wind and twisted into an Archimedean spiral by the Sun's rotation.

1561 **Interplanetary Medium:** The volume of space in the solar system that lies between the Sun and
1562 the planets. The solar wind flows in the interplanetary medium.

1563 **Interplanetary Coronal Mass Ejection (ICME):** The evolutionary part of a CME as it propagates
1564 through interplanetary space. Typically after the CME has propagated 1 AU from the Sun,
1565 the ICME only contains the magnetic cloud (MC) portion of the initial three parts of a
1566 CME. The MC may also have been compressed/expanded or rotated by the time it reaches
1567 1 AU.

1568 **Interplanetary Shock:** A fast forward shock is characterized by a sharp increase in solar wind
1569 speed, plasma density, plasma temperature and magnetic field magnitude. The shock
1570 reduces the upstream plasma from a supermagnetosonic state to a subsonic state, much as
1571 an airplane wing sonic shock reduces the relative flow of air from a supersonic speed
1572 (relative to the airplane) to a subsonic speed. A fast (magnetosonic) forward (propagating
1573 in the direction of the "piston", in this case the propagation of the ICME in the antisolar
1574 direction) shock is detected upstream (antisolarward) of fast ICMEs. A reverse shock
1575 propagates in the direction of the Sun. Planetary bow shocks are reverse shocks. There
1576 are other types of shocks not discussed in this paper: slow shocks and intermediate shocks.



1577 **Interstellar** (gas, neutral gas, ions, cosmic rays, wind, magnetic field, etc.) Literally, between
1578 the stars. In practical terms, it is anything beyond the outer boundary of the solar wind
1579 (the "heliopause") yet within the Milky Way.

1580 **Ion**: (1). An electrically charged atom or molecule. (2). An atom or molecular fragment that has
1581 a positive electrical charge due to the loss of one or more electrons; the simplest ion is the
1582 hydrogen nucleus, a single proton.

1583 **Ionization State**: The number of electrons missing from an atom.

1584 **Ionosphere**: The region of the Earth's upper atmosphere containing free (not bound to an atom
1585 or molecule) electrons and ions. This ionization is produced from the neutral atmosphere
1586 by solar ultraviolet radiation at very short wavelengths (<100 nm) and also by
1587 precipitating energetic particles.

1588 **Ionospheric Storm**: A positive ionospheric storm is where the ionospheric total electron content
1589 (TEC) increases. A negative ionospheric storm is an event where the ionospheric TEC
1590 decreases.

1591 **Ionospheric Connection Explorer (ICON)**: is a NASA 2-year mission that will give new views
1592 of the boundary between our atmosphere and space, where planetary weather and space
1593 weather meet.

1594 **Irradiance**: Radiant energy flux density on a given surface (e. g. ergs cm⁻²s⁻¹).

1595 **keV**: 1000 electron Volts (kiloelectron Volt). See electron Volt. See also Anisotropic Plasma;
1596 Plasma.

1597 **Loop** (solar-loop prominence system): A magnetic loop is the flux tube which crosses from one
1598 polarity to another. A loop prominence bridges a magnetic inversion line across which
1599 the magnetic field changes direction. See also Magnetic Foot Point; Prominence.

1600 **Loss Cone**: A small cone angle about the ambient magnetic field direction where
1601 magnetospheric charged particles with velocity vectors within the cone will mirror at
1602 sufficiently low altitudes such that the particle will have collisions with atmospheric
1603 atoms and molecules and will be "lost" from returning to the magnetosphere.



1604 **Loss Cone Instability:** An instability generated by a plasma anisotropy where the temperature
1605 perpendicular to the magnetic field is greater than the temperature parallel to the field.
1606 This instability gets its name because this condition exists in the Earth's magnetosphere
1607 and the "loss cone" particles are those that are lost into the upper atmosphere.

1608 **Magnetic Cloud:** A region in the solar wind of about 0.25 AU or more in radial extent in which
1609 the magnetic field strength is high and the direction of one component of the magnetic
1610 field changes appreciably by means of a rotation nearly parallel to a plane. Magnetic
1611 clouds may be parts of the driver gases (coronal mass ejections) in the interplanetary
1612 medium.

1613 **Magnetic Foot Point:** For the Earth's magnetic field lines, where the magnetic field enters the
1614 surface of the Earth.

1615 **Magnetic Mirror:** Charged particles moving into a region of converging magnetic flux (as at the
1616 pole of a magnet) will experience "Lorentz" forces that slow the particles and "mirror"
1617 them by eventually reversing their direction if the particles are initially moving slowly
1618 enough along the field line. See also Mirror Point.

1619 **Magnetic Reconnection:** The act of interconnection between oppositely directed magnetic field
1620 lines.

1621 **Magnetic Storm:** see Geomagnetic Storm.

1622 **Magnetopause:** The boundary surface between the solar wind and magnetosphere, where the
1623 pressure of the magnetic field of the object effectively equals the ram pressure of the
1624 solar wind plasma.

1625 **Magnetosheath:** The region between the bow shock and the magnetopause, characterized by
1626 very turbulent plasma. This plasma has been heated (shocked) and slowed as it passed
1627 through the bow shock. For the Earth, along the Sun-Earth axis, the magnetosheath is
1628 about 3 Earth radii thick.

1629 **Magnetosonic Speed** (acoustic speed): The speed of the fastest low frequency magnetic waves
1630 in a magnetized plasma. It is the equivalent of the sound speed in a neutral gas or non-
1631 magnetized plasma.



1632 **Magnetosphere:** The magnetic cavity surrounding a magnetized planet, carved out of the
1633 passing solar wind by virtue of the planetary magnetic field, which prevents, or at least
1634 impedes, the direct entry of the solar wind plasma into the cavity.

1635 **Magnetospheric Multiscale Mission (MMS):** A NASA mission designed to spend extensive
1636 periods in locations where magnetic reconnection at the magnetopause/magnetotail is
1637 expected to occur. The critical electron diffusion region will be studied. The mission
1638 consists of 4 spacecraft flown in a tetrahedron configuration.

1639 **Magnetotail:** The extension of the magnetosphere in the anti-sunward direction as a result of
1640 interaction with the solar wind. In the inner magnetotail, the field lines maintain a
1641 roughly dipolar configuration. But at greater distances in the anti-sunward direction, the
1642 field lines are stretched into northern and southern lobes, separated by a plasmashell.
1643 There is observational evidence for traces of the Earth's magnetotail as far as 1000 Earth
1644 radii downstream, in the anti-solar direction.

1645 **Maxwellian Distribution:** The minimum energy particle distribution for a given temperature. It
1646 is also the equilibrium distribution in the absence of losses due to radiation, collisions,
1647 etc.

1648 **Mean Free Path:** The statistically most probable distance a particle travels before undergoing a
1649 collision with another particle or interacting with a wave.

1650 **Mesosphere:** The region of the Earth's atmosphere between the upper limit of the stratosphere
1651 (approximately 30 km altitude) and the lower limit of the thermosphere (approximately
1652 80 km altitude).

1653 **MeV:** One million electron Volts (Megaelectron Volt). See also Electron Volt.

1654 **Mirror Point:** The point where the charged particles reverse direction (mirrors). At this point, all
1655 of the particle motion is perpendicular to the local ambient magnetic field. See also
1656 Magnetic Mirror.

1657 **Parker Solar Probe:** a NASA robotic spacecraft to probe the outer corona of the Sun. It will
1658 approach to within 9.9 solar radii (6.9 million kilometers or 4.3 million miles from the



1659 center of the Sun and will travel, at closest approach, as fast as 690,000 km/h
1660 (430,000 mph).

1661 **Photosphere:** The lowest visible layer of the solar atmosphere; corresponds to the solar surface
1662 viewed in white light. Sunspots and faculae are observed in the photosphere.

1663 **Pickup Ion:** An ion which has entered the solar system as a neutral particle and then becomes
1664 ionized either through charge exchange or photoionization. It is called a pickup ion
1665 because as soon as the neutral atom is ionized, it becomes attached to the magnetic field
1666 carried by the solar wind and so is "picked up" by the solar wind.

1667 **Pitch Angle:** In a plasma, the angle between the instantaneous velocity vector of a charged
1668 particle and the direction of the ambient magnetic field.

1669 **Plasma** (ions, electrons): A gas that is sufficiently ionized so as to affect its dynamical behavior.
1670 A plasma is a good electrical conductor and is strongly affected by magnetic fields. See
1671 also Anisotropic Plasma; Isotropic Plasma.

1672 **Plasma Instability** (ion, electron): When a plasma is sufficiently anisotropic, plasma waves
1673 grow, which in turn alter the distribution via wave-particle interactions. The plasma is
1674 "unstable."

1675 **Plasma Sheet:** A region in the center of the magnetotail between the north and south lobes. The
1676 plasma sheet is characterized by hot, dense plasma and is a high beta plasma region, in
1677 contrast to the low beta lobes. The plasma sheet bounds the neutral sheet where the
1678 magnetic field direction reverses from Earthward (north lobe direction) to anti-Earthward
1679 (south lobe direction).

1680 **Plasma Wave** (electrostatic/electromagnetic): A wave generated by plasma instabilities or other
1681 unstable modes of oscillation allowable in a plasma. "Chorus" and "Plasmasheric Hiss"
1682 are whistler wave modes. These are electromagnetic waves with frequencies below the
1683 electron cyclotron frequency. Electromagnetic ion cyclotron (EMIC) waves are ion
1684 cyclotron waves with frequencies below the proton cyclotron frequency.

1685 **Polar Cap Absorption Event (PCA):** An anomalous condition of the polar ionosphere whereby
1686 HF and VHF (3-300 MHz) radio waves are absorbed, and LF and VLF (3-300 kHz) radio



1687 waves are reflected at lower altitudes than normal. The cause is energetic particle
1688 precipitation into the ionosphere/atmosphere. The enhanced ionization caused by this
1689 precipitation leads to cosmic radio noise absorption and attenuation of that noise at the
1690 surface of the Earth. PCAs generally originate with major solar flares, beginning within a
1691 few hours of the event (after the flare particles have propagated to the Earth) and
1692 maximizing within a day or two after onset. As measured by a riometer (relative
1693 ionospheric opacity meter), the PCA event threshold is 2 dB of absorption at 30 MHz for
1694 daytime and 0.5 dB at night. In practice, the absorption is inferred from the proton flux at
1695 energies greater than 10 MeV, so that PCAs and proton events are simultaneous.
1696 However, the transpolar radio paths may still be disturbed for days, up to weeks,
1697 following the end of a proton event, and there is some ambiguity about the operational
1698 use of the term PCA.

1699 **Prominence:** A term identifying cloud-like features in the solar atmosphere. The features appear
1700 as bright structures in the corona above the solar limb and as dark filaments when seen
1701 projected against the solar disk. Prominences are further classified by their shape (for
1702 example, mound prominence, coronal rain) and activity. They are most clearly and most
1703 often observed in H alpha. See also Loop.

1704 **Radiation Belt:** Regions of the magnetosphere roughly 1.2 to 6 Earth radii above the equator in
1705 which charged particles are stably trapped by closed geomagnetic field lines. There are
1706 two belts. The inner belt's maximum proton density lies near 5000 km above the Earth's
1707 surface. Inner belt protons (10s of MeV) and electrons (100s of keV) and originate from
1708 the decay of secondary neutrons created during collisions between cosmic rays and upper
1709 atmospheric particles. The outer belt extends on to the magnetopause on the sunward side
1710 (10 Earth radii under normal quiet conditions) and to about 6 Earth radii on the nightside.
1711 The altitude of maximum proton density is near 16,000-20,000 km. Outer belt protons
1712 and electrons are lower energy (about 200 eV to 1 MeV). The origin of the particles
1713 (before they are energized to these high energies) is a mixture of the solar wind and the
1714 ionosphere. The outer belt is also characterized by highly variable fluxes of energetic
1715 electrons. The radiation belts are often called the "Van Allen radiation belts" because



1716 they were discovered in 1958 by a research group at the University of Iowa led by
1717 Professor J. A. Van Allen. See also Trapped Particle.

1718 **Ram Pressure:** Sometimes called “dynamic pressure”. The pressure exerted by a streaming
1719 plasma upon a blunt object.

1720 **Reconnection:** A process by which differently directed field lines link up allowing topological
1721 changes of the magnetic field to occur, determining patterns of plasma flow, and resulting
1722 in conversion of magnetic energy to kinetic and thermal energy of the plasma.
1723 Reconnection is invoked to explain the energization and acceleration of the
1724 plasmas/energetic particles that are observed in solar flares, magnetic substorms and
1725 storms, and elsewhere in the solar system.

1726 **Relativistic:** Charged particles (ions or electrons) which have speeds comparable to the speed of
1727 light.

1728 **Ring Current:** In the magnetosphere, a region of current that flows near the geomagnetic
1729 equator in the outer belt of the two Van Allen radiation belts. The current is produced by
1730 the gradient and curvature drift of the trapped charged particles of energies of 10 to 300
1731 keV. The ring current is greatly augmented during magnetic storms because of the hot
1732 plasma injected from the magnetotail and upwelling oxygen ions from the ionosphere.
1733 Further acceleration processes bring these ions and electrons up to ring current energies.
1734 The ring current (which is a diamagnetic current) causes a worldwide depression of the
1735 horizontal geomagnetic field during a magnetic storm.

1736 **Solar Energetic Particle (SEP):** An energetic particle of solar flare/interplanetary shock origin.

1737 **Sheath:** The plasma and magnetic fields in the downstream subsonic region after collisionless
1738 shocks. See Shock Wave.

1739 **Shock Wave:** A shock wave is characterized by a discontinuous change in pressure, density,
1740 temperature, and particle streaming velocity, propagating through a compressible fluid or
1741 plasma. Fast collisionless shock waves occur in the solar wind when fast solar wind
1742 overtakes slow solar wind with the difference in speeds being greater than the
1743 magnetosonic speed. Collisionless shock thicknesses are determined by the proton and

1744 electron gyroradii rather than the collision lengths. See also Diffusive Shock
1745 Acceleration; Solar Wind Shock.

1746 **Solar Activity:** Transient perturbations of the solar atmosphere as measured by enhanced x-ray
1747 emission (see x-ray flare class), typically associated with flares. Five standard terms are
1748 used to describe the activity observed or expected within a 24-h period:

1749 Very low - x-ray events less than C-class.

1750 Low - C-class x-ray events.

1751 Moderate - isolated (one to 4) M-class x-ray events.

1752 High - several (5 or more) M-class x-ray events, or isolated (one to 4).

1753 M5 or greater x-ray events.

1754 Very high - several (5 or more) M5 or greater x-ray events.

1755 **Solar Corona:** See Corona.

1756 **Solar Cycle:** The approximately 11 year quasi-periodic variation in the sunspot number. The
1757 polarity pattern of the magnetic field reverses with each cycle. Other solar phenomena,
1758 such as the 10.7-cm solar radio emission, exhibit similar cyclical behavior. The solar
1759 magnetic field reverses each sunspot cycle so there is a corresponding 22 year solar
1760 magnetic cycle.

1761 **Solar Energetic Particle (SEP) Event:** A high flux event of solar (low energy) cosmic rays.
1762 This is commonly generated by larger solar flares or CME shocks, and lasts, typically
1763 from minutes to days. See also Cosmic Ray.

1764 **Solar Maximum:** The month(s) during the sunspot cycle when the smoothed sunspot number reaches a maximum.

1766 **Solar Minimum:** The month(s) during the sunspot cycle when the smoothed sunspot number reaches a minimum.

1768 **Solar Orbiter:** A European Space Agency-led (ESA) mission intended to perform detailed
1769 measurements of the inner heliosphere and nascent solar wind to answer the question "How does



1770 the Sun create and control the heliosphere?" The mission will make observations of the Sun from
1771 an eccentric orbit moving as close as ~60 solar radii (R_S), or 0.284 astronomical units (AU) from
1772 the Sun.

1773

1774 **Solar Wind:** The outward flow of solar particles and magnetic fields from the Sun. Typically at
1775 1 AU, solar wind velocities are 300-800 km/s and proton and electron densities of 3-7 per
1776 cubic centimeter (roughly inversely correlated with velocity). The total intensity of the
1777 interplanetary magnetic field is nominally 3-8 nT.

1778 **Space Weather:** Dynamic variations at the Sun, in interplanetary space, in the Earth's and
1779 planetary magnetospheres, ionospheres and atmospheres associated with space
1780 phenomena.

1781 **Stratosphere:** That region of the Earth's atmosphere between the troposphere and the
1782 mesosphere. It begins at an altitude of temperature minimum at approximately 13 km and
1783 defines a layer of increasing temperature up to about 30 km.

1784 **Streamer:** A feature of the white light solar corona (seen in eclipse or with a coronagraph) that
1785 looks like a ray extending away from the Sun out to about 1 solar radius, having an arch-
1786 like base containing a cavity usually occupied by a prominence.

1787 **Substorm:** A substorm corresponds to an injection of charged particles from the magnetotail into
1788 the nightside magnetosphere. Plasma instabilities lead to the precipitation of the particles
1789 into the auroral zone ionosphere, producing intense aurorae. Potential drops along
1790 magnetic field lines lead to the acceleration of ~1 to 10 keV electrons with brilliant
1791 displays of aurora as the electrons impact the upper atmosphere. Enhanced ionospheric
1792 conductivity and externally imposed electric fields lead to the intensification of the
1793 auroral electrojets.

1794 **Sudden Impulse (SI):** An abrupt (10s of seconds) jump in the Earth's surface magnetic field.
1795 The positive sudden impulses (SI⁺s) are caused by fast forward shock impingement onto
1796 the magnetosphere.



1797 **Sunspot:** An area seen as a dark spot, in contrast with its surroundings, on the photosphere of the
1798 Sun. Sunspots are concentrations of magnetic flux, typically occurring in bipolar clusters
1799 or groups. They appear dark because they are cooler than the surrounding photosphere.
1800 Larger and darker sunspots sometimes are surrounded (completely or partially) by
1801 penumbrae. The dark centers are umbrae. The smallest, immature spots are sometimes
1802 called pores.

1803 **SWARM:** A European Space Agency (ESA) mission originally instrumented to study the Earth's
1804 magnetic field. The current goals are to study magnetospheric-ionospheric coupling and
1805 auroral space weather problems.

1806 **Tesla:** A unit of magnetic flux density (Weber/m²). A nanoTesla (nT) is 10⁻⁹ Teslas.

1807 **Termination Shock:** The shock wave in the solar wind which is caused by the abrupt
1808 deceleration of the solar wind as it runs into the local interstellar medium (LISM). It is
1809 thought to lie somewhere between 70 and 150 AU from the Sun.

1810 **Thermal Speed** (ion, electron): The random velocity of a particle associated with its
1811 temperature.

1812 **Thermosphere:** That region of the Earth's atmosphere where the neutral temperature increases
1813 with height. It begins above the mesosphere at about 80-85 km and extends upward to the
1814 exosphere.

1815 **Total Electron Content (TEC):** The column density of electrons in the Earth's ionosphere.

1816 **Trapped Particle:** Particles gyrating about magnetic field lines (e.g., in the Earth's
1817 magnetosphere). See also Magnetic Mirror and Pitch Angle.

1818 **Troposphere:** The lowest layer of the Earth's atmosphere, extending from the ground to the
1819 stratosphere, approximately 13 km altitude. In the troposphere, temperature decreases
1820 with height.

1821 **Ultraviolet (UV):** That part of the electromagnetic spectrum between 5 and 400 nm.

1822 **Ultra Low Frequency (ULF):** 1 milliHertz to 1 Hertz.



1823 **Very High Frequency (VHF):** That portion of the radio frequency spectrum from 3 to 300
1824 MHz.

1825 **Very Low Frequency (VLF):** That portion of the radio frequency spectrum from 3 to 300 kHz.

1826 **Van Allen Radiation Belt:** See Radiation Belt.

1827

REFERENCES

1829

1830 Acero, F.J., Vaquero, J.M., Gallego, M.C., and Garcia, J.A.: A limit for the values of the Dst
1831 geomagnetic index, *Geophys. Res. Lett.*, 45, doi.org/10.1029/2018GL079676, 2018.

1832 Agostinelli, S., et al.: GEANT4-A simulation toolkit, *Nucl. Instr. Meth. In Phys. Res. Sect. A*, 506,
1833 250, doi:10.1016/S0168-9002(03)01368-8, 2003.

1834 Aikio, A. T., Sergeev, V. A., Shukhtina, M. A., Vagina, L. I., Angelopoulos, V., and Reeves, G.
1835 D.: Characteristics of pseudobreakups and substorms observed in the ionosphere, at the
1836 geosynchronous orbit, and in the midtail, *J. Geophys. Res.*, 104, 12263-12287, doi:
1837 10.1029/1999JA900118, 1999.

1838 Akasofu, S.-I.: The development of the auroral substorm, *Plan. Spa. Phys.*, 12, 273-282, 1964.

1839 Akasofu, S.-I.: Magnetospheric substorms, a model, in *Solar Terrestrial Physics, Part III*, edited
1840 by D. Dyer, p. 131, D. Reidel Publ., Norwell, Mass, 1972.

1841 Akasofu, S.-I., and Chao, J. K.: Interplanetary shock waves and magnetospheric substorms,
1842 *Planetary and Space Science*, 28, 381-385, 1980.

1843 Akasofu, S.-I., and Kamide, Y.: Comment on “The extreme magnetic storm of 1-2 September
1844 1859” by B.T. Tsurutani, W.D. Gonzalez, G.S. Lakhina and S. Alex, *J. Geophys. Res.*, 110,
1845 A09226, doi:10.1029/2005JA011005, 2005.

1846 Alfvén, H.: *Cosmical Electrodynamics*, Oxford at the Clarendon Press, 1950.

1847 Anderson, B. J., and Hamilton, D.C.: Electromagnetic ion cyclotron waves stimulated by modest
1848 magnetospheric compressions, *J. Geophys. Res.*, 98, A7, 11369, 1993.

1849 Anderson, D. N., Decker, D. T., and Valladares, C. E.: Global theoretical ionospheric model
1850 (GTIM) in *Solar-Terrestrial Energy Program: Handbook of Ionospheric Models*, Natl. Oceanic
1851 and Atmos. Admin, Boulder, CO, 133-152, 1996.



1852 Araki, T., Tsunomura, S., and Kikuchi, T.: Local time variation of the amplitude of geomagnetic
1853 sudden commencements (SC) and SC-associated polar cap potential, *Earth Plan. Spa.*, 61, e13-
1854 e16, 2009.

1855 Araki, T.: Historically largest geomagnetic sudden commencement (SC) since 1868, *Earth, Plan.*
1856 *Spa.*, 66:164, <http://www.earth-planets-space.com/66/1/164>, 2014.

1857 Baker, D.N., Higbie, P.R., Belian, R.D., and Hones Jr., E.W.: Do Jovian electrons influence the
1858 terrestrial outer radiation zone?, *Geophys. Res. Lett.*, 6, 531-534,
1859 <https://doi.org/10.1029/GL006i006p00531>, 1979.

1860 Baker, D.N., Pulkkinen, T.I., Angelopoulos, V., Baumjohann, W., McPherron, R.L.: Neutral line
1861 model of substorms: Past results and present view, *J. Geophys. Res.*, 101, 12975-13010, 1996.

1862 Baker, D.N., Li, X., Blake, J.B., and Kanekal, S.: Strong electron acceleration in the Earth's
1863 magnetosphere, *Adv. Space Res.*, 21, 609-613, 1998.

1864 Barnes, C.W., and Simpson, J.A.: Evidence for interplanetary acceleration of nucleons in
1865 corotating interaction regions, *Astrophys. J.*, 210, L91, 1976.

1866 Bartels, J.: Terrestrial-magnetic activity in the years 1931 and 1932, *Terrestrial Magnetism and*
1867 *Atmospheric Electricity*, 39, 1-4, 1934.

1868 Belcher, J.W., and Davis Jr., L.: Large-amplitude Alfvén waves in the interplanetary medium, 2,
1869 *J. Geophys. Res.*, 76, 16, 3534-3563, 1971.

1870 Bieber, J. W., Clem, J., Evenson, P., Pyle, R., Sáiz, A., and Ruffolo, D.: *Astrophys. J.*, 771, 92,
1871 2013.

1872 Blake, J.B., Kolasinski, W.A., Filius, R.W., and Mullen, E.G.: Injection of electrons and protons
1873 with energies of tens of MeV into $L < 3$ on March 24, 1991, *Geophys. Res. Lett.*, 19, 821, 1992.

1874 Bombardieri, D. J., Duldig, M. L., Humble, J. E., and Michael, K. J.: An improved model for
1875 relativistic solar proton acceleration applied to the 2005 January 20 and earlier events,
1876 *Astrophysical J.*, 682, 1315-1327, 2008.

1877 Boyd, A.J., Spence, H.E., Claudepierre, S.G., Fennell, J.F., Blake, J.B., Baker, D.N., Reeves, G.D.,
1878 and Turner, D.L.: Quantifying the radiation belt seed population in the March 17, 2013 electron
1879 acceleration event, *Geophys. Res. Lett.*, 41, 2275-2281, <https://doi.org/10.1002/2014GL059626>,
1880 2014.



1881 Boyd, A.J., Spence, H.E., Huang, C.L., Reeves, G.D., Baker, D.N., Turner, D.L., Claudepierre,
1882 S.G., Fennell, J.F., Blake, J.B., and Shprits, Y.Y.: Statistical properties of the radiation belt seed
1883 population, *J. Geophys. Res.* 121, 7636-7646, <https://doi.org/10.1002/2016JA022652>, 2016.

1884 Brice, N.: Fundamentals of very low frequency emission generation mechanisms, *J. Geophys. Res.*,
1885 69, 4701, 1964.

1886 Burlaga, L., Sittler, E., Mariani, F., and Schwenn, R.: Magnetic loop behind an interplanetary
1887 shock: Voyager, Helios and IMP 8 observations, *J. Geophys. Res.*, 86, A8, 6673-6684, 1981.

1888 Burlaga, L., Fitzenreiter, R., Lepping, R., et al.: A magnetic cloud containing prominence material:
1889 January, 1997, *J. Geophys. Res.*, 103, A1, 77-285, 1998.

1890 Burton, R. K., McPherron, R. L., and Russell, C. T.: An empirical relationship between
1891 interplanetary conditions and Dst, *J. Geophys. Res.*, 80, 4204-4214, 1975.

1892 Carlson, C. W., McFadden, J. P., Ergun, R. E., Temerin, M., Peria, W., Mozer, F. S., Klumpar, D.
1893 M., Shelley, E. G., Peterson, W. K., Moebius, E., Elphic, R., Strangeway, R., Cattell, C., and Pfaff,
1894 R.: FAST observations in the downward auroral current region: Energetic upgoing electron beams,
1895 parallel potential drops, and ion heating, *Geophys. Res. Lett.*, 25, 2017-2020, 1998.

1896 Carrington, R.C: Description of a singular appearance seen in the Sun on September 1, 1859, *Mon.*
1897 *Not. R. Astron. Soc.*, XX, 13, 1859.

1898 Chan, A.A., Xia, M., and Chen, L.: Anisotropic Alfvén-ballooning modes in Earth's
1899 magnetosphere, *J. Geophys. Res.*, 99, 17351-17366, 1994.

1900 Chapman, S., and Bartels, J.: *Geomagnetism*, vol. 1, Oxford Univ. Press, New York, 1940.

1901 Choe, G.S., LaBelle-Hamer, N., Tsurutani, B.T., and Lee, L.C.: Identification of a driver gas
1902 boundary layer, *EOS Trans. AGU*, 73, 485, 1992.

1903 Chree, C.: Review of Maunder's recent investigations on the causes of magnetic disturbances,
1904 *Terr. Mag.*, 10, 9-14, 1905.

1905 Chree, C.: Some phenomena of sunspots and of terrestrial magnetism at Kew Observatory,
1906 *Philosophical Transactions of the Royal Society A*, 212, 75-116, 1913.

1907 Christon, S.P., and Simpson, J.A.: Separation of corotating nucleon fluxes from solar flare fluxes
1908 by radial gradients and nuclear composition, *Astrophys. J. Lett.*, 227, L49, 1979.

1909 Cliver, E.W.: The 1859 space weather event : Then and now, *Adv. Spa. Res.*, 38, 119-129, 2006.



1910 Cornwall, J.M.: Cyclotron instabilities and electromagnetic emission in the ultra low frequency
1911 and very low frequency ranges, *J. Geophys. Res.*, 70, 61-69, doi:10.1029/JA0761004p00900,
1912 1965.

1913 Daglis, I. A., Thorne, R.M., Baumjohann, W., and Orsini, S.: The terrestrial ring current: origin,
1914 formation and decay, *Rev. Geophys.*, 37, 4, 407-438, 1999.

1915 Dasso, S., Gómez, D., and Mandrini, C. H.: Ring current decay rates of magnetic storms: A
1916 statistical study from 1957 to 1998, *J. Geophys. Res.*, 107(A5), 1059, doi:10.1029/2000JA000430,
1917 2002.

1918 Davis, T. N., and Sugiura, M.: Auroral electrojet activity index AE and its universal time
1919 variations, *Journal of Geophysical Research*, 71, 785-801,
1920 <https://doi.org/10.1029/JZ071i003p00785>, 1966.

1921 Deng, Y., Sheng, C., Tsurutani, B.T., and Mannucci, A.J.: Possible influence of extreme magnetic
1922 storms on the thermosphere in the high latitudes, *Spa. Weath.*, 16,
1923 <https://doi.org/10.1029/2018SW001847>, 2018.

1924 Dessler, A.J., and Parker, E.N.: Hydromagnetic theory of magnetic storms, *J. Geophys. Res.*, 64,
1925 2239, 1959.

1926 Dryer, M., Smith, Z. K., Steinolfson, R. S., Mihalov, J. D., Wolfe, J. H., and Chao, J.-K.:
1927 Interplanetary disturbances caused by the August 1972 solar flares as observed by Pioneer 9, *J.*
1928 *Geophys. Res.*, 81, 4651-4663, doi: 10.1029/JA081i025p04651, 1976.

1929 Dungey, J.W.: Interplanetary magnetic field and the auroral zones, *Phys. Rev. Lett.*, 6, 47, 1961.

1930 Ebihara, Y., and Ejiri, M.: Modeling of solar wind control of the ring current buildup: A case study
1931 of the magnetic storms in April 1997, *Geophys. Res. Lett.*, 25(20), 3751-3754,
1932 doi:10.1029/1998GL900006, 1998.

1933 Echer, E., Gonzalez, W.D., Tsurutani, B.T., and Gonzalez, A.L.C.: Interplanetary conditions
1934 causing intense geomagnetic storms ($Dst \leq -100$ nT) during solar cycle 23 (1996-2006), *J.*
1935 *Geophys. Res.*, 113, A05221, doi:10.1029/2007JA012744, 2008a.

1936 Echer, E., Gonzalez, W.D., and Tsurutani, B.T.: Interplanetary conditions leading to superintense
1937 geomagnetic storms ($Dst \leq -250$ nT) during solar cycle 23, *Geophys. Res. Lett.*, 35, L06S03,
1938 doi:10.1029/2007GL031755, 2008b.

1939 Echer, E., Tsurutani, B.T., and Guarneri, F.L.: Solar and interplanetary origins of the November
1940 2004 superstorms, *Adv. Spa. Res.*, 44, 615-620, 2009.



1941 Echer, E., Tsurutani, B.T., Guarneri, F.L., and Kozyra, J.U.: Interplanetary fast forward shocks
1942 and their geomagnetic effects: CAWSES events, *J. Atmosph. Sol.-Terr. Phys.*, 73, 1330-1338,
1943 2011.

1944 Elkington, S.R., Hudson, M.K., and Chan, A.A.: Acceleration of relativistic electrons via drift-
1945 resonant interaction with toroidal-mode Pc-5 ULF oscillations, *Geophys. Res. Lett.*, 26, 3273,
1946 1999.

1947 Elkington, S.R., Hudson, M.K., and Chan, A.A.: Resonant acceleration and diffusion of outer zone
1948 electrons in an asymmetric geomagnetic field, *J. Geophys. Res.*, 108, doi: 10.129/2001JA009202,
1949 2003.

1950 Elvey, C. T.: Problems in auroral morphology, *Proceedings of the National Academy of Sciences*
1951 *Jan 1957*, 43 (1) 63-75; DOI: 10.1073/pnas.43.1.63, 1957.

1952 Engebretson, M.J., Peterson, W.K., Posch, J.L., Klatt, M.R., Anderson, B.J., Russell, C.T., Singer,
1953 H.J., Arnoldy, R.L., and Fukunishi, H.: Observations of two types of Pc 1-2 pulsations in the outer
1954 dayside magnetosphere, *J. Geophys. Res.* 107, A12, 1415, doi:10.1029/2001JA00198, 2002.

1955 Firoz, K. A., Gan, W. Q., Moon, Y.-J., and Li, C.: An interpretation of the possible mechanisms
1956 of two ground-level enhancement events, *Astrophys. J.*, 758, 119, 2012.

1957 Foster, J.C., Wygant, J.R., Hudson, M.K., Boyd, A.J., Baker, D.N., Erikson, P.J., and Spence,
1958 H.E.: Shock-induced prompt relativistic electron acceleration in the inner magnetosphere, *J.*
1959 *Geophys. Res. Spa. Phys.*, 120, 1661-1674, doi:10.1002/2014JA020642, 2015.

1960 Gonzalez, W.D., and Tsurutani, B.T.: Criteria of interplanetary parameters causing intense
1961 magnetic storms (Dst < -100 nT), *Planet. Spa. Sci.*, 35, 1101, 1987.

1962 Gonzalez, W.D., Joselyn, J.A., Kamide, Y., Kroehl, H.W., Rostoker, G., Tsurutani, B.T., and
1963 Vasyliunas, V.M.: What is a geomagnetic storm?, *J. Geophys. Res.*, 99, A4, 5571-5792, 1994.

1964 Gonzalez, W.D., Gonzalez, A.L.C., Dal Lago, A., Tsurutani, B.T., Arballo, J.K., Lakhina, G.S.,
1965 Buti, B., Ho, C.M., and Wu, S.-T.: Magnetic cloud field intensities and solar wind velocities,
1966 *Geophys. Res. Lett.*, 25, 963-966, 1998.

1967 Gopalswamy, N.: Coronal mass ejections and their heliospheric consequences, in First Asia-
1968 Pacific Sol. Phys. Meet, vol. 2, edited by A. Choudhuri and D. Banerjee, *Astron. Soc. India Conf.*
1969 *Series*, pp. 241–258, 21024 Mrach, Bengaluru, India, 2011.

1970 Gosling, J.T., Bame, S.J., and Feldman, W.C.: Solar wind speed variations: 1962, *J. Geophys.*
1971 *Res.*, 81, 5061, 1976.



1972 Guarnieri, F. L.: The nature of auroras during high-intensity long-duration continuous AE activity
1973 (HILDCAA) events: 1998–2001, in *Recurrent Magnetic Storms: Corotating Solar Wind Streams*,
1974 Geophys. Monogr. Ser., vol. 167, edited by B. T. Tsurutani et al., pp. 235–243, AGU, Washington,
1975 D.C., 2006.

1976 Guarnieri, F. L., Tsurutani, B. T., Gonzalez, W. D., Echer, E., Gonzalez, A. L. C., Grande, M., and
1977 Soraas, F.: ICME and CIR storms with particular emphasis on HILDCAA events, *ILWS Workshop*
1978 2006, Goa, 2006.

1979 Guarnieri, F.L., Tsurutani, B.T., Vieira, L.E.A., Hajra, R., Echer, E., Mannucci, A.J., and
1980 Gonzalez, W.D.: A correlation study regarding the AE index and ACE solar wind data for Alfvénic
1981 intervals using wavelet decomposition and reconstruction, *Nonl. Proc. Geophys.*, 25, 67-76,
1982 <https://doi.org/10.5194/npg-25-67-2018>, 2018.

1983 Haerendel, G.: Acceleration from field-aligned potential drops, *Astrophys. J. Suppl. Ser.*, 90, 765,
1984 1994.

1985 Hajra, R., Echer, E., Tsurutani, B.T., and Gonzalez, W.D.: Solar cycle dependence of high-
1986 intensity long-duration continuous AE activity (HILDCAA) events, relativistic electron
1987 predictors?, *J. Geophys. Res. Spa. Phys.*, 118, doi:10.1002/jgra.50530, 2013.

1988 Hajra, R., Echer, E., Tsurutani, B.T., and Gonzalez, W.D.: Solar wind-magnetosphere energy
1989 coupling efficiency and partitioning: HILDCAAs and preceding CIR storms during solar cycle 23,
1990 *J. Geophys. Res. Spa. Phys.*, 119, 2675-2690, 2014a.

1991 Hajra, R., Echer, E., Tsurutani, B. T., and Gonzalez, W. D.: Superposed epoch analyses of
1992 HILDCAAs and their interplanetary drivers: solar cycle and seasonal dependences, *J. Atmos. Sol.*
1993 *Ter. Phys.*, 121, 24-31, 2014b.

1994 Hajra, R., Tsurutani, B. T., Echer, E., and Gonzalez, W. D.: Relativistic electron acceleration
1995 during high-intensity, long-duration, continuous AE activity (HILDCAA) events: solar cycle
1996 phase dependences, *Geophys. Res. Lett.*, 41, 1876-1881, 2014c.

1997 Hajra, R., Tsurutani, B.T., Echer, E., Gonzalez, W.D., and Santolik, O.: Relativistic ($E > 0.6, > 2.0$,
1998 and > 4.0 MeV) electron acceleration at geosynchronous orbit during high-intensity long-duration
1999 continuous AE activity (HILDCAA) events, *Ap. J.*, 799:39, doi:10.1088/0004-637X/799/1/39,
2000 2015a.

2001 Hajra, R., Tsurutani, B. T., Echer, E., Gonzalez, W. D., Brum, C. G. M., Vieira, L. E. A., and
2002 Santolik, O.: Relativistic electron acceleration during HILDCAA events: are precursor CIR



2003 magnetic storms important?, *Earth, Planets and Space*, 67, 109, doi:10.1186/s40623-015-0280-5,

2004 2015b.

2005 Hajra, R., Tsurutani, B.T., Echer, E., Gonzalez, W.D., and Gjerloev, J.W.: Supersubstorms (SML
2006 < -2500 nT): Magnetic storm and solar cycle dependences, *J. Geophys. Res. Spa. Phys.*, 121, 7805-
2007 7816, doi:10.1002/2015JA021835, 2016.

2008 Hajra, R., Tsurutani, B. T., Brum, C. G. M., and Echer, E.: High-speed solar wind stream effects
2009 on the topside ionosphere over Arecibo: a case study during solar minimum, *Geophys. Res. Lett.*,
2010 44, 7607-7617, doi:10.1002/2017GL073805, 2017.

2011 Hajra, R., and Tsurutani, B. T.: Magnetospheric “killer” relativistic electron dropouts (REDs) and
2012 repopulation: a cyclical process, in *Extreme Events in Geospace: Origins, Predictability, and*
2013 *Consequences*, N. Buzulukova (Eds), pages 373-400, Elsevier, <https://doi.org/10.1016/B978-0-12-812700-1.00014-5>, 2018a.

2015 Hajra, R., and Tsurutani, B. T.: Interplanetary shock inducing magnetospheric supersubstorms
2016 (SML < -2500 nT): Unusual auroral morphologies and energy flow, *Astrophys. J.*, 858:123,
2017 <https://doi.org/10.3847/1538-4357/aabaed>, 2018b.

2018 Hale, G.E.: The spectrohelioscope and its work Part III. Solar eruptions and their apparent
2019 terrestrial effects, *Astrophys. J.*, 73:379-412, 1931.

2020 Halford, A.J., Fraser, B.J., and Morley, S.K.: EMIC wave activity during geomagnetic storm and
2021 nonstorm periods: CRRES results, *J. Geophys. Res.*, 115, A12248, doi:10.1029/2010JA015716,
2022 2010.

2023 Halford, A.J., McGregor, S.L., Murphy, K.R., Millan, R.M., Hudson, M.K., Woodger, L.A.,
2024 Cattel, C.A., Breneman, A.W., Mann, I.R., Kurth, W.S., Hospodarsky, G.B., Gkioulidou, M., and
2025 Fennel, J.F.: BARREL observations of an ICME-shock impact with the magnetosphere and the
2026 resultant radiation belt electron loss, *J. Geophys. Res. Spa. Phys.*, 120, 2557-2570, 2015.

2027 Halford, A.J., McGregor, S.L., Hudson, M.K., Milan, R.M., and Kress, B.T.: BARREL
2028 observations of a solar energetic electron and solar energetic proton event, *J. Geophys. Res. Spa.*
2029 *Phys.*, 121, 4205-4216, doi:10.1002/2016JA022462, 2016.

2030 Hamilton, D. C., Gloeckler, G., Ipavich, F. M., Stüdemann, W., Wilken, B., and Kremser, G.: Ring
2031 current development during the great geomagnetic storm of February 1986, *J. Geophys. Res.*,
2032 93(A12), 14343-14355, doi:10.1029/JA093iA12p14343, 1988.



2033 Harada, Y., Goto, A., Hasegawa, H., Fujikawa, N., Naoe, H., and Hirooka, T.: A major
2034 stratospheric sudden warming event in January 2009, *J. Atmos. Sci.*, 67, 2052,
2035 doi:10.1175/2009JA53310.1, 2010.

2036 Hellinger, P., and Travnicek, P.M.: Oblique proton fire hose instability in the expanding solar
2037 wind: Hybrid simulations, *J. Geophys. Res.*, 113, A10109, <https://doi.org/10.1029/2008JA013416>,
2038 2008.

2039 Heppner, J.P.: Note on the occurrence of world-wide SSCs during the onset of negative bays at
2040 College, Alaska, *J. Geophys. Res.*, 60, 29, 1955.

2041 Hodgson, R.: On a curious appearance seen in the Sun, *Mon. Not. R. Astron. Soc.*, XX, 15, 1859.

2042 Hollweg, J.V.: The solar wind: Then and now, in *Recurrent Magnetic Storms: Corotating Solar*
2043 *Wind Streams* (Vol. 167, pp. 19-27), edited by B.T. Tsurutani, R.L. McPherron, W.D. Gonzalez,
2044 G. Lu, J.H.A. Sobral and N. Gopalswamy, AGU Press, Wash D.C., 2006.

2045 Hones, E.W. Jr.: Transient phenomena in the magnetotail and their relation to substorms, *Spa. Sci.*
2046 *Rev.*, 23, 393-410, 1979.

2047 Horne, R. B., and Thorne, R. M.: Potential waves for relativistic electron scattering and stochastic
2048 acceleration during magnetic storms, *Geophys. Res. Lett.*, 25, 3011-3014,
2049 <https://doi.org/10.1029/98GL01002>, 1998.

2050 Huba, J.D., Joyce, G., and Fedder, J.A.: Sami2 is another model of the ionosphere (SAMI2): A
2051 new low-latitude ionosphere model, *J. Geophys. Res.*, 105 (A10), 23035, 2000.

2052 Huba, J.D., Dymond, K.F., Joyce, G., Budzien, S.A., Thonnard, S.E., Fedder, J.A., and McCoy,
2053 R.P.: Comparison of O+ density from ARGOS LORAAS data analysis and SAMI2 model results,
2054 *Geophys. Res. Lett.*, 29 (7), 6-1, doi:10.1029/2001GL013089, 2002.

2055 Hudson, M.K., Elkington, S.R., Lyon, J.G., Goodrich, C.C., and Rosenberg, T.J.: Simulations of
2056 radiation belt dynamics driven by solar wind variations, in *Sun-Earth Plasma Connections*, edited
2057 by J. Burch, R.L. Carovillano, and S.K. Antiochos, Amer. Geophys. Un. Press, Wash. D.C., 171,
2058 1999.

2059 Illing, R.M.E. and Hundhausen, A.J.: Disruption of a coronal streamer by an eruptive prominence
2060 and coronal mass ejection, *J. Geophys. Res.*, 91, A10, 10,951-10,960, 1986.

2061 Inan, U.S., Bell, T.F., and Helliwell, R.A.: Nonlinear pitch angle scattering of energetic electrons
2062 by coherent VLF waves in the magnetosphere, *J. Geophys. Res.*, 83, 3235-3253, 1978.



2063 Iyemori, T.: Storm-time magnetospheric currents inferred from midlatitude geomagnetic field
2064 variations, *J. Geomag. Geoelectr.* 42, 1249, 1990.

2065 Jordanova, V. K., Farrugia, C.J., Janoo, L., Quinn, J.M., Torbert, R.B., Ogilvie, K.W., and Belian,
2066 R.D.: October 1995 magnetic cloud and accompanying storm activity: Ring current evolution, *J.*
2067 *Geophys. Res.*, 103, 79-92, <https://doi.org/10.1029/97JA02367>, 1998.

2068 Joselyn, J. A., and Tsurutani, B. T.: Geomagnetic sudden impulses and storm sudden
2069 commencements, A note of terminology, *EOS*, 71, 47, 1808-1809, 1990.

2070 Kellerman, A.C., and Shprits, Y.Y.: On the influence of solar wind conditions on the outer-
2071 electron radiation belts, *J. Geophys. Res.*, 117, A05127, doi:0.1029/2011JA017253, 2012.

2072 Kellerman, A.C., Shprits, Y.Y., Kondrashov, D., Subbotin, D., Makarevich, R.A., Donovan, E.,
2073 and Nagal, T.: Three-dimensional data assimilation and reanalysis of radiation belt electrons:
2074 Observations of a four-zone structure using five spacecraft and the VERB code, *J. Geophys. Res.*
2075 *Spa. Phys.*, 119, doi:10.1002/2014JA020171, 2014.

2076 Kelley, M.C., Fejer, B.G., and Gonzales, C.A.: An explanation for anomalous equatorial
2077 ionospheric electric field associated with a northward turning of the interplanetary magnetic field,
2078 *Geophys. Res. Lett.*, 6(4), 301, 1979.

2079 Kelley, M.C., Makela, J.J., Chau, J.L., and Nicolls, M.J.: Penetration of the solar wind electric
2080 field into the magnetosphere/ionosphere system, *Geophys. Res. Lett.*, 30(4), 1158,
2081 doi:10.1029/2002GL016321, 2003.

2082 Kennel, C.F., and Petschek, H.E.: Limit of stably trapped particle fluxes, *J. Geophys. Res.* 71, 1-
2083 28, 1966.

2084 Kennel, C.F., Edmiston, J.P., and Hada, T.: A quarter century of collisionless shock research in
2085 Collisionless Shocks in the Heliosphere: A Tutorial Review, *Geophys. Mon. Ser.*, vol. 34, 1, AGU,
2086 Wash. D.C., 1985.

2087 Kikuchi, T., and Hashimoto, K.K.: Transmission of the electric fields to the low latitude
2088 ionosphere in the magnetosphere-ionosphere current circuit, *Geosc. Letts.*, 3:4,
2089 doi:10.1186/s40562-016-0035-6, 2016.

2090 Kimball, D.S.: A study of the aurora of 1859, *Sci. Rept.* 6, UAG-R109, Univ. of Alaska, Fairbanks,
2091 Alaska, 1960.

2092 Klein, L.W., and Burlaga, L.F.: Interplanetary magnetic clouds at 1 AU, *J. Geophys. Res.*, 87, 613,
2093 1982.



2094 Kozyra, J.U., Jordanova, V.K., Horne, R.B., and Thorne, R.M.: Modeling of the contribution of
2095 electromagnetic ion cyclotron (EMIC) waves to stormtime ring current erosion, in *Magnetic*
2096 *Storms*, Geophys. Mon. Ser., 98, edited by B.T. Tsurutani et al., 187-202, 1997.

2097 Kozyra, J. U., Liemohn, M. W., Clauer, C. R., Ridley, A. J., Thomsen, M. F., Borovsky, J. E.,
2098 Roeder, J. L., Jordanova, V. K., and Gonzalez, W. D.: Multistep Dst development and ring current
2099 composition changes during the 4-6 June 1991 magnetic storm, *J. Geophys. Res.*, 107(A8), 1224,
2100 doi:10.1029/2001JA000023, 2002.

2101 Kozyra, J.U., Nagy, A.F., Slater, D.W.: High-altitude energy source(s) for stable auroral red arcs,
2102 *Rev. Geophys.*, 35, 155-190, 2006a.

2103 Kozyra, J. U., Crowley, G., Emery, B. A., Fang, X., Maris, G., Mlynczak, M. G., Niciejewski, R.
2104 J., Palo, S. E., Paxton, L. J., Randal, C. E., Rong, P. P., III Russell, J. M., Skinner, W., Solomon,
2105 S. C., Talaat, E. R., Wu, Q., and Yee, J. H.: Response of the upper/middle atmosphere to coronal
2106 holes and powerful high-speed solar wind streams in 2003, in *Recurrent Magnetic Storms:*
2107 *Corotating Solar Wind Streams*, Geophys. Monogr. Ser., vol. 167, edited by B. T. Tsurutani et al.,
2108 pp. 319, AGU, Washington, D.C., doi: 10.1029/167GM24, 2006b.

2109 Kozyra, J.U., Manchester IV, W.B., Escoubet, C.P. et al.: Earth's collision with a solar filament
2110 on 21 January 2005: Overview, *J. Geophys. Res. Spa. Phys.*, 118, doi:10.1002/jgra.50567, 2013.

2111 Krieger, A.S., Timothy, A.F., and Roelof, E.C.: A coronal hole and its identification as the source
2112 of a high velocity solar wind stream, *Sol. Phys.* 23, 123, 1973.

2113 Lakhina, G.S.: Magnetic reconnection, *Bull. Astr. Soc. India*, 28, 593-646, 2000.

2114 Lakhina, G.S., Alex, S., Tsurutani, B.T., and Gonzalez, W.D.: Supermagnetic storms: Hazards to
2115 society, in *Extreme Events and Natural Hazards: The Complexity Perspective*, Geophys. Mon.,
2116 196, 267-278, 2012.

2117 Lakhina, G.S., and Tsurutani, B.T.: Superg geomagnetic storms: Past, present and future, Chapter 7
2118 in *Extreme Events in Geospace*, 157, edited by N. Buzulokova, Elsevier, 2017.

2119 Lam, M.M., Chisham, G., and Freeman, M.P.: The interplanetary magnetic field influences mid-
2120 latitude surface atmospheric pressure, *Env. Res. Lett.*, 8, doi:10.1088/1748-9326/8/4/045001,
2121 2013.

2122 Lario, D.: Estimation of the solar flare neutron worst-case fluxes and fluences for missions
2123 traveling close to the Sun, *Space Weather*, 10, S03002, doi: 10.1029/2011SW000732, 2012.



2124 Lee, K. H.: Generation of parallel and quasi-perpendicular EMIC waves and mirror waves by fast
2125 magnetosonic shocks in the solar wind, *J. Geophys. Res.*, 122, 7307-7322, 2017.

2126 Lepri, S.T., and Zurbuchen, T.H.: Direct observational evidence of filament material within
2127 interplanetary coronal mass ejections, *Astrophys. J. Lett.*, 723(1), L22-L27.
2128 <https://doi.org/10.1088/2041-8205/723/1/L22>, 2010.

2129 Li, X., Roth, I., Temerin, M., Wygant, J.R., Hudson, M.K., and Blake, J.B.: Simulation of the
2130 prompt energization and transport of radiation belt particles during the March 24, 1991 SSC,
2131 *Geophys. Res. Lett.*, 20, 22, 2423-2426, 1993.

2132 Li, X.-L., Temerin, M., Baker, D.N., Reeves, G.D., and Larson, D.: Quantitative prediction of
2133 radiation belt electrons at geostationary orbit based on solar wind measurements, *Geophys. Res.*
2134 *Lett.*, 28, 1887, 2001.

2135 Li, X., Baker, D.N., Temerin, M., Reeves, G., Friedel, R., and Shen, C.: Energetic electrons, 50
2136 keV to 6 MeV, at geosynchronous orbit: their responses to solar wind variations, *Space Weather*,
2137 3. S04001. <https://doi.org/10.1029/2004SW000105>, 2005.

2138 Li, X., Temerin, M., Tsurutani, B.T., and Alex, S.: Modeling of 1-2 September 1859 super
2139 magnetic storm, *Adv. Spa. Res.*, 38(2), 273-279, <https://doi.org/10.1016/j.asr.2005.06.070>, 2006.

2140 Lui, A.T.Y, Chang, C.-L., Mankofsky, A., Wong, H.-K., and Winske, D.: A cross-field current
2141 instability for substorm expansions, *J. Geophys. Res.*, 96, 11389, 1991.

2142 Lui, A.T.Y.: Current disruption in the Earth's magnetosphere: Observations and models, *J.*
2143 *Geophys. Res.*, 101, 13067-13088, doi:10.1029/96JA00079, 1996.

2144 Manchester, W.B. IV, Ridley, A.J., Gombosi, T.I., and Dezeeuw, D.L.: Modeling the Sun-to-Earth
2145 propagation of a very fast CME, *Adv. Space Res.*, 38, 253-262, 2006.

2146 Mann, I.R., O'Brien, T.P., and Milling, D.K.: Correlations between ULF wave power, solar wind
2147 speed, and relativistic electron flux in the magnetosphere: solar cycle dependence, *J. Atmosph.*
2148 *Solar-Terr. Phys.*, 66, 187, 2004.

2149 Mannucci, A.J., Tsurutani, B.T., Iijima, B.A., Konjathy, A., Saito, A., Gonzalez, W.D., Guarneri,
2150 F.L., Kozyra, J.U., and Skoug, R.: Dayside global ionospheric response to the major interplanetary
2151 events of October 29-30, 2003 "Halloween storms", *Geophys. Res. Lett.*, 32, L12S02,
2152 doi:10.1029/2004GL021467, 2005.

2153 Mannucci, A.J., Tsurutani, B.T., Abdu, M.A., Gonzalez, W.D., Komjathy, A., Echer, E., Iijima,
2154 B.A., Crowley, G., and Anderson, D.: Superposed epoch analysis of the dayside ionospheric



2155 response to four intense geomagnetic storms, *J. Geophys. Res.*, 113, A00A02,
2156 doi:10.1029/2007JA012732, 2008.

2157 Matteini, L., Landi, S., Hellinger, P., and Velli, M.: Parallel proton fire hose instability in the
2158 expanding solar wind: Hybrid simulations, *J. Geophys. Res.*, 111, A10101,
2159 <https://doi.org/10.1029/2006JA011667>, 2006.

2160 Matteini, L., Landi, S., Hellinger, P., Pantellini, F.G., Maksimovic, M., Velli, M., et al.: The
2161 evolution of the solar wind proton temperature anisotropy from 0.3 to 2.5 AU, *Geophys. Res. Lett.*,
2162 34, L20105, <https://doi.org/10.1029/2007GL030920>, 2007.

2163 Maunder, E. W.: Magnetic Disturbances, 1882 to 1903, as recorded at the Royal Observatory,
2164 Greenwich, and their Association with Sun-spots, *Monthly Notices of the Royal Astronomical
2165 Society*, 65, 2-18, <https://doi.org/10.1093/mnras/65.1.2>, 1904.

2166 Mays, M. L., Thompson, B.J., Jian, L.K., Colaninno, R.C., Odstrcil, D., Mostl, C., Temmer, M.,
2167 Savani, N.P., Collinson, G., Taktakishvili, A., MacNeice, P.J., and Zheng, Y.: *Astrophys J.*,
2168 812:145, doi:10.1088/004-637X/812/2/145, 2015.

2169 McComas, D.J. et al.: Ulysses second fast latitude scan; complexity near solar maximum and the
2170 reformation of polar coronal holes, *Geophys. Res. Lett.*, 29(9), 1290, doi:10.1029/2001GL014164,
2171 2002.

2172 McDonald, F.B., Teegarden, B.J., Trainor, J.H., Von Rosenvinge, T.T., and Webber, W.R.: The
2173 interplanetary acceleration of energetic nucleons, *Astrophys. J. Lett.*, 203, L149, 1976.

2174 Mendes, O., Domingues, M. O., Echer, E., Hajra, R., and Menconi, V. E.: Characterization of
2175 high-intensity, long-duration continuous auroral activity (HILDCAA) events using recurrence
2176 quantification analysis, *Nonlin. Processes Geophys.*, 24, 407-417, 2017.

2177 Meng, X., Tsurutani, B.T., and Mannucci, A.J.: The solar and interplanetary causes of superstorms
2178 (minimum $Dst \leq -250$ nT) during the space age, *J. Geophys. Res.*, 124. <https://doi.org/10.1029/2018JA026425>, 2019.

2179

2180 Meredith, N. P., Horne, R.B., Iles, R.H.A., Thorne, R.M., Heynderickx, D., and Anderson, R. R.:
2181 Outer zone relativistic electron acceleration associated with substorm-enhanced whistler mode
2182 chorus, *J. Geophys. Res.*, 107, A7, 1144, doi:10.1029/2001JA900146, 2002.

2183 Miyake, F., Nagaya, K., Masuda, K., and Nakamura, T.: A signature of cosmic-ray increase in AD
2184 774-775 from tree rings in Japan, *Nature Lett.*, doi:10.1038/nature11123, 2012.



2185 Miyoshi, Y., Jordanova, V.K., Morioka, A., and Evans, D.S.: Solar cycle variations of the electron
2186 radiation belts: Observations and radial diffusion simulation, *Space Weather*, 2, S10S02,
2187 doi:10.1029/2004SW000070, 2004.

2188 Montreal MacMahon, R., and Llop, C.: Ring current decay time model during geomagnetic storms:
2189 A simple analytical approach, *Ann. Geophys.*, 26, 2543-2550, 2008.

2190 Mostl, C., Rollett, T., Frahm, R.A., Liu, Y.D., Long, D.M., Colaninno, R.C., Reiss, M.A., Temmer,
2191 M., Farrugia, C.J., Posner, A., Dumbovic, M., Janvier, M., Demoulin, P., Boakes, P., Devos, A.,
2192 Kraaijkamp, E., Mays, M.L., and Vršnak, B.: Strong coronal channeling and interplanetary
2193 evolution of a solar storm up to Earth and Mars, *Nat. Comm.*, 6:7135, doi:10.1038/ncomms8135,
2194 2015.

2195 Newton, H.W.: Solar flares and magnetic storms, *Mon. Not. R. Astron. Soc.*, 103, 244, 1943.

2196 Ngwira, C.M., Pulkkinen, A., Kuznetsova, M.M., and Glocer, A.: Modeling extreme “Carrington-
2197 type” space weather events using three dimensional global MHD simulations, *J. Geophys. Res.
Spa. Phys.* 119, 4456-4474, <https://doi.org/10.1002/2013JA019661>, 2014.

2199 Nishida, A., and Jacobs, J.A.: Equatorial enhancement of world-wide changes, *J. Geophys. Res.*,
2200 67, 12, 4937-4940, 1962.

2201 Nishida, A.: Coherence of geomagnetic DP2 fluctuations with interplanetary magnetic variations,
2202 *J. Geophys. Res.*, 73, 5549, 1968.

2203 Nishida, A.: *Geomagnetic Diagnosis of the Magnetosphere*, Springer-Verlag, New York, 1978.

2204 Nishiura, M., Yoshida, Z., Saitoh, H., Yano, Y., Kawazura, Y., Nogami, T., Yamasaki, M.,
2205 Mushiake, T., and Kashyap, A.: Improved beta (local beta > 1) and density in electron cyclotron
2206 resonance heating on the RT-1 magnetosphere plasma, *Nuc. Fus.*, 55, 053019, doi:10.1088/0029-
2207 5515/5/053019, 2015.

2208 Obayashi, T.: The interaction of solar plasma with geomagnetic field, disturbed conditions, in *Sol.
Terr. Phys.*, edited by J.W. King and W.S. Newman, 107 pp., Academic Press, London, 1967.

2210 O’Brien, T. P., and McPherron, R. L.: An empirical phase space analysis of ring current dynamics:
2211 Solar wind control of injection and decay, *J. Geophys. Res.*, 105(A4), 7707-7719,
2212 doi:10.1029/1998JA000437, 2000.

2213 O’Brien, T.P., McPherron, R.L., Sornette, D., Reeves, G.D., Friedel, R., and Singer, H.J.: Which
2214 magnetic storms produce relativistic electrons at geosynchronous orbit?, *J. Geophys. Res.*, 106,
2215 15533, 2001.



2216 Olsen, J.V., and Lee, L.C.: PC1 wave generation by sudden impulses, *Plan. Spa. Sci.*, 31, 295,
2217 1983.

2218 Pérez-Peraza, J., Vashenyuk, E. V., Miroshnichenko, L. I., Balabin, Yu. V., and Gallegos-Cruz,
2219 A.: Impulsive, stochastic, and shock wave acceleration of relativistic protons in large solar events
2220 of 1989 September 29, 2000 July 14, 2003 October 28, and 2005 January 20, *Astrophys. J.*, 695,
2221 865-873, 2009.

2222 Perreault, P., and Akasofu, S. I.: A study of geomagnetic storms, *Geophysical Journal
2223 International*, 54, 547-573, <https://doi.org/10.1111/j.1365-246X.1978.tb05494.x>, 1978.

2224 Pesses, M.E., Van Allen, J.A., and Goertz, C.K.: Energetic protons associated with interplanetary
2225 active regions 1-5 AU from the sun, *J. Geophys. Res.*, 83, 553, 1978.

2226 Pesses, M.E., Tsurutani, B.T., Van Allen, J.A., and Smith, E.J.: Acceleration of energetic protons
2227 by interplanetary shocks, *J. Geophys. Res.*, 84, 7297, 1979.

2228 Phillips, J.L., Bame, S.J., Feldman, W.C., Goldstein, B.E., Gosling, J.T., Hammond, C.M.,
2229 McComas, D.J., Neugebauer, M., Scime, E.E., and Suess, S.T.: Ulysses solar wind plasma
2230 observations at high southerly latitudes, *Science*, 268, 1030, 1995.

2231 Reames, D.V.: Particle acceleration at the Sun and in the heliosphere, *Spa. Sci. Rev.*, 90, 413-491,
2232 1999.

2233 Reeves, G. D., Cayton, T. E., Gary, S. P., and Belian, R. D.: The great solar energetic particle
2234 events of 1989 observed from geosynchronous orbit, *J. Geophys. Res.*, 97, 6219-6226, 1992.

2235 Reeves, G.D., Spence, H.E., Henderson, M.G., Morley, S.K., Friedel, R.H.W., Funsten, H.O.,
2236 Baker, D.N., Kanekal, S.G., Blake, J.B., Fennell, J.F., Claudepierre, S.G., Thorne, R.M., Turner,
2237 D.L., Kletzing, C.A., Kurth, W.S., Larsen, B.A., and Niehof, J.T.: Electron acceleration in the
2238 heart of the Van Allen radiation belts, *Science*, 341, 991-994,
2239 <https://doi.org/10.1126/science.1237743>, 2013.

2240 Reeves, G.D., Friedel, R.H.W., Larsen, B.A., Skoug, R.M., Funsten, H.O., Claudepierre, S.G.,
2241 Fennell, J.F., Turner, D.L., Denton, M.H., Spence, H.E., Blake, J.B., and Baker, D.N.: Energy
2242 dependent dynamics of keV to MeV electrons in the inner zone, outer zone, and slot regions, *J.
2243 Geophys. Res.* 121, 397-412, <https://doi.org/10.1002/2015JA021569>, 2016.

2244 Remya, B., Tsurutani, B.T., Reddy, R.V., Lakhina, G.S., and Hajra, R.: Electromagnetic cyclotron
2245 waves in the dayside subsolar outer magnetosphere generated by enhanced solar wind pressure:



2246 EMIC wave coherency, *J. Geophys. Res. Spa. Phys.*, **120**, 7536-7551, doi:10.1002/2015JA021327,
2247 2015.

2248 Riley, P., Caplan, R.M., Giacalone, J., Lario, D., and Liu, Y.: Properties of the fast forward shock
2249 driven by the 2012 July 23 extreme coronal mass ejection, *Astrophys. J.*, **819**:57,
2250 doi:10.3847/0004-637X/819/1/57, 2016.

2251 Saikin, A.A., Zhang, J.-C., Smith, C., Spence, H.E., Torbert, R.B., and Kletzing, C.A.: The
2252 dependence on geomagnetic conditions and solar wind dynamic pressure of the spatial
2253 distributions of EMIC waves observed by the Van Allen Probes, *J. Geophys. Res. Spa. Phys.*, **121**,
2254 4362-4377, doi:10.1002/2016JA022523, 2016.

2255 Saitoh, H., Yano, Y., Yoshida, Z., Nishiura, M., Morikawa, J., Kawazura, Y., Nogami, T., and
2256 Yamasaki, M.: Observation of a new high- β and high-density state of a magnetospheric plasma in
2257 RT-1, *Phys. Plas.* **21**, 082511, 2014.

2258 Saldanha, R., Krucker, S., and Lin, R. P.: Hard x-ray spectral evolution and production of solar
2259 energetic particle events during the January 2005 x-class flares, *Astrophys. J.*, **673**, 1169-1173,
2260 2008.

2261 Scherhag, R.: Stratospheric temperature changes and the associated changes in pressure
2262 distribution, *J. Meteor.*, **17**, 575, doi:10.1175/1520-0469(1960)017<0575:STCATA>2.0.CO;2,
2263 1960.

2264 Sckopke, N.: A general relation between the energy of trapped particles and the disturbance field
2265 near the Earth, *J. Geophys. Res.*, **71**, 3125, 1966.

2266 Schrijver, C. J., Beer, J., Baltensperger, U., Cliver, E. W., Güdel, M., Hudson, H. S., McCracken,
2267 K. G., Osten, R. A., Peter, T., Soderblom, D. R., Usoskin, I. G., and Wolff, E. W.: Estimating the
2268 frequency of extremely energetic solar events, based on solar, stellar, lunar, and terrestrial records,
2269 *J. Geophys. Res.*, **117**, A08103, doi: 10.1029/2012JA017706, 2012.

2270 Sheeley, N.R. Jr., Harvey, J.W., and Feldman, W.C.: Coronal holes, solar wind streams and
2271 recurrent geomagnetic disturbances: 1973-1976, *Sol. Phys.*, **49**, 271, 1976.

2272 Sheeley, N.R. Jr., Asbridge, J.R., Bame, S.J., and Harvey, J.W.: A pictoral comparison of
2273 interplanetary magnetic field polarity, solar wind speed and geomagnetic disturbance index during
2274 the sunspot cycle, *Sol. Phys.*, **52**, 485, 1977.

2275 Simpson, J.A., Lentz, G.A., McKibben, R.B., O'Gallagher, J.J., Schroeder, W., and Tuzzolino,
2276 A.J.: Preliminary documentation for the University of Chicago charged particle instrument data



2277 from the Pioneer 10.11 spacecraft as submitted to NASA NSSDG, *NSSDC Doc. B.*, GSFC,
2278 Greenbelt, Md, 1974.

2279 Siscoe, G. L.: A quasi-self-consistent axially symmetric model for the growth of a ring current
2280 through earthward motion from a pre-storm configuration, *Planet. Spa. Sci.*, 27, 285-295, 1979.

2281 Smith, E.J., Connor, B.V., and Foster Jr., G.T.: Measuring the magnetic fields of Jupiter and the
2282 outer solar system, *IEE Trans. Magn.*, MAG-11, 962, 1975.

2283 Smith, E.J., and Wolfe, J.H.: Observations of interaction regions and corotating shocks between
2284 one and five AU: Pioneers 10 and 11, *Geophys. Res. Lett.*, 3, 137-140, 1976.

2285 Smith, E.J., Tsurutani, B.T., and Rosenberg, R.L.: Observations of the interplanetary sector
2286 structure up to heliographic latitudes of 16°: Pioneer 11, *J. Geophys. Res.*, 83, 717-723, 1978.

2287 Soraas, F., Aarsnes, K., Oksavik, K., Sandanger, M.I., Evans, D.S., and Greer, M.S.: Evidence for
2288 particle injection as the case of Dst reduction during HILDCAA events, *J. Atmos. Sol.-Terr. Phys.*,
2289 66, 177-187, 2004.

2290 Souza, A. M., Echer, E., Bolzan, M. J. A., and Hajra, R.: A study on the main periodicities in
2291 interplanetary magnetic field Bz component and geomagnetic AE index during HILDCAA events
2292 using wavelet analysis, *J. Atmos. Sol. Terr. Phys.*, 149, 81-86, 2016.

2293 Souza, A. M., Echer, E., Bolzan, M. J. A., and Hajra, R.: Cross-correlation and cross-wavelet
2294 analyses of the solar wind IMF Bz and auroral electrojet index AE coupling during HILDCAAs,
2295 *Ann. Geophys.*, 36, 205-211, 2018.

2296 Stern, D.P.: The motion of a proton in the equatorial magnetosphere, *J. Geophys. Res.*, 80, 595,
2297 1975.

2298 Sugiura, M.: Hourly values of equatorial Dst for the IGY, *Annual International Geophysical Year*,
2299 vol. 35, Pergamon, New York, p. 9, 1964.

2300 Summers, D., Ni, B., and Meredith, N.P.: Timescale for radiation belt electron acceleration and
2301 loss due to resonant wave-particle interactions: 2. Evaluation for VLF chorus, ELF hiss, and
2302 electromagnetic ion cyclotron waves, *J. Geophys. Res.*, 112, A04207,
2303 <https://doi.org/10.1029/2006JA011993>, 2007.

2304 Tan, B.: Small-scale microwave bursts in long-duration solar flares, *Astrophys. J.*, 773, 165, 2013.

2305 Thomson, N. R., Rodger, C. J., and Clilverd, M. A.: Large solar flares and their ionospheric D
2306 region enhancements, *J. Geophys. Res.*, 110, A06306, doi: 10.1029/2005JA011008, 2005.



2307 Thorne, R.M., Smith, E.J., Fiske, K.J., and Church, S.R.: Intense variation of ELF hiss and chorus
2308 during isolated substorms, *Geophys. Res. Lett.*, 1, 193-196, doi:10.1029/GL001i005p00193, 1974.

2309 Thorne, R.M., O'Brien, T.P., Shprits, Y.Y., Summers, D., and Horne, R.B.: Timescale for MeV
2310 electron microburst loss during geomagnetic storms, *J. Geophys. Res.*, 110, A09202,
2311 <https://doi.org/10.1029/2004JA010882>, 2005.

2312 Thorne, R.M., Li, W., Ni, B., Ma, Q., Bortnik, J., Chen, L., Baker, D.N., Spence, H.E., Reeves,
2313 G.D., Henderson, M.G., Kletzing, C.A., Kurth, W.S., Hospodarsky, G.B., Blake, J.B., Fennell,
2314 J.F., Claudepierre, S.G., and Kanekal, S.G.: Rapid local acceleration of relativistic radiation-belt
2315 electrons by magnetospheric chorus, *Nature* 504, 411-414, 2013.

2316 Thomson, N.R., Rodger, C.J., and Dowden, R.L.: Ionosphere gives the size of the greatest solar
2317 flare, *Geophys. Res. Lett.*, 31, L06803, doi:10.1029/2003GL019345, 2004.

2318 Tinsley, B.A., and Deen, G.W.: Apparent tropospheric response to MeV-GeV particle flux
2319 variations: A connection via electrofreezing of supercooled water in high-level clouds?, *J.*
2320 *Geophys. Res.*, 96, 22,283, doi:10.1029/91JD02473, 1991.

2321 Tsurutani, B.T., and Smith, E.J.: Postmidnight chorus: A substorm phenomenon, *J. Geophys. Res.*,
2322 79, 1, 118-127, 1974.

2323 Tsurutani, B.T., Smith, E.J., West Jr., H.I., and Buck, R.M.: Chorus, energetic electrons and
2324 magnetospheric substorms, in *Wave Instabilities in Space Plasmas*, edited by P.J. Palmadesso and
2325 K. Papadopoulos, 55, 1979.

2326 Tsurutani, B.T., Smith, E.J., Pyle, K.R., and Simpson, J.A.: Energetic protons accelerated at
2327 corotating shocks: Pioneer 10 and 11 observations from 1 to 6 AU, *J. Geophys. Res.*, 87, A9, 7389-
2328 7404, 1982.

2329 Tsurutani, B.T., and Lin, R.P.: Acceleration of >47 keV ions and > 2 keV electrons by
2330 interplanetary shocks at 1 AU, *J. Geophys. Res.*, 90, A1, 1-11, 1985.

2331 Tsurutani, B.T., and Gonzalez, W.D.: The cause of high-intensity long-duration continuous AE
2332 activity (HILDCAAs): Interplanetary Alfvén wave trains, *Plan. Spa. Sci.*, 35, 4, 405-412, 1987.

2333 Tsurutani, B.T., Gonzalez, W.D., Tang, F., Akasofu, S.-I., and Smith, E.J.: Origin of interplanetary
2334 southward magnetic fields responsible for major magnetic storms near solar maximum (1978-
2335 1979), *J. Geophys. Res.*, 93, A8, 8518-8531, 1988.

2336 Tsurutani, B.T., Gonzalez, W.D., Tang, F., and Lee, Y.T.: Great magnetic storms, *Geophys. Res.*
2337 *Lett.*, 19, 73-76, 1992a.



2338 Tsurutani, B.T., Gonzalez, W.D., Tang, F., Lee, Y.T., Okada, M., and Park, D.: Reply to L.J.
2339 Lanzerotti: Solar wind ram pressure corrections and an estimation of the efficiency of viscous
2340 interaction, *Geophys. Res. Lett.*, 19, 19, 1993-1994, 1992b.
2341 Tsurutani, B.T., and Gonzalez, W.D.: The causes of geomagnetic storms during solar maximum,
2342 *EOS*, 75, 5, 49-56, 1994.
2343 Tsurutani, B.T., Gonzalez, W.D., Zhou, X.-Y., Lepping, R.P., and Bothmer, V.: Properties of slow
2344 magnetic clouds, *J. Atmos. Sol.-Terr. Phys.*, 66, 147-151, 1994.
2345 Tsurutani, B.T., Gonzalez, W.D., Gonzalez, A.L.C., Tang, F., Arballo, J.K., and Okada, M.:
2346 Interplanetary origin of geomagnetic activity in the declining phase of the solar cycle, *J.*
2347 *Geophys. Res.*, 100, 21,717, 1995.
2348 Tsurutani, B.T., and Lakhina, G.S.: Some basic concepts of wave-particle interactions in
2349 collisionless plasmas, *Rev. Geophys.*, 35, 4, 491-502, 1997.
2350 Tsurutani, B.T., and Gonzalez, W.D.: The interplanetary causes of magnetic storms: A review, in
2351 *Magnetic Storms*, edited by Tsurutani, Gonzalez, Kamide and Arballo, AGU Press, Wash. D.C.,
2352 98, 77-89, 1997.
2353 Tsurutani, B.T., Arballo, J.K., Lakhina, G.S., Ho, C.M., Ajello, J., Pickett, J.S., Gurnett, D.A.,
2354 Lepping, R.P., Peterson, W.K., Rostoker, G., Kamide, Y., and Kokubun, S.: The January 10, 1997
2355 auroral hot spot, horseshoe aurora and first substorm: A CME loop?, *Geophys. Res. Lett.*, 25, 15,
2356 3047-3050, 1998.
2357 Tsurutani, B. T., Arballo, J. K., Lakhina, G. S., Ho, C. M., Ajello, J., Pickett, J. S., Gurnett, D. A.,
2358 Lepping, R. P., Peterson, W. K., Rostoker, G., Kamide, Y., and Kokubun, S.: The January 10,
2359 1997 auroral hot spot, horseshoe aurora and first substorm: A CME loop?, *J. Geophys. Res.*, 25,
2360 3047-3050, 1998.
2361 Tsurutani, B.T.: Solar/interplanetary plasma phenomena causing geomagnetic activity at Earth, in
2362 *Proc. Inter. Sch. Phys. "Enrico Fermi" Course CXLII*, edited by B. Coppi, A. Ferrari and E.
2363 Sindoni, IOS Prss, Amsterdam, 273, 2000.
2364 Tsurutani, B.T., Gonzalez, W.D., Lakhina, G.S., and Alex, S.: The extreme magnetic storm of 1-
2365 2 September 1859, *J. Geophys. Res.* 108, A7, 1268, doi:10.1029/JA009504, 2003.
2366 Tsurutani, B.T., Gonzalez, W.D., Zhou, X.-Y., Lepping, R.P., and Bothmer, V.: Properties of slow
2367 magnetic clouds, *J. Atmos. Sol.-Terr. Phys.*, 66, 147-151, 2004a.



2368 Tsurutani, B.T., Gonzalez, W.D., Guarnieri, F., Kamide, Y., Zhao, X., and Arballo, J.K.: Are high-
2369 intensity long-duration continuous AE activity (HILDCAA) events substorm expansion events?,
2370 *J. Atmos. Sol.-Terr. Phys.*, 66, 167-176, 2004b.

2371 Tsurutani, B.T., Mannucci, A., Iijima, B., Abdu, M.A., Sobral, J.H.A., Gonzalez, W., Guarnieri,
2372 F., Tsuda, T., Saito, A., Yumoto, K., Fejer, B., Fuller-Rowell, T.J., Kozyra, J., Foster, J.C., Coster,
2373 A., and Vasyliunas, V.M.: Global dayside ionospheric uplift and enhancement associated with
2374 interplanetary electric fields, *J. Geophys. Res.* 109, A08302, doi:10.1029/2003JA010342, 2004c.

2375 Tsurutani, B.T., Gonzalez, W.D., Lakhina, G.S., and Alex, S.: Reply to comment by S.-I. Akasofu
2376 and Y. Kamide on “The extreme magnetic storm of 1-2 September 1859”, *J. Geophys. Res.*, 110,
2377 A09227, doi:10.1029/2005JA011121, 2005a.

2378 Tsurutani, B.T., Judge, D.L., Guarnieri, F.L., Gangopadhyay, P., Jones, A.R., Nuttall, J., Zambon,
2379 G.A., Didkovsky, L., Mannucci, A.J., Iijima, B., Meier, R.R., Immel, T.J., Woods, T.N., Prasad,
2380 S., Floyd, L., Huba, J., Solomon, S.C., Straus, P., and Viereck, R.: The October 38, 2003 extreme
2381 EUV solar flare and resultant extreme ionospheric effects: Comparison to other Halloween events
2382 and the Bastille day event, *Geophys. Res. Lett.*, 32, L03S09, doi:10.1029/2004GL021475, 2005b.

2383 Tsurutani, B.T., Gonzalez, W.D., Gonzalez, A.L.C., Guarnieri, F.L., Gopalswamy, N., Grande,
2384 M., Kamide, Y., Kasahara, Y., Lu, G., Mann, I., McPherron, R., Soraas, F., and Vasyliunas, V.:
2385 Corotating solar wind streams and recurrent geomagnetic activity: A review, *J. Geophys. Res.*,
2386 111, A07S01, doi:10.1029/2005JA011273, 2006a.

2387 Tsurutani, B.T., McPherron, R.L., Gonzalez, W.D., Lu, G., Gopalswamy, N., and Guarnieri, F.L.:
2388 Magnetic storms caused by corotating solar wind streams, in *Recurrent Magnetic Storms*
2389 *Corotating Solar Wind Streams*, edited by B.T. Tsurutani et al., AGU Press, Wash. DC, 167, 1-17,
2390 2006b.

2391 Tsurutani, B.T., Echer, E., Guarnieri, F.L., and Kozyra, J.U.: CAWSES November 7-8, 2004
2392 superstorm: Complex solar and interplanetary features in the post-solar maximum phase, *Geophys.*
2393 *Res. Lett.*, 35, L06S05, doi:10.1029/2007GL031473, 2008a.

2394 Tsurutani, B.T., Verkhoglyadova, O.P., Mannucci, A.J., Saito, A., Araki, T., Yumoto, K., Tsuda,
2395 T., Abdu, M.A., Sobral, J.H.A., Gonzalez, W.D., McCreadie, H., Lakhina, G.S., and Vasyliunas,
2396 V.M.: *J. Geophys. Res.*, 113, A05311, doi:10.1029/2007HA012879, 2008b.

2397 Tsurutani, B.T., Horne, R.B., Pickett, J.S., Santolik, O., Schriver, D., and Verhoglyadova, O.P.: *J.*
2398 *Geophys. Res.*, 115, AF0010, doi:10.1029/2010JA015870, 2010.



2399 Tsurutani, B.T., Lakhina, G.S., Verkhoglyadova, O.P., Gonzalez, W.D., Echer, E., and Guarnieri,
2400 F.L.: A review of interplanetary discontinuities and their geomagnetic effects, *J. Atmos. Sol.-Terr.*
2401 *Phys.*, 73, 5-19, 2011.

2402 Tsurutani, B.T., Verkhoglyadova, O.P., Mannucci, A.J., and Lakhina, G.S.: Extreme changes in
2403 the dayside ionosphere during a Carrington-type magnetic storm, *J. Spa. Weath. Spa. Clim.*, 2,
2404 A05, doi:10.1051/swsc/2012004, 2012.

2405 Tsurutani, B.T., and Lakhina, G.S.: An extreme coronal mass ejection and consequences for the
2406 magnetosphere and Earth, *Geophys. Res. Lett.*, 41, doi:10.1002/203GL058825, 2014.

2407 Tsurutani, B.T., Echer, E., Shibata. K., Verkhoglyadova, O.P., Mannucci, A.J., Gonzalez, W.D.,
2408 Kozyra, J.U., and Paetzold, M.: The interplanetary causes og geomagnetic activity during the 7-
2409 17 March 2012 interval: a CAWSES II overview, *J. Spa. Weath. Spa. Clim.*, 4, A02,
2410 doi:10.1051/swsc/2013056, 2014.

2411 Tsurutani, B. T., Hajra, R., Echer, E., and Gjerloev, J. W.: Extremely intense (SML ≤ -2500 nT)
2412 substorms: isolated events that are externally triggered?, *AnGeo Comm.*, 33, 519-524, 2015.

2413 Tsurutani, B. T., Hajra, R., Echer, E., Gonzalez, W. D., and Santolik, O.: Predicting
2414 magnetospheric relativistic >1 MeV electrons, *NASA Tech Briefs*, 40, 20, 2016a.

2415 Tsurutani, B.T., Hajra, R., Tanimori, T., Takada, A., Bhanu, R., Mannucci, A.J., Lakhina, G.S.,
2416 Kozyra, J.U., Shiokawa, K., Lee, L.C., Echer, E., Reddy, R.V., and Gonzalez, W.D.: Heliospheric
2417 plasma sheet (HPS) impingement onto the magnetosphere as a cause of relativistic electron
2418 dropouts (REDs) via a coherent EMIC wave scattering with possible consequences for climate
2419 change mechanisms, *J. Geophys. Res. Spa. Phys.*, 121, doi:10.1002/2016JA022499, 2016b.

2420 Tsurutani, B.T., Lakhina, G.S., Echer, E., Hajra, R., Nayak, C., Mannucci, A.J., and Meng, X.:
2421 Comment on “Modeling extreme “Carrington-type” space weather events using three-dimensional
2422 global MHD simulations” by C.M. Ngwira, A. Pulkkinen, M.M Kuznetsova and A. Glocer”, *J.*
2423 *Geophys. Res. Spa. Phys.*, 123, 1388-1392, <https://doi.org/10.1002/2017JA024779>, 2018a.

2424 Tsurutani, B.T., Lakhina, G.S., Sen, A., Hellinger, P., Glassmeier, K.-H., and Mannucci, A.J.: A
2425 review of Alfvénic turbulence in high-speed solar wind streams: Hints from cometary plasma
2426 turbulence, *J. Geophys. Res. Spa. Phys.*, 123, <https://doi.org/10.1002/2017JA024203>, 2018b.

2427 Turner, N. E., Mitchell, E. J., Knipp, D. J., and Emery, B. A.: Energetics of magnetic storms driven
2428 by corotating interaction regions: a study of geoeffectiveness, in *Recurrent Magnetic Storms*:



2429 *Corotating Solar Wind Streams*, Geophys. Monogr. Ser., vol. 167, edited by B. T. Tsurutani et al.,
2430 pp. 113, AGU, Washington, D.C., doi:10.1029/167GM11, 2006.

2431 Turner, D.L., and Li, X.: Quantitative forecast of relativistic electron flux at geosynchronous orbit
2432 based on low energy electron flux, *Space Weather*, 6, S05005,
2433 <https://doi.org/10.1029/2007SW000354>, 2008.

2434 Usanova, M.E., Mann, I.R., Bortnik, J., Shao, L., and Angelopoulos, V.: THEMIS observations of
2435 electromagnetic ion cyclotron wave occurrence: Dependence on AE, SYMH and solar wind
2436 dynamic pressure, *J. Geophys. Res.*, 117, A10218, doi:10.1029/2012JA018049, 2012.

2437 Usoskin, I.G., and Kovaltsov, G.A.: Occurrence of extreme solar particle events: Assessment from
2438 historical proxy data, *Astrophys. J.*, 757:92, doi:10.1088/0004-637X/757/1/92, 2012.

2439 Usoskin, I.G., Kromer, B., Ludlow, F., Beer, J., Friedrich, M., Kovaltsov, G.A., Solanki, S.K., and
2440 Wacker, L.: The AD775 cosmic event revisited: the Sun is to blame, *Astron. Astrophys.*, L3,
2441 doi:10.1051/0004-6361/201321080, 2013.

2442 Vaisberg, O.L., and Zastenker, G.N.: Solar wind and magnetosheath observations at Earth during
2443 August 1972, *Spa. Sci. Rev.*, 19, 687, 1976.

2444 Volland, H.: A semi-empirical model of large-scale magnetospheric electric fields, *J. Geophys.*
2445 *Res.*, 78, 171, 1973.

2446 Wang, C. B., Chao, J. K., and Lin, C.-H.: Influence of the solar wind dynamic pressure on the
2447 decay and injection of the ring current, *J. Geophys. Res.*, 108(A9), 1341,
2448 doi:10.1029/2003JA009851, 2003.

2449 Wang, J., Zhao, M., and Zhou, G.: Magnetic changes in the course of the X7.1 solar flare on 2005
2450 January 20, *Astrophys. J.*, 690, 862-874, 2009.

2451 Wanliss, J. A., and Showalter, K. M.: High-resolution global storm index: Dst versus SYM-H,
2452 *Journal of Geophysical Research*, 111, A02202. <https://doi.org/10.1029/2005JA011034>, 2006.

2453 West, H.I., Jr., Buck, R.M, and Walton, J.R.: Shadowing of electron azimuthal-drift motions near
2454 the noon magnetopause, *Nature Phys. Sci.*, 240, 6, doi:10.1038/physci240006a0, 1972.

2455 Weygand, J. M., and McPherron, R. L.: Dependence of ring current asymmetry on storm phase, *J.*
2456 *Geophys. Res.*, 111, A11221, doi:10.1029/2006JA011808, 2006.

2457 Wilcox, J.M., Scherrer, P.H., Svalgaard, L., Roberts, W.O., and Olson, R.H.: Solar magnetic sector
2458 structure: Relation to circulation of the Earth's atmosphere, *Science*, 180, 185,
2459 doi:10.1126/science.180.4082.185, 1973.



2460 Williams, D. J., Mitchell, D. G., Huang, C. Y., Frank, L. A., and Russell, C. T.: Particle
2461 acceleration during substorm growth and onset, *Geophys. Res. Lett.*, 17, 587-590,
2462 <https://doi.org/10.1029/GL017i005p00587>, 1990.

2463 Winterhalter, D.E., Smith, E.J., Burton, M.E., Murphy, N., and McComas, D.J.: The heliospheric
2464 plasma sheet, *J. Geophys. Res.*, 99, 6667, doi:10.1029/93JA03481, 1994.

2465 Wolff, E.W., Bigler, M., Curran, M.A.J., Dibb, J.E., Frey, M.M., Legrand, M., and McConnell,
2466 J.R.: The Carrington event not observed in most ice core nitrate records, *Geophys. Res. Lett.*, 39,
2467 L08503, doi:10.1029/2012GL051603, 2012.

2468 Wygant, J., Mozer, F., Temerin, M., Blake, J., Maynard, N., Singer, H., and Smiddy, M.: Large
2469 amplitude electric and magnetic field signatures in the inner magnetosphere during injection of 15
2470 MeV electron drift echos, *Geophys. Res. Lett.*, 21, 16, 1739-1742, 1994.

2471 Wygant, J., Rowland, D., Singer, H.J., Temerin, M., Mozer, F., and Hudson, M.K.: Experimental
2472 evidence on the role of the large spatial scale electric field in creating the ring current, *J. Geophys.*
2473 *Res.*, 103, A12, 29527-29544, 1998.

2474 Yashiro, S., Gopalswamy, N., Michalek, G., St. Cyr, O. C., Plunkett, S. P., Rich, N. B., and
2475 Howard, R. A.: A catalog of white light coronal mass ejections observed by the SOHO spacecraft,
2476 *J. Geophys. Res.*, 109, A07105, doi:10.1029/2003JA010282, 2004.

2477 Yermolaev, Y.I., Lodkina, I.G., Nikolaeva, N.S., and Yermolaev, M.Y.: Influence of the
2478 interplanetary driver type on the durations of the main and recovery phases of magnetic storms, *J.*
2479 *Geophys. Res. Spa. Phys.* 119, 8126-8136, doi:10.1002/2014JA019826, 2014.

2480 Zastenker, G.N., Temny, V.V., d'Uston, C., and Bosqued, J.M.: The form and energy of the shock
2481 waves from the solar flares of August 2, 4 and 7, 1972, *J. Geophys. Res.*, 83, 1035, 1978.

2482 Zhao, X., and Dryer, M.: Current status of CME/shock arrival time prediction, *Spa. Weath.*, 12,
2483 448-469, doi:10.1002/2014SW001060, 2014.

2484 Zhang, J., Woch, J., and Solanki, S.: Polar coronal holes during solar cycles 22 and 23, *Chin. J.*
2485 *Astron. Astrophys.*, 5, 5, 531-538, 2005.

2486 Zhou, X., and Tsurutani, B. T.: Rapid intensification and propagation of the dayside aurora: Large
2487 scale interplanetary pressure pulses (fast shocks), *Geophys. Res. Lett.*, 26, 8, 1097-1100, 1999.

2488 Zhang, J., et al.: Solar and interplanetary sources of major geomagnetic storms ($Dst \leq -100$ nT)
2489 during 1996-2005, *J. Geophys. Res.*, 112, A10102, doi:10.1029/2007JA012321, 2007.



2490 Zhou, X., and Tsurutani, B.T.: Interplanetary shock triggering of nightside geomagnetic activity:
2491 Substorms, pseudobreakups, and quiescent events, *J. Geophys. Res.*, 106, A9, 18,957-18,967,
2492 2001.
2493 Zhou, X.-Y., Strangeway, R.J., Anderson, P.C., Sibeck, D.G., Tsurutani, B.T., Haerendel, G., Frey,
2494 H.U., and Arballo, J.K.: Shock aurora: FAST and DMSP observations, *J. Geophys. Res.*, 108, A4,
2495 doi:10.1029/2002JA009701, 2003.
2496
2497 Acknowledgements. Portions of this research were performed at the Jet Propulsion Laboratory,
2498 California Institute of Technology under contract with NASA. GSL thanks the National Academy of
2499 Sciences, India for support under the NASI-Senior Scientist Platinum Jubilee Fellowship Scheme. The
2500 work of RH is funded by the Science & Engineering Research Board (SERB), a statutory body of
2501 the Department of Science & Technology (DST), Government of India through the Ramanujan
2502 Fellowship.